

**International Doctorate School in Information and  
Communication Technologies**

DIT - University of Trento

**DESIGN, MODELLING AND CONTROL OF IRST  
CAPACITIVE MEMS MICROPHONE**

Daide Cattin

Advisor:

Prof. R. Oboe

Dipartimento di Tecnica e Gestione dei Sistemi Industriali

Università di Padova



## **Abstract**

Condenser MEMS microphones are becoming a promising technology to substitute the current standard microphones, and modelling such systems has become very important for designing a condenser microphone fulfilling the given constraints. In this dissertation a deep analysis of capacitive MEMS microphone has been presented coming up with a complete model which is able to fit the experimental data of the microphone sensitivity. Furthermore, a simple noise model, able to fit the experimental data, has been developed considering the well-known Brownian noise and the more subtle  $1/f$  component, usually neglected. With such models, it is possible to have a reliable estimation of the microphone SNR.

Many characterizations have been performed on the produced samples and different problems of the manufacturing process have been highlighted, gaining a deeper understanding on the structure of the microphone and on the production process.

Finally, to reply to the more and more demanding constraints, two applications of control law have been applied: a force feedback and a controller to tune the resonant frequency of the microphone.

This last application shows how a controller can make the system more flexible and reduce the problem of some defects on the production.

The force feedback is a technique already used in MEMS systems, such as gyroscopes and accelerometers, where it has shown to be able to improve the performance of the systems.

In the presented configuration, a force feedback has been implemented in a digital readout interface, realizing the so-called electromechanical sigma delta converter. Its stability has been evaluated and the improvements have been verified experimentally: due to the extra filtering action of the embedded MEMS system inside the converter loop, the A-weighted in-band noise has been reduced from -63dBA to -73dBA.

### **Keywords**

[MEMS, microphone, modelling, control]



# Contents

<b>1. INTRODUCTION.....</b>	<b>1</b>
<b>2. STATE OF THE ART .....</b>	<b>5</b>
<b>3. MODELLING .....</b>	<b>11</b>
3.1. ELECTRO-MECHANO-ACOUSTICAL ANALOGY .....	11
3.1.1 <i>Mechanical elements</i> .....	12
3.1.2 <i>Acoustical elements</i> .....	15
3.2. MICROPHONE STRUCTURE.....	20
3.2.1 <i>Membrane mass</i> .....	21
3.2.2 <i>Membrane compliance</i> .....	23
3.2.3 <i>Air gap resistance</i> .....	25
3.2.4 <i>Air gap mass</i> .....	29
3.2.5 <i>Acoustic holes resistance</i> .....	29
3.2.6 <i>Acoustic hole mass</i> .....	31
3.2.7 <i>Backplate compliance</i> .....	31
3.2.8 <i>Backplate mass</i> .....	32
3.2.9 <i>Flow-by slots</i> .....	32
3.2.10 <i>Backchamber compliance</i> .....	34
3.2.11 <i>Electrostatic Force</i> .....	35
3.2.12 <i>Package model</i> .....	38
3.2.13 <i>Schematic</i> .....	40
3.3. SIMULATION AND EXPERIMENTAL RESULTS .....	41
3.3.1 <i>Noise</i> .....	45
3.3.2 <i>Experimental setup and results</i> .....	48
3.4. MODEL SIMPLIFICATION .....	53
<b>4. MICROPHONE DESIGN AND TESTING.....</b>	<b>55</b>
4.1. MICROPHONE DESIGN .....	55
4.2. MICROPHONE TESTING.....	58
4.2.1 <i>CV characteristic</i> .....	58
4.2.2 <i>Integrated resistances</i> .....	62
4.2.3 <i>Parasitic capacitances</i> .....	67
4.2.4 <i>Acoustic Test</i> .....	74
<b>5. CONTROL APPLICATIONS .....</b>	<b>79</b>
5.1. FORCE FEEDBACK ANALYSIS .....	79
5.1.1 <i>SDM stability</i> .....	80
5.1.2 <i>SDM + microphone stability</i> .....	84
5.1.3 <i>Experimental measurements</i> .....	86
5.2. FREQUENCY TUNING .....	87
5.2.1 <i>Extremum seeking control</i> .....	89
5.2.2 <i>Stability analysis</i> .....	92
5.2.3 <i>Simulation results</i> .....	97
<b>6. CONCLUSIONS .....</b>	<b>103</b>
6.1. FUTURE WORKS.....	104
<b>BIBLIOGRAPHY .....</b>	<b>105</b>



# Chapter 1

## 1. Introduction

In the last fifty years, microphone construction technology has not changed much, and the common electret microphone was produced forty years ago. About two decades ago, however, MEMS technology started a new and promising manufacturing process and the capacitive MEMS microphone has become one of the interesting product.

There are several applications where it can be applied: automotive, space, industrial applications, but the most promising are hearing aid and consumer products such as mobile phones and cameras. A capacitive microphone has many advantages with respect to traditional microphones: smaller size, high sensitivity, flat response, suitable for mass production, less sensitivity to temperature and mechanical shock and it can be integrated with electronic circuit realizing a smart sensors, which can reduce costs and offer new functionalities [1,2].

A capacitive MEMS microphone is a device which converts an acoustic wave into a suitable output signal for post-processing, usually a voltage signal. A typical configuration is shown in figure 1.1.

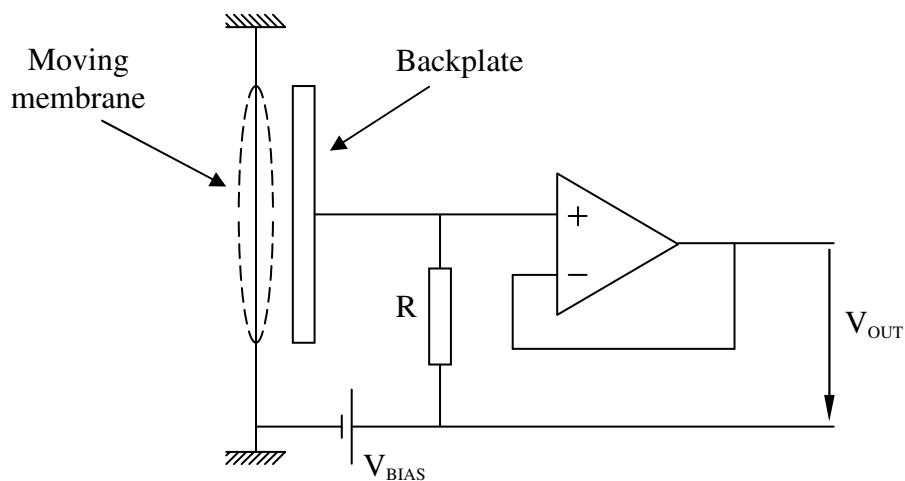


Figure 1.1 Typical readout schematic for a condenser MEMS microphone

The microphone is polarized through a large resistor R and charge is stored in the moving membrane and the backplate, which are the electrodes of the capacitive microphone. The resistor is used to keep constant the charge stored in the microphone. When a sound wave hits the

membrane, the distance between the two electrodes changes and the capacitance of the microphone changes as well. With the hypothesis of constant charge, due to the resistor  $R$ , a voltage is generated at the output of the microphone as a function of the displacement of the moving membrane.

The range of pressure the microphone has to be sensitive to is very wide and ranges from  $20\mu\text{mPa}$ , which is the minimum audible sound for a human ear, to sounds which can reach  $10\text{Pa}$ , equivalent to a jet takeoff at 60 meters. The sound is very loud at that pressure, but well below to the atmospheric value. Furthermore, if the microphone is used as audio transducer, the frequency range of the acoustic pressure is from  $20\text{Hz}$  to  $20\text{kHz}$ .

Therefore, besides the aforementioned advantages, some challenging issues come up, especially in modelling and testing of devices.

A microphone for audio purpose has to guarantee high sensitivity in a wide range of pressure and frequency, so that an accurate and efficient layout of the microphone has to be developed. Thus, modelling becomes a key issue to understand how to design properly a microphone in order to fulfil all the requirements.

On the other hand, the requirements on the microphone are becoming more and more demanding, so that a more sophisticated integrated control is necessary, sometime including on-chip actuation as well.

For this reasons control laws have starting to be applied to MEMS technologies and even to capacitive microphone, in order to improve their performances.

The aim of this dissertation is to treat the main issues of modelling a capacitive MEMS microphone, then the characterization of the produced devices and some method concerning the improvement of microphone performances applying a proper readout electronics and control law. The thesis will be developed as follows:

In chapter 2 a brief review of the main models used to describe the behaviour of the microphone and a couple of solution to improve the performance of the microphone were presented, pointing out the chosen method.

Chapter 3 will present the complete model of the microphone, along with a comparison between the simulation and experimental results for a microphone designed in Omron, Japan.

Chapter 4 will briefly present some technological aspect of the manufacturing process, highlighting the main difficulties we ran into and the adopted solutions. Then a complete characterization of the produced microphones has been performed and experimental results are used to better understand the behaviour of the devices.



Finally, chapter 5 presents a brief analysis of a force feedback readout interface and a control law to tune the resonance frequency of the microphone, applying an extremum seeking controller.



# Chapter 2

## 2. State of the Art

Silicon condenser microphones are becoming more and more relevant and they are replacing the electret microphones, the current standard in many applications.

With respect to them, condenser microphones present higher sensitivity, flatter frequency response, smaller size, lower temperature coefficient, compatibility with surface and batch fabrication normally used for electronic components and thus the possibility of integration of electronic circuit with microphones [3–5]. Due to these characteristics, silicon condenser microphones are drawing more and more attention.

Since the first MEMS microphone, that was described in 1983 [6], many configurations have been developed. The typical configuration comprises a fixed electrode, the backplate, which is separated from a flexible membrane by a small air gap. At the beginning, the backplate and the moving membrane were fabricated using bulk silicon micromachining techniques in different wafer and then put together by wafer bonding. This approach was very difficult due to the complicated procedures and the yields were not satisfactory. In the last decade the fabrication process has been improved, surface micromachining in a single-wafer has been applied and many microphones were presented in literature [6-9]. Many structures and configurations appear, with square or circular membrane, fully clamped membrane, simply supported or corrugated membrane, different configuration of backplate and different materials [10-13], and modelling has become very important for designing condenser microphones.

Figure 2.1 shows the schematic of the condenser MEMS microphone, where the main elements common to almost all the condenser microphone are pointed out.

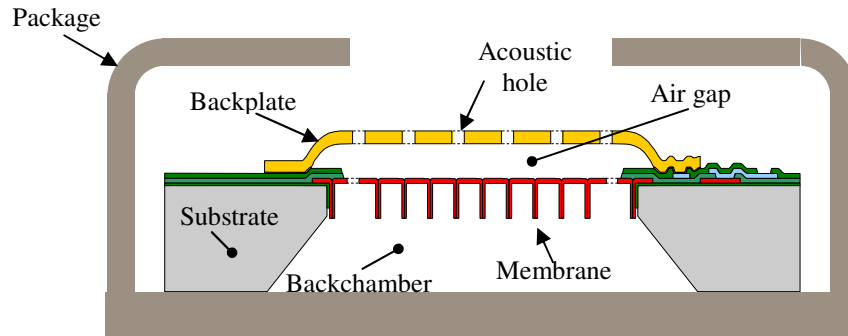


Figure 2.1 Schematic of IRST-ITC MEMS microphone, where we can see a typical structure of a condenser microphone.

Several papers concerning modelling were presented, and both analytically and numerically approaches were adopted analyzing each element of the microphone [14-16]. Efforts were spent to model the deflection of the membrane [17, 18], because the membrane is the active part of the microphone which makes the conversion of the acoustical energy. Each configuration shows pros and cons, and in our case we prefer to use a piston-like membrane. This type of membrane is developed as a rigid plate supported at the corner by flexural beam. This configuration has been preferred because almost all the surface of the moving membrane works actively in the transduction process. Usually the membrane is modelled with FEM, and all the necessary parameters are obtained through simulations. In our case, besides the FEM model, an analytical model has been developed to better understand the behaviour of the moving membrane and to find the reasons of mismatching between simulation and experimental results.

Another main element is the air gap. This component is very important, because it affects the microphone dynamic performance and noise performance.

The first and basic work was written by Skvor in [21] and almost all the models of condenser MEMS microphone use its model. More accurate but more complex theoretical expressions have been developed in [22]. Recently, new studies have been performed to better characterize the air gap, especially concerning the micro-switches. Indeed, these devices have almost the same structure of a condenser microphone, but their working principle is different. A condenser MEMS microphone is biased, the charge is stored in the backplate and the moving membrane, which represent the electrodes of a capacitor. When an acoustic sound wave hits the moving membrane, it moves. Under the hypothesis to keep constant the stored charge, the capacitance between the electrodes changes, thus a signal appears at the output of the microphone. To work properly the backplate and the moving membrane do not have to touch each other, otherwise they short-circuit and risk to stitch each other. As to a micro-switch is like a normal switch,

namely, it has to be open, the two electrodes do not touch each other, or closed, there is a contact between the two electrodes. The switch operation between open and closed state has to be as fast as possible. The air gap between the two electrodes affects the dynamic of the micro-switch, so that recently many studies on the behaviour of the squeezing of the air film between the two electrodes have been presented. In [23-26] the squeezing film damping phenomenon has been deeply developed. In those papers were presented several correction coefficients due to the adaptation of the current formulae to the micro-domain, where some law are no longer valid and some effect, usually negligible in micro-scale, becomes relevant. Using these corrections it was possible to model almost all channels present in the microphone layout and describe the behaviour of the air film when it is squeezed between the moving membrane and the backplate. Another element, often missing in many models, is the package. The package can heavily influence the dynamic performance of the microphone. In the package we can consider the backchamber and the volume enclosed by the package. Usually the backchamber is considered in the model and it is modelled as a volume subject to compression. Its behaviour is like a spring. It can be described with well-established model, such as in [27]. The main issue on designing the backchamber is to find a proper trade-off between its volume, space constrains and stiffness of the moving membrane. Indeed, a small backchamber is like having a hard spring behind the moving membrane that makes the system stiffer, no longer dependent on the membrane stiffness and reducing the sensitivity of the microphone. On the other hand, having a huge backchamber is also to avoid in order to keep limited the size of the microphone. A trade-off was therefore necessary to optimize our design with respect the given constrains.

As to the volume of the package, usually it is considered has an Helmholtz resonator [28, 29]. Such a resonator is due to the vibration of the air inside the inlet hole of the package. When the sound pressure comes, the volume in the inlet hole moves inside the package and it compresses the internal volume. The compressed internal volume tends to pull the air of the inlet hole out. When this air goes out, it gives rise to a depression inside the package. This depression sucks the air of the inlet hole inside the package and the cycle starts again. It behaves like a spring-mass system, and the oscillations are damped by the viscous resistance of the walls of the inlet hole. Sometimes the damping coefficient is neglected, but in our case is very important to model it, because if the resonance frequency of the package falls inside the band, it has to be limited, otherwise the model can crash. Helmholtz resonance is a well-known effect, but if it is not considered properly it can interfere with the dynamic response of the microphone. A detailed characterization can be found in [30], where an exhaustive model has been developed and applied in our model.

One of the main issue of a condenser microphone is the signal to noise ratio (SNR). If we manage to produce a very sensitive microphone but with high noise level, this device is almost useless. The SNR is an index that highlights this property in a device. The noise of a microphone is due mainly to the mechanical noise, because of the microphone itself, and the readout electronics. A decade ago, the noise due to the electronics was dominant [31, 32], but with the new low power consumption and low noise electronics, the mechanical noise has become the main limit for microphone performances. In [33] it was highlighted that the main noise is due to Brownian motion, which is well correlated to the dissipative elements present in the device. The main dissipative element in the microphone is the air gap resistance, and this is the reason of modelling it in such a deep detail. The Brownian noise is due to the random motion of air particles which randomly hit the moving membrane causing an output signal without any input signal. It can be described as a white noise whose power spectral density can be estimated from the value of the dissipative element. Usually only the Brownian noise is considered, but Zuckerwar in [34] found evidence of the presence of a  $1/f$  source noise well correlated with air gap resistance again. In he developed model both contributions are considered.

Collecting all the descriptions and characterizations of each element of the microphone it was possible to build a complete model which is able to predict the behaviour of the microphone and verify if all the constraints are fulfilled.

Besides the model activity of the capacitive MEMS microphone, the project involved the design of a digital readout electronic interface for the microphone as well. This task was accomplished by the Smart Optical Sensors and Interfaces group of FBK in Trento and a detailed description can be found in [35]. The readout interface implements two different solutions to improve the performances of the microphone, and the force feedback is one of them.

This technique is widely used to improve performances of MEMS devices, such as gyroscopes and accelerometers. The idea of force feedback is to counterbalance the acoustic force acting on the moving membrane feeding back the output signal of the interface which is in some way related to the acoustical input. The main advantage of this solution is reduction of the intrinsic nonlinearity of the microphone [36], increasing of the dynamic range and opportunity to increase the bias voltage, but the main difficult to characterize the system was concerned about the stability of the closed loop. The readout interface uses a sigma delta modulator (SDM) as analog to digital converter. It is very efficient, but it has a heavy nonlinearity due to the presence of a quantizer. This nonlinearity complicates the full understanding of the behaviour of a SDM converter, and many methods were used to deal with this issue, using wavelets [37], describing function [38] and others, but the simpler and most used method is the root locus [39]. It uses the

quasi-linear model, where the quantizer is approximate with a variable gain and a noise generator, which represents the distortion due to the quantizer. The variable gain is defined as the ratio between the output of the quantizer and its input, and it ranges between zero to infinity. Thus the root locus of the SDM has been drawn with respect to the variable gain. Then, the stability of the whole system microphone+SDM has been estimated using the root locus method as well.

Besides the common use for voice purposes, a microphone can be applied in other field, such as automotive. One of the possible applications is as park assist sensor. In this case a tone is emitted and the microphone receives the reflected sound wave. To optimize the system, the microphone should have its resonant frequency matching with the frequency of the emitted signal in order to amplify as much as possible the output signal at such a frequency. However, due to technical issues in the mass production, the microphone could have the resonant frequency far away from the desired value.

One way to tune the resonance frequency of a microphone is using an extremum seeking controller. This controller is a special case of adaptive control, and it makes possible to tune a parameter in order to maximize or minimize a given function. Many implementation has been used [40, 41], but here we have chosen to use the simplest one, as described in [42]. A slow perturbation is applied to the system and the slowly varying output is used to infer information about the gradient of the function to maximize or minimize, thus the tuneable parameter is regulated accordingly.





# Chapter 3

## 3. Modelling

This chapter presents the model of the microphone. First, the electro-mechano-acoustical analogy is presented. It will be the fundamental tool to develop the model of the microphone. Then, once drawn the microphone model, a comparison between simulation and experimental results permits to validate the built model.

### 3.1. Electro-mechano-acoustical analogy

A sound is defined as a vibration which propagates through an elastic medium causing an alteration in pressure or displacement of the particles which can be detected by a person or an instrument [27]. Dealing with acoustic waves, the elastic material concerning us is air and the propagation of sound in air can be predicted and described using wave equation.

In classical mechanics, vibrations are represented by differential equations, which are easy to formulate in simpler case, but they can become complex when considering a complete acoustic system. Since early, to cope with these difficulties, it became common to use a schematic representation. This representation has two main advantages: first, it is possible to have a visualization of each component of the system; second, the differential equations can be derived directly from the schematic, instead of formulating them mathematically directly from the physical system.

The schematic can use lumped or distributed parameters: in the former case the independent variable is only time; in the latter case, besides time there are the three space variables as well. In our case, treating with MEMS microphones, we can neglect the dependency on spatial variables because we are not affected by propagation phenomenon, hence we can use properly a lumped schematic. It is indeed in this case where the schematic shows its usefulness in helping to represent and understand the acoustic system under study.

The schematic is based on the electrical circuit theory and each element has its own mathematical and physical meaning. From now on, we shall consider schematic with lumped elements. Following, the main mechanical and acoustical elements shall be presented, explaining their meaning and the mathematical analogy with the electric circuit theory.

### 3.1.1 Mechanical elements

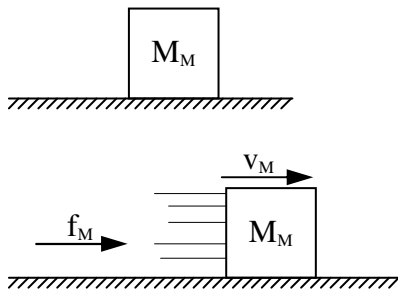
We define the mechanical impedance as the complex ratio between the force ( $f_M$ ) acting on a specific area and the resulting linear velocity ( $v_M$ ) of that area. The unit is Newton second per meter.

$$Z_M = \frac{f_M}{v_M} \left[ \frac{\text{Ns}}{\text{m}} \right] \quad (3.1)$$

The complex ratio is intended as in electric circuit theory: force and velocity are assumed to be sinusoidal, than both of them can be represented by their complex phasors [43]. Their ratio defines the mechanical impedance.

Now the three main mechanical elements will be defined: mass, compliance and mechanical resistance.

- Mechanical Mass ( $M_M$ ) is defined as the quantity which, when acted on by a force, accelerates proportionally to that force; the unit is kilogram [kg] and it follows the Newton's second law:



$$f_M(t) = M_M a_M(t) = M_M \frac{dv_M(t)}{dt} \quad (3.2)$$

where  $f_M(t)$  is the mechanical force acting on the mechanical mass  $M_M$ ,  $a_M(t)$  and  $v_M(t)$  are the mechanical acceleration and the velocity respectively.

In steady state, when  $f_M(t)$  is a sinusoidal force with angular frequency  $\omega=2\pi f$  where  $f$  is the vibrating frequency and the mechanical mass  $M_M$  is constant, we can express the Newton's second law in complex variables

$$f_M = j\omega M_M v_M$$

where  $j = \sqrt{-1}$  and  $f_M$  and  $v_M$  are expressed as phasors.

In electric circuit theory we can find the same differential equation describing the relationship between the voltage and the current through an inductor.

$$v_E(t) = L_E \frac{di_E(t)}{dt}$$

where  $v_E(t)$  is the voltage across the inductor  $L_E$  and  $i_E(t)$  is the current flowing through it.

In this analogy, the force applied to a mass is like applying a voltage across the inductor and the variation of the mass velocity correspond to the variation of the current flowing through the inductor. In this analogy the mass is represented by an equivalent inductor and indeed the symbol of the mass in the equivalent schematic is an inductor.

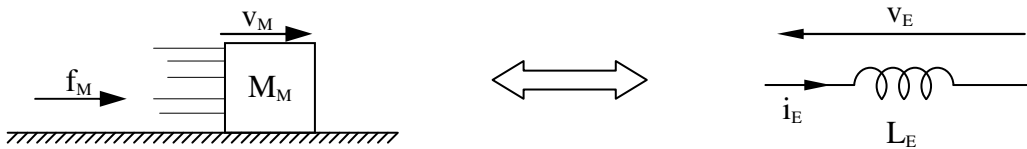


Figure 3.1 Mechanical mass and its equivalent symbol in electro-mechanical analogy

- Mechanical Compliance ( $C_M$ ) is defined as the displacement of a mechanical system directly proportional to the force acting on it. The opposite of the compliance is the stiffness. The unit of the mechanical compliance is meter per Newton [m/N]. It obeys to the following physical law:

$$f_M(t) = \frac{1}{C_M} x_M(t) = \frac{1}{C_M} \int v_M(t) dt \quad (3.3)$$

where  $f_M(t)$  is the force acting on the mechanical system,  $C_M$  is the mechanical compliance and  $x_M(t)$  and  $v_M(t)$  is the mechanical displacement and velocity respectively.

In steady state, when  $f_M(t)$  is sinusoidal with angular frequency  $\omega=2\pi f$  and the compliance  $C_M$  is constant, the displacement  $x_M(t)$  and the velocity  $v_M(t)$  are sinusoidal as well. We can express the integral relation (3.3) with phasors:

$$f_M = \frac{v_M}{j\omega C_M}$$

Keeping the same analogy as before, with voltage drop and current equivalent to mechanical force and velocity respectively, (3.3) is equivalent to the relationship between voltage ( $v_E$ ) and current ( $i_E$ ) through a capacitor  $C_E$ . The equivalent electric variable to the mechanical position is the integral of the current through the capacitor, that is charge ( $q_E$ ).

$$v_E(t) = \frac{1}{C_E} \int i_E(t) dt = \frac{q_E(t)}{C_E}$$

The mechanical symbol of compliance is a spring, and its equivalent electric element in circuit theory is a capacitor.

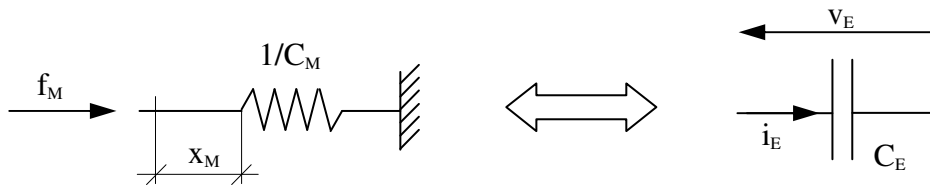


Figure 3.1 Mechanical compliance and its equivalent symbol in electro-mechanical analogy

- Mechanical Resistance ( $R_M$ ) is defined as a mechanical element which dissipates energy which is never reconverted in kinetic nor potential energy [43]. This definition is general and embraces many mechanical elements, linear and nonlinear. In our particular case, we can simplify and consider only viscous friction, which is the main source of dissipation in the microphone. In this case the mechanical resistance is a mechanical element which moves at a velocity proportional to the force acting on it. Usually it is represented by a dashpot:

$$f_M(t) = R_M v_M(t) \tag{3.4}$$

where  $R_M$  is the mechanical resistance representing the viscous friction,  $f_M(t)$  and  $v_M(t)$  are the force acting on and the mechanical velocity respectively.

In steady state, if  $f_M(t)$  is sinusoidal with angular frequency  $\omega=2\pi f$  and the mechanical resistance is constant, the force and the velocity can be expressed as phasors and the (3.4) becomes

$$F_M = R_M v_M$$

The analogous component in electric circuit theory to the mechanical resistance is a resistor. Indeed, the relationship between the voltage drop applied to a resistor and the current flowing through it is the same expressed by (3.4):

$$v_E(t) = R_E i_E(t)$$

In the schematic, the symbol of the mechanical resistance describing the viscous friction is a dashpot, whereas its equivalent symbol in the electric circuit is a resistor.

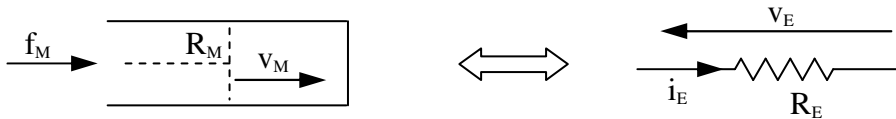


Figure 3.3 Mechanical resistance and its equivalent symbol in electro-mechanical analogy

### 3.1.2 Acoustical elements

As done for the mechanical elements, we can define an acoustic impedance as the complex ratio between the instantaneous pressure ( $p_A$ ) and the volume velocity ( $v_A$ ):

$$Z_A = \frac{p_A}{v_A} \left[ \frac{N s}{m^5} \right] \quad (3.5)$$

Before defining the instantaneous pressure we have to define the static pressure as the pressure presents at a point without any acoustic wave. The instantaneous pressure is then defined as the incremental change from the static pressure at a given point and instant due to the presence of an acoustic wave. The unit is Newton per square meter.

The volume velocity is defined as the rate of flow of air due only to an acoustic wave perpendicularly through a specific area, namely, if the air particles passing through a specific section  $S_A$  have a velocity  $v_p(t)$  the volume velocity is defined as  $v_A(t) = S_A v_p(t)$ . The unit is cube meter per second.

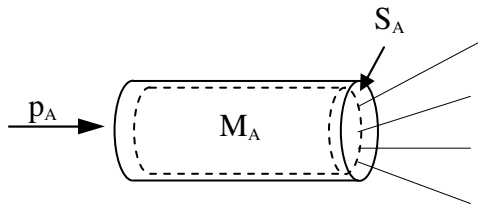
Once defined the acoustical impedance it is possible to define the main three acoustic elements and their equivalent in electrical circuit theory.

- Acoustic Mass ( $M_A$ ) is defined as the quantity of mass of air accelerated by a force acting on it, neglecting compression of the air itself. The main point in this definition is that the air is not compressed and this feature allows to distinguish the acoustic mass from other acoustic elements.

Usually, acoustic mass is represented with a tube of section  $S_A$  filled with air. The behaviour of an acoustic mass is described by the Newton's second law like (3.2) and can be made suitable for acoustic field considering the force  $f_M(t)$  as the force acting on the air mass, and the velocity  $v_M(t)$  as the particle velocity  $v_P(t)$  and the mass  $M_M$  as the mass of the moving air:

$$f_M(t) = M_M \frac{dv_P(t)}{dt}$$

Referring the force to the specific surface which the particles pass through, we can express the Newton's second law in acoustical terms:



$$\begin{aligned} \frac{f_M(t)}{S_A} &= p_A(t) = \frac{M_M}{S_A} \frac{d[v_P(t) S_A]}{dt S_A} = \frac{M_M}{S_A^2} \frac{dv_A(t)}{dt} \\ p_A(t) &= M_A \frac{dv_A(t)}{dt} \end{aligned} \quad (3.6)$$

where  $p_A(t)$  is the instantaneous difference pressure at each end of the air mass  $M_M$  undergoing the force  $f_M(t)$ .

$M_A$  is the acoustic mass defined as the ratio between the air mass  $M_M$  undergoing the force  $f_M(t)$  and the square of the specific surface the air pass through. The unit is kilogram per meter powered four [ $\text{kg}/\text{m}^4$ ].

$v_A(t)$  is the volume velocity, namely the ratio of flow of the air mass  $M_M$  through the specific surface  $S_A$ .

In steady state, if the pressure  $p_A(t)$  is sinusoidal with angular frequency  $\omega=2\pi f$  and the acoustic mass  $M_A$  is constant, the (3.6) can be expressed with phasors

$$p_A = j\omega M_A v_A$$

As the mechanical mass, the analogous electrical element to the acoustic mass is an inductor.

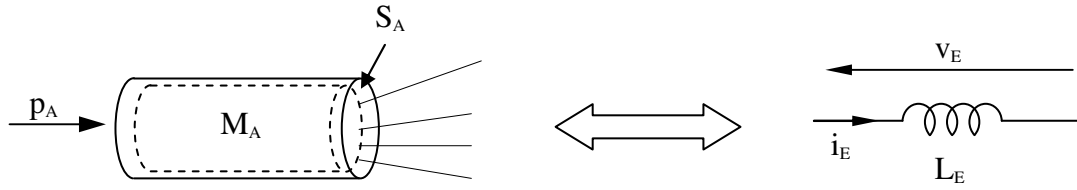


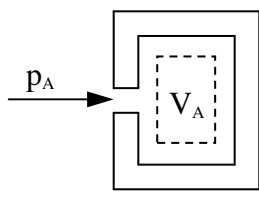
Figure 3.4 Acoustical mass and its equivalent symbol in electro-mechanical analogy

- Acoustic Compliance ( $C_A$ ) is a characteristic of a volume  $V_A$  of gas compressed by a force without causing acceleration to the gas itself. The acoustic compliance is like a mechanical spring which counteracts the compressing force acting on it. Indeed, the mathematical relationship of acoustic compliance can be derived from the (3.3) of the mechanical compliance where  $f_M(t)$  becomes the force compressing the volume and the displacement  $x_M$  becomes the compressed volume  $V_A$  with respect to its section  $S_A$ .

$$f_M(t) = \frac{1}{C_M} x_M = \frac{1}{C_M} \frac{V_A}{S_A} = \frac{1}{C_M S_A} \int v_A(t) dt$$

From the schematic point of view, the acoustic compliance is usually represented using a box containing the volume  $V_A$  and an opening for the entrance of pressure variation.

Referring the force  $f_M(t)$  to the specific area  $S_A$  the previous equation can be expressed in acoustical terms:



$$\begin{aligned} \frac{f_M(t)}{S_A} &= p_A(t) = \frac{1}{S_A^2 C_M} \int v_A(t) dt \\ p_A(t) &= \frac{1}{C_A} \int v_A(t) dt \end{aligned} \quad (3.7)$$

where  $p_A(t)$  is the instantaneous pressure acting on the volume  $V_A$

$v_A(t)$  is the volume velocity of air flowing into the volume  $V_A$  undergoing the pressure  $p_A(t)$ .

$C_A$  is the acoustic compliance of the volume  $V_A$  undergoing the compression. The unit is meter powered five per Newton [ $m^5/N$ ].

If the pressure acting on the volume  $V_A$  is sinusoidal with angular frequency  $\omega=2\pi f$  and the acoustic compliance  $C_A$  is constant, the relationship (3.7) can be expressed with phasors

$$p_A = \frac{1}{j\omega C_A} v_A$$

As the mechanical compliance, the analogous electrical element of the acoustical compliance is a capacitor.

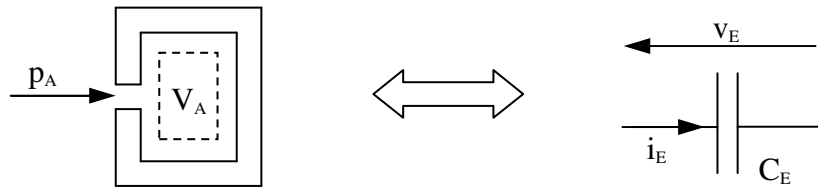


Figure 3.5 Acoustical compliance and its equivalent symbol in electro-mechanical analogy

- Acoustic Resistance ( $R_A$ ) is defined as the element causing losses due to the flowing of gas through it. In our case, the main cause of losses is the viscous movement of gas through a fine mesh screen or a tube with a very small section [27]. The mathematical relationship between acoustic variables and  $R_A$  can be derived from the mechanical case described by (3.4) where  $f_M(t)$  in this case is the force acting on the air flowing through the specific area  $S_A$ , and  $v_M(t)$  is the velocity of the air particles  $v_p(t)$  through that section.

$$f_M(t) = R_M v_P(t) = \frac{R_M}{S_A} v_P(t) S_A = \frac{R_M}{S_A} v_A(t)$$

Referring the force  $f_M(t)$  to the specific section  $S_A$ , we can express the early expression in acoustical terms:

$$\frac{f_M(t)}{S_A} = p_A(t) = \frac{R_M}{S_A^2} v_A(t) \Rightarrow p_A(t) = R_A v_A(t) \quad (3.8)$$



where  $p_A(t)$  is the pressure acting on the air volume

$v_A(t)$  is the volume velocity of the air passing through the specific area  $S_A$ .

$R_A(t)$  is the acoustical resistance due to the viscosity friction of the air passing through the specific section  $S_A$ . The unit is Newton second per meter powered five  $[Ns/m^5]$ .

If the force acting on it is sinusoidal with angular frequency  $\omega=2\pi f$  and the acoustical resistance is constant, the (3.8) can be expressed with phasors:

$$p_A = R_A v_A$$

As can be inferred by the previous relations, the analogous electrical element of the acoustical resistance is a resistor. In acoustical schematic,  $R_A$  is usually represented as a fine mesh screen, whereas in the analogous electric circuit schematic with a resistor, as shown in the following figure.

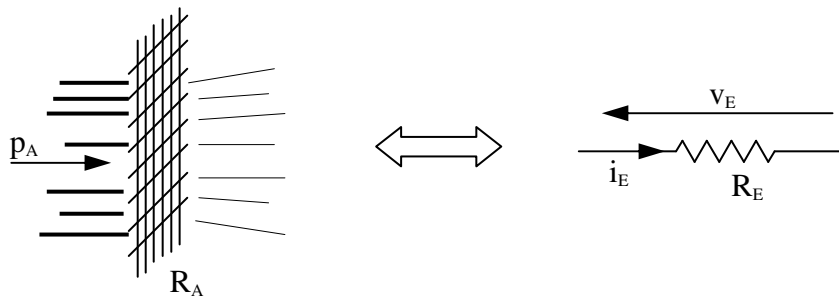


Figure 3.6 Acoustical resistance and its equivalent symbol in electro-mechanical analogy

The following table summarizes all the analogy for mechanical and acoustical impedance with their respective analogous element in electric circuit theory.

Variables		
Mechanical	Acoustical	Electrical
Force ( $f_M$ )	Instantaneous pressure ( $p_A$ )	Voltage ( $v_E$ )
Velocity ( $v_M$ )	Volume velocity ( $v_A$ )	Current ( $i_E$ )

Element	Mechanical		Acoustical		Electrical	
	Physical Law	Unit	Physical Law	Unit	Physical Law	Unit
Mass	$f_M(t) = M_M \frac{dv_M(t)}{dt}$	[kg]	$p_A(t) = M_A \frac{dv_A(t)}{dt}$	$\left[ \frac{\text{kg}}{\text{m}^4} \right]$	$v_E(t) = L_E \frac{di_E(t)}{dt}$	[H]
Compliance	$f_M(t) = \frac{1}{C_M} \int v_M(t) dt$	$\left[ \frac{\text{m}}{\text{N}} \right]$	$p_A(t) = \frac{1}{C_A} \int v_A(t) dt$	$\left[ \frac{\text{m}^5}{\text{N}} \right]$	$v_E(t) = \frac{1}{C_E} \int i_E(t) dt$	[F]
Resistance	$f_M(t) = R_M v_M(t)$	$\left[ \frac{\text{kg}}{\text{s}} \right]$	$p_A(t) = R_A v_A(t)$	$\left[ \frac{\text{kg}}{\text{s m}^4} \right]$	$v_E(t) = R_E i_E(t)$	[Ω]
Impedance	$Z_M = \frac{f_M}{v_M}$	$\left[ \frac{\text{kg}}{\text{s}} \right]$	$Z_A = \frac{p_A}{v_A}$	$\left[ \frac{\text{kg}}{\text{s m}^4} \right]$	$Z_E = \frac{v_E}{i_E}$	[Ω]

### 3.2. Microphone structure

A schematic of the IRST MEMS microphone in a package is shown in figure 3.7.

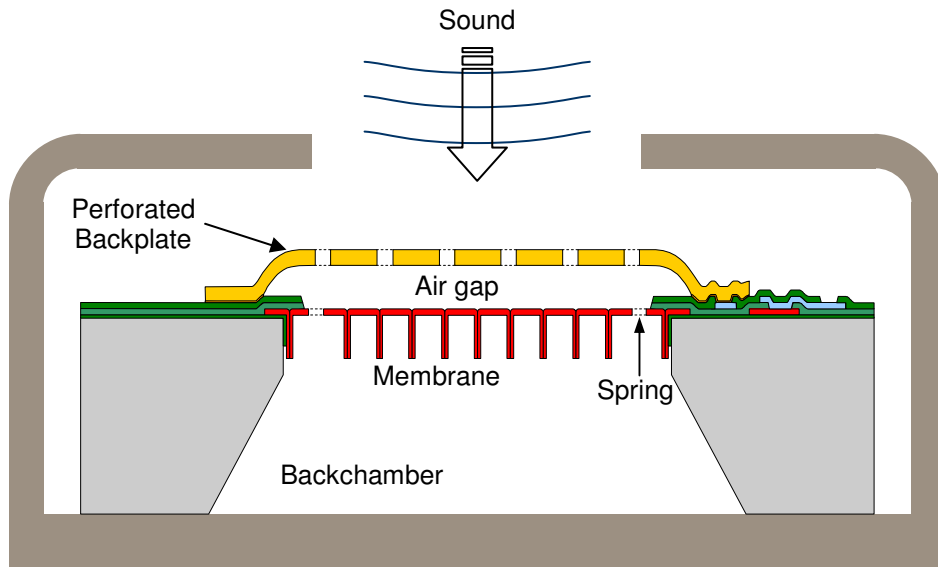


Figure 3.7 Schematic of FBK MEMS microphone inside a package

Figure 3.7 shows the main parts of the microphone: the sound enters through the inlet hole of the package, it passes through the acoustic holes of the perforated backplate and hits the moving

membrane which vibrates. The displacement of the moving membrane is damped by the air gap and the backchamber compliance. Following the path of sound wave it is possible to recognize the main elements of the microphone and design them in order to achieve the desired sensitivity and dynamic response.

Two models have been realized, one for the Omron's MEMS microphone and another one for the IRST MEMS microphone. As to the Omron's microphone, it was possible to perform acoustical and mechanical characterizations, so that simulation results have been compared with experimental results and the model has been tuned accordingly.

The IRST MEMS microphone has a layout slightly different from the Omron's one, but they have many parts in common and it was possible to develop the IRST MEMS microphone model using the knowledge acquired developing the Omron's model.

MEMS systems are not easy to model especially because of their dimensions. Indeed, some physical law is no longer true because a scale down rule cannot always be applied [44]. Due to the impossibility of realizing the proper experimental setup to characterize each element of the MEMS microphone in our laboratories, each part of the microphone is modelled accordingly to models found in literature.

Besides microphone, the package and the mechanical noise will be modelled as well, because both of them influence the microphone performance. The former is like a filter to the incoming sound wave, and the latter limits the minimum detectable sound.

In the following sections the package, the noise source and the main parts of the microphone will be analysed and modelled and a complete schematic will be drawn.

### **3.2.1 Membrane mass**

The mass of the moving membrane can be easily calculated knowing the geometrical dimensions, the material it is made of and its physical properties. With these information it is possible to determine the mass of the moving membrane:

$$M_D = \rho V_D$$

where  $\rho$  is the density of the material the diaphragm is made of and  $V_D$  is the volume of the moving membrane. In this way the mass of the moving membrane of both Omron's microphone and IRST MEMS microphone has been calculated. We can not go into detail for the Omron's MEMS microphone but the complete calculation will be carried out for the IRST MEMS microphone.

As to the moving membrane of the FKB MEMS microphone, figure 3.8 shows a cross section of its moving membrane.

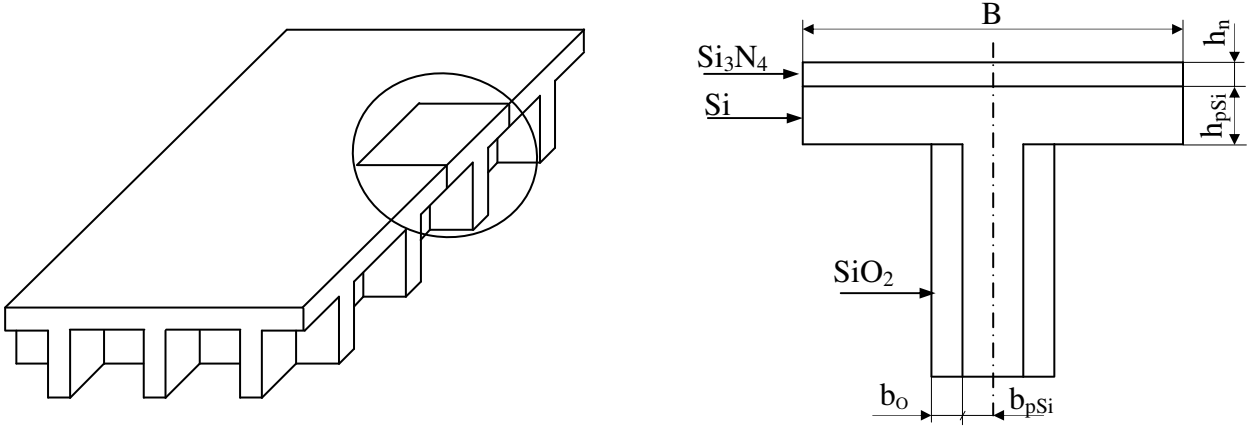


Figure 3.8 Cross section of the IRST moving membrane

The membrane is made of a layer of silicon nitride ( $\text{Si}_3\text{N}_4$ ), polysilicon (Si) to make the conductive layer of the moving membrane and the ridges, then the silicon oxide ( $\text{SiO}_2$ ) to isolate the ridges. Figure 3.8 shows also a unit cell used to evaluate the volume and thus the mass of the membrane. The mass of a unit cell of silicon nitride and polysilicon is

$$M_n = \rho_n B^2 h_n$$

$$M_{pSi} = \rho_{pSi} B^2 h_{pSi}$$

where  $\rho_n$ ,  $\rho_{pSi}$ ,  $h_n$  and  $h_{pSi}$  are respectively density and thickness of silicon nitride and polysilicon,  $B$  is the side of the square unit cell.

The mass of the ridges relative to one unit cell is

$$M_{ridges} = 4 (b_0 + b_{pSi}) [B - (b_0 + b_{pSi})] h_r$$

The total mass of one unit cell is the sum of all three elements:

$$M_D^1 = M_n + M_{pSi} + M_{ridges}$$

thus, the mass of the whole moving membrane is

$$M_D = \frac{S_D}{B^2} M_D^1$$

where  $S_D$  is the surface of the moving membrane.

### 3.2.2 Membrane compliance

The stiffness of an element is defined as the ratio between the force acting on it and the respective extension with respect to its own resting position. The reciprocal of the stiffness is defined as compliance.

The moving membrane is anchored at its own corners and, on first approximation, we can suppose the membrane is rigid and has a piston-like movement. In this hypothesis, the anchors behave like springs and have deformation. The stiffness of these springs can be roughly estimated as follows [45].

We can recognize three main sources of spring deformation: flexion due to the force acting on the moving membrane, axial strain and internal stress.

In the case of deformation due only to the flexion, springs can be considered a flat spring cantilever, where the axial spring constant is given by [45]

$$k_r = \frac{1}{2} \frac{E}{1-\nu^2} \left( \frac{t}{l_s} \right)^2 \frac{b t}{l_s}$$

where  $E$  and  $\nu$  are respectively the Young module and the Poisson's ratio,  $t$  is the thickness,  $b$  the width and  $l_s$  is the length of the spring.

The spring constant due to the stretch of the spring when the membrane moves can be estimated considering the extension of the spring due to the vertical force acting on the moving membrane.

Figure 3.9 shows the case.

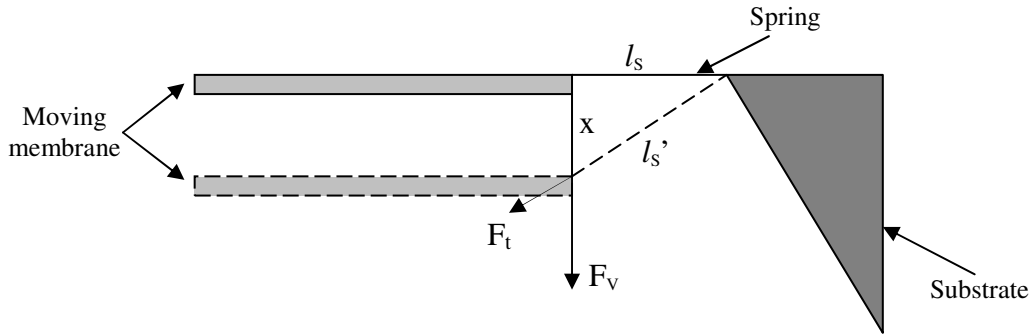


Figure 3.9 Schematic of the model used to estimate the spring stretching after (dashed line) force acting on moving membrane.

When the membrane moves, the length of the spring changes from  $l_s$  to  $l_s'$ . The increment is

$$l_s' - l_s = l_s - \sqrt{l_s^2 + x^2}$$

The strain is then

$$\varepsilon = \frac{l_s' - l_s}{l_s} = 1 - \sqrt{1 + \left(\frac{x}{l_s}\right)^2} \cong \frac{1}{2} \left(\frac{x}{l_s}\right)^2$$

where the last approximation is true if  $\frac{x}{l_s} \ll 1$ .

The stress in the spring can be derived from the strain previously evaluated:

$$\sigma_t = \frac{E}{1-\nu^2} \varepsilon = \frac{1}{2} \frac{E}{(1-\nu^2)} \left(\frac{x}{l_s}\right)^2$$

From the axial stress of the spring, it can be evaluated the axial force acting on the spring:

$$F_t = \sigma_t t b$$

where  $t$  and  $b$  are respectively the thickness and the width of the spring.

If the vertical displacement is small ( $x \ll l_s$ ), the vertical force  $F_v$  can be calculated directly knowing  $x$  and  $l_s$ :

$$F_V \cong \frac{x}{l_s} F_t$$

Thus, the spring constant due to the axial extension is

$$k_{EX} = \frac{F_V}{x} = \frac{1}{2} \frac{E}{(1-\nu^2)} \left( \frac{x}{l_s} \right)^2 \frac{t b}{l_s}$$

The spring constant due to the internal stress can be simply evaluated as

$$k_i = \sigma_i \frac{t b}{l_s}$$

The overall spring constant of the anchor is the sum of the three contribution previously evaluated:

$$k_D = k_f + k_{EX} + k_i$$

The compliance of the moving membrane is calculated as the reciprocal of the spring constant  $k_D$ . Anyway, this evaluation is just a rough approximation of the true spring constant, because it does not take into account other effects, such as the non-ideal piston-like displacement of the membrane, the deformation of the moving membrane, residual stress of the membrane which is released over the springs. For this reasons, usually this calculation are used just for a rough estimation, but the value used in the simulation is the spring constant obtained in FEM simulation. This procedure is used both in the Omron's microphone and the IRST MEMS microphone design.

### 3.2.3 Air gap resistance

The space between the moving membrane and the backplate is called air gap. When the moving membrane moves the gas film in the air gap is squeezed and gives rise to losses. The element representing these losses is the air gap resistance.

The air gap resistance is one of the main elements of the MEMS microphone model, because it influences the behaviour of the frequency response at high frequency, the sensitivity and it is the main source of thermal noise. For this reason it is important to have a good approximation of it.

There are several works on it, from [21] which is still the basis for many models, and more recent papers [46] which slightly modify the Škvor's model introducing correction due to end effect and keeping into account different flow regimes inside the air gap depending on the dimensions of the air gap itself and acoustic holes in the backplate.

To calculate the air gap resistance, Škvor made two hypotheses: the compression of the gas in the air gap is negligible and the flowing of the gas through the acoustic holes of the backplate is laminar. The first hypothesis holds if there the backplate holes are small enough and they are placed in a regular pattern; the second hypothesis depends on the dimension of the acoustic holes which determines the flow regimes.

Having a regular distribution of acoustical holes, it is possible to divide the surface of the backplate in regular regions as many as the number of acoustical holes and suppose that the air in that region is collected only from the relative acoustical hole. Then, the air gap resistance is calculated for one single region of each acoustic hole.

The volume velocity of that area is given by the following integral

$$v_A = \int v \, dS$$

where  $v_A$  is the volume velocity,  $v$  is the normal velocity of the moving membrane squeezing the air film and  $dS$  is the elementary surface of the air film where the moving membrane is acting on.

The pressure drop of the air film for a path of length  $l$  is given by the Hagen-Poiseuille's law [23]:

$$p = \int \frac{12\eta v_A}{2\pi l h^3} dl$$

where  $\eta$  is the dynamic viscosity of air and  $h$  is the height of the air gap.

Using the definition of acoustical impedance, the air gap resistance is obtained by the ratio between the pressure drop and the volume velocity

$$R_{\text{AIRGAP}} = \frac{p}{v_A}$$

We can not go into detail about the formulation of the air gap resistance of the Omron's microphone, but we can express a detailed expression for the IRST MEMS microphone.

The layout of the acoustic holes is at honeycomb with a hole in the centre, as shown is figure 3.10.



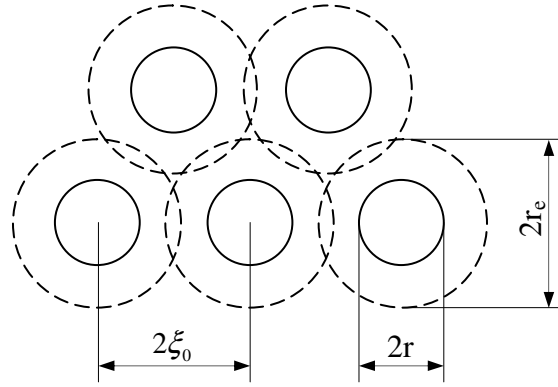


Figure 3.10 Honeycomb pattern of acoustic holes on the backplate

In this layout each hole as the following area ( $S_1$ ) with the equivalent radius ( $r_e$ ):

$$S_1 = 2\sqrt{3}\xi_0 \Rightarrow r_e = \sqrt{\frac{S_1}{\pi}} = \sqrt{\frac{2\sqrt{3}\xi_0}{\pi}} \cong 1.05\xi_0$$

The dynamic viscosity is evaluated using the Poiseuille flow rate [23] function of the Knudsen number defined as  $K_n = \frac{\lambda}{h}$  where  $\lambda$  is the mean free path of air and  $h$  is the characteristic dimension of the flow channel, in this case the air gap height.

The dynamic viscosity is usually defined for channel of infinite length, whereas in short channel there are fringe flow effects due to the entrance and the escape of the air through the channel itself. These effects are taken into account including an extra elongation on the length of the channel. This evaluation has been approximated numerically in [46,23] and the relative elongation with respect to the air gap height ( $h$ ) is

$$\Delta l^r = \frac{8}{3\pi} \frac{1 + 2.471D^{-0.659}}{1 + 0.5D^{-0.5} \left(\frac{l}{h}\right)^{-0.238}}$$

The effective viscosity with end effect correction is given by [23]

$$\eta_{\text{eff}} = \eta \frac{v_A(\infty)}{v_A(D)}$$

where  $v_A(\infty)$   $v_A(D)$  are the volume velocity considering infinite and finite length channel respectively.  $D = \frac{\sqrt{\pi}}{2K_n}$  is the inverse Knudsen number. The volume velocity for infinite length channel for a rectangular channel is  $v_A^R(\infty) = \frac{D}{6}$ , calculated considering a continuum flow regime using the Poiseuille's law. The volume velocity considering end effects of a finite length rectangular channel has been approximated numerically in [24]:

$$v_A^R \cong \frac{D}{6} + \frac{1.396}{D^{0.159}}$$

Substituting the value of the volume velocities in the equation of  $\eta_{\text{eff}}$

$$\eta_{\text{eff}} = \frac{\eta}{1 + 9.638K_n^{1.159}}$$

Finally, using the ratio between the pressure drop evaluated in [21] and the volume velocity with end effect correction, the air gap resistance of the air flowing through a single acoustic hole is given by [24]

$$R_{\text{AIRGAP}}^1 = \frac{2\pi D \eta_{\text{eff}} l_{\Delta}^4}{v_A h^3} \left( \frac{1}{2} \ln \frac{l_{\Delta}}{r} - \frac{3}{8} + \frac{1}{2} \frac{r^2}{l_{\Delta}^2} - \frac{1}{8} \frac{r^4}{l_{\Delta}^4} \right)$$

where  $l_{\Delta}$  is the length of the channel with end effect correction  $l_{\Delta} = l + h\Delta l$ ,  $r$  is the radius of the acoustic hole,  $D$  is the inverse Knudsen number,  $h$  is the air gap height,  $\eta_{\text{eff}}$  the effective viscosity early defined.

The backplate has  $N$  acoustic holes and each of them has the same resistance under its section  $S_1$ , thus the overall air gap resistance will be  $N$  times the resistance of a single section:

$$R_{\text{AIRGAP}} = N R_{\text{AIRGAP}}^1$$

### 3.2.4 Air gap mass

The air in the air gap follows the second Newton's law which can be expressed as

$$p(t) S = \rho l \frac{dv_A(t)}{dt}$$

where  $p(t)$  is the pressure acting on the specific surface  $S$ ,  $\rho$  is the air density,  $l$  is the length of the path the air pass through and  $v_A(t)$  is the volume velocity. Supposing a sinusoidal pressure and volume velocity, they can be both transformed in phasors.

The pressure drop due to the mass of a single section relative to one acoustic hole of the backplate can be expressed as

$$p = \int j\omega v_A \rho \frac{dl}{2\pi l h}$$

where  $p$  is the pressure drop,  $\omega=2\pi f$  is the angular frequency,  $l$  is the length of the path of the air in a single section relative to one acoustic hole,  $\rho$  is the air density,  $v_A$  is the volume velocity and  $h$  is the height of the air gap.

In this way, the mechanical mass of a single section relative to one acoustic hole is given by [21]

$$M_{\text{AIRGAP}}^1 = \omega \rho \frac{\pi r_e^4}{h} \left( \frac{1}{2} \ln \frac{r_e}{r} - \frac{3}{8} + \frac{1}{2} \frac{r^2}{r_e^2} - \frac{1}{8} \frac{r^4}{r_e^4} \right)$$

where  $r$  and  $r_e$  are respectively the radius of the acoustic hole and the equivalent radius of the surface relative to that hole and  $h$  is the air gap height.

On the backplate there are  $N$  acoustic holes, then the total mass of the air gap is

$$M_{\text{AIRGAP}} = N M_{\text{AIRGAP}}^1$$

### 3.2.5 Acoustic holes resistance

The resistance of the acoustic holes is modelled as the flowing of air through a short channel taking into account end effects as done for the air gap resistance.[23].

The relative extra-elongation of the channel with respect to the radius of the acoustic hole ( $r$ ) is given by [23]

$$\Delta t_{BP}^r = \frac{3\pi}{8} \frac{1 + 1.7D^{-0.858}}{1 + 0.688D^{-0.858} \left( \frac{t_{BP}}{r} \right)^{-0.125}}$$

where  $D$  is the inverse Knudsen number and  $t_{BP}$  is the length of the acoustic hole, that is the thickness of the backplate. The infinite length  $v_A(\infty)$  and short circular channel  $v_A^C$  volume velocity is respectively [23]

$$v_A(\infty) = \frac{D}{4} \quad v_A^C = \frac{D}{4} + 1.485 \frac{1.78D + 1}{2.625D + 1}$$

Thus, the effective density for the acoustic hole resistance is given by:

$$\eta_{eff} = \eta \frac{v_A^C(\infty)}{v_A^C(D)} \cong \eta \frac{11,573 + 9.029K_n}{1 + 2,326K_n}$$

where  $K_n$  is the Knudsen number.

The resistance of one acoustic hole with end effect correction can be calculated as done for the air gap resistance:

$$R_{AH}^1 = 2\pi t_{BP}^\Delta \eta_{eff} \frac{D}{v_A^C}$$

where  $t_{BP}^\Delta = t_{BP} + r \Delta t_{BP}^r$  is the acoustic hole length accounting for the end effect and  $D$  is the inverse Knudsen number with respect to the radius of the acoustic hole.

The backplate has  $N$  acoustic holes, hence it like having  $N$  resistances in parallel. Thus, the resistance of all acoustic holes will be  $N$  times smaller:

$$R_{AH} = \frac{R_{AH}^1}{N}$$

### 3.2.6 Acoustic hole mass

The acoustic hole mass is calculated from [27] where end effect were considered, and it is given by:

$$M_{AH}^1 = \rho \left[ t_{BP} + 1.7 \left( 1 - \frac{r}{a} \right) \right] \pi r^2$$

where  $\rho$  is the air density,  $t_{BP}$  is the thickness of the backplate,  $r$  is the radius of acoustic holes and  $a$  is the distance between the centres of two acoustic holes.

The backplate has  $N$  acoustic holes, so that the mass of all acoustic hole is

$$M_{AH} = N M_{AH}^1$$

### 3.2.7 Backplate compliance

The backplate is usually supposed to be much more stiffer than the moving membrane, hence its compliance is often neglected in models. However, in order to reduce air gap resistance, improving the frequency response and the noise performances, the backplate has a large amount of acoustic holes, thus reducing its rigidity. Increasing the backplate compliance makes, in some case, no longer negligible its displacement, influencing the sensitivity of the device.

Ideally the backplate has an infinite stiffness, so that, when an acoustic wave comes, only the moving membrane moves. The displacement of the membrane gives rise to a capacitance variation which is sensed by the electronic read-out interface.

Actually, the stiffness of the backplate is finite and the backplate moves as well. The displacement of the backplate is almost in phase with the displacement of the moving membrane, thus the relative displacement between them is reduced, thus the sensitivity is reduced as well. For this reason, it becomes important to have at least an approximation of the compliance of the backplate in order to avoid unexpected results once the device has been produced.

A common assumption was to approximate the compliance of the backplate with the compliance of a solid plate with the same dimensions but the thickness, which is reduced of the same fraction as the surface occupied by the acoustic holes [1]. A more precise method was presented in [47] using energy method and an equivalent elastic constant is derived:

$$C_{BP}^{EQ} = \frac{E}{a^2} \left( \frac{a(a - r\sqrt{\pi})}{1 - \nu^2} + \frac{r\sqrt{\pi}(a - r\sqrt{\pi})^2}{2a} \right) \quad (3.1)$$

where  $E$  is the Young modulus,  $\nu$  is the Poisson's ratio,  $a$  is the distance between the centres of two acoustic holes and  $r$  is the acoustic hole radius.

Supposing the backplate free from internal stress, using (3.1) the compliance of the perforated backplate is given by [48]:

$$C_{BP} = \frac{32 S_{BP}}{\pi^6 (2\pi C_{BP}^{EQ})} \quad (3.2)$$

where  $S_{BP}$  is the surface of the backplate.

### 3.2.8 Backplate mass

The mass of the backplate can be easily calculated knowing the geometry and the physical properties of the backplate:

$$M_{BP} = \rho_{BP} h_{BP} (S_{BP} - N\pi r^2) \quad (3.3)$$

where  $\rho_{BP}$ ,  $h_{BP}$  and  $S_{BP}$  are respectively the density, the thickness and the surface of the backplate,  $N$  and  $r$  are the number and the radius of the acoustic holes.

### 3.2.9 Flow-by slots

A MEMS microphone measures the instantaneous differential pressure. To sense properly an acoustic wave, the static pressure on both sides of the moving membrane has to be the same. If the membrane is fully clamped, to guarantee the static pressure compensation the backchamber has a small hole connected to the environment.

In Omron and IRST MEMS microphones the membrane moves like a piston and it is only supported at the corners, thus between the substrate and the moving membrane there is a little space which plays the role of equalization pressure hole.

The design of these channels is very important, because they represent an acoustic short circuit. Indeed, if their impedance is too small most of the air flows through them and only a small fraction of that makes the membrane moves, reducing the sensitivity of the device.

The impedance of these channels is represented by a resistance, which considers losses due to viscous resistance of air passing through them, and an inductor, which represents the inertial effect of the air mass in the channels. At low frequency the resistance is dominant, but at high frequency the dominant part is the mass.

To cope with this problem, Omron and IRST have adopted different solutions. Omron's microphone cannot be unveiled, but the structure of IRST MEMS microphone will be analyzed and calculation of resistance and mass of the flow-by slots were done.

The moving membrane of the IRST microphone is suspended over the hole of the backchamber and it is surrounded by narrow slots as shown in the figure 3.11.

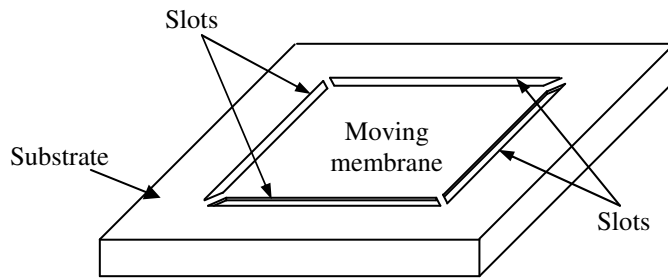


Figure 3.11 Schematic of slits around the moving membrane

The impedance of a narrow slots is given in [27] without any end effect correction. Being a short channel, we can apply the correction made in [23] using the effective viscosity and increasing the height of slots using the same correction for the air gap resistance:

$$\Delta t_{\text{SLOT}}^r = \frac{8}{3\pi} \frac{1 + 2.471D^{-0.659}}{1 + 0.5D^{-0.5} \left( \frac{t_{\text{SLOT}}}{w_{\text{SLOT}}} \right)^{-0.238}}$$

where  $\Delta t_{\text{SLOT}}^r$  is the relative elongation of the height of slots with respect to  $w_{\text{SLOT}}$ ,  $D$  is the inverse Knudsen number and  $w_{\text{SLOT}}$  is the slot width.

The acoustic resistance of one slot with end correction is thus given by [27, 23]

$$R_{\text{SLOT}}^1 = 12\eta_{\text{eff}} \frac{t_{\text{SLOT}} + w_{\text{SLOT}} \Delta t_{\text{SLOT}}}{\sqrt{S_D} w_{\text{SLOT}}^3}$$

where  $\eta_{\text{eff}}$  is the effective density,  $t_{\text{SLOT}}$  is height of the slot,  $S_D$  is the surface of the moving membrane and  $w_{\text{SLOT}}$  is the width of the slot.

Around the moving membrane there are four slots, so it is like having four resistance in parallel. Thus, the resistance is reduced four times:

$$R_{\text{SLOT}} = \frac{R_{\text{SLOT}}^1}{4}$$

As to the acoustical mass of a slot is given by [27]:

$$M_{\text{SLOT}}^1 = \frac{6}{5} \rho \frac{t_{\text{SLOT}}}{w_{\text{SLOT}}}$$

The complete mass of all four slots surrounding the moving membrane will be four times the mass of a single slot:

$$M_{\text{SLOT}} = 4 M_{\text{SLOT}}^1$$

### 3.2.10 Backchamber compliance

The backchamber is an important element because it avoids the sound pressure acts on the back side of the diaphragm. Otherwise the sound pressure would be present on both sides of the moving membrane reducing considerably the effective pressure acting on the moving membrane.

When the membrane moves toward the backchamber, the inside air is compressed adding stiffness to that one of the membrane. Making a too much small backchamber reduces the sensitivity of the microphone because it increases the stiffness of the overall system, but on the other hand a big backchamber is to avoid, in order to keep small the size of the microphone.

Assuming adiabatic compression, the acoustic compliance is given by [27]

$$C_{\text{BC}} = \frac{V_{\text{BC}}}{\rho c^2 S_t^2}$$



where  $V_{BC}$  is the volume of the backchamber,  $\rho$  is the air density,  $c$  the sound velocity and  $S_t$  is the inlet hole of the backchamber.

### 3.2.11 Electrostatic Force

Applying a voltage to the microphone results in an attractive electrostatic force acting on the moving membrane and the backplate. In static condition, the potential energy stored in the microphone capacitor is given by

$$E = \frac{1}{2} C_{\text{MIKE}} V_{\text{BIAS}}^2 \quad (3.4)$$

where  $C_{\text{MIKE}}$  is the capacitance of the microphone between the moving membrane and the backplate and  $V_{\text{BIAS}}$  is the applied bias voltage. Supposing parallel plate configuration, the capacitance of the microphone is given by

$$C_{\text{MIKE}} = \frac{\epsilon_0 S_{\text{BP}}^E}{x_D} \quad (3.5)$$

where  $\epsilon_0$  is the dielectric constant of air,  $S_{\text{BP}}^E$  is the active electrical surface of the backplate and  $x_D$  is the distance between the moving membrane and the backplate.

The acoustic holes in the backplate reduce the conductive surface and hence the capacitance. Nevertheless, the active electrical surface is larger than the simple difference between the surface of the backplate and that one of the acoustic holes, because the fringing fields present at the rim of the holes reduce the effective diameter of the holes. This phenomenon has been reported in literature [57-59] where they reports capacitance value higher than what estimated via simulation and then they calculated an approximation of the fringing field. One simple way is to consider the acoustic hole dimension reduced by a rim around the edge of the same width of the distance between the backplate and the moving membrane [56], increasing the effective electrical area of the backplate. The force is given by the derivative of (3.4) with respect to the distance between the moving membrane and the backplate.

$$F_{EL} = \frac{\partial E}{\partial x_D} = \frac{1}{2} \epsilon_0 S_{BP}^E \frac{V_{BIAS}^2}{x_D^2} \quad (3.6)$$

As shown in (3.6), the electrostatic force is proportional to the bias voltage but inversely proportional to the distance between membrane and backplate, so that when the membrane moves toward the backplate the distance is reduced and the electrostatic force increases and acts like a softening of the membrane stiffness. An equivalent electrostatic spring constant can be estimated as the derivative of the electrostatic force (3.6) with respect to  $x_D$ :

$$k_{EL} = \frac{\partial F_{EL}}{\partial x_D} = -\epsilon_0 S_{BP}^E \frac{V_{BIAS}^2}{x_D^3} \quad (3.7)$$

The (3.7) highlights  $k_{EL}$  is negative, that is it makes the system more compliant. The electrostatic force is counterbalanced by the spring restoring force of the membrane, but if the bias voltage is too high then the electrostatic force overwhelms the restoring force and the moving membrane snaps down to the backplate. Figure 3.12 shows the behaviour of the electrostatic force and the restoring force as a function of the distance between moving membrane and backplate.

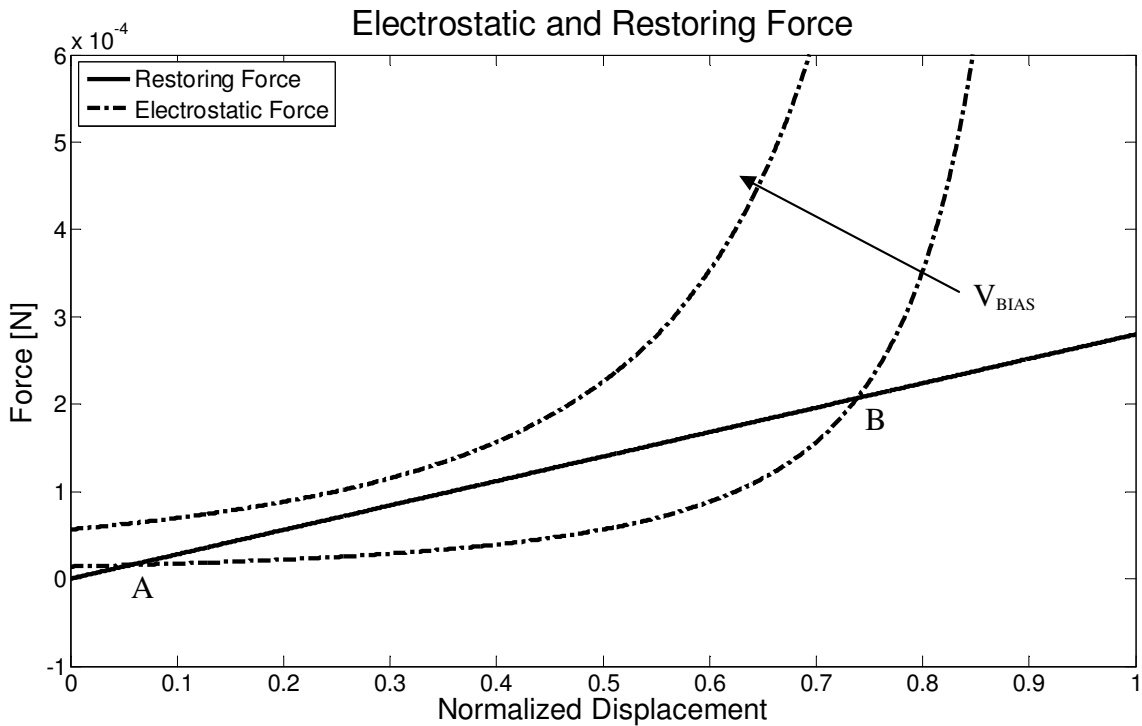


Figure 3.12 Electrostatic (---) and restoring force (—) as function of the normalized displacement of the moving membrane and parameterized with respect to the bias voltage. The direction of the arrow shows the increasing bias voltage.

As shown in figure 3.12, if the bias voltage is low enough there are two equilibrium points (A and B) where the electrostatic force is counterbalanced by the restoring force. The presence of two equilibrium points is due to the nonlinearity of the system, because the electrostatic force is inversely proportional to the square of the distance between the moving membrane and the backplate. Looking at figure 3.12 it is possible to have a qualitative assessment of stability of each point. A is a stable equilibrium point because if the membrane gets closer to the backplate, the displacement increases, the restoring force is greater than the electrostatic force and pulls the membrane back in A. On the other hand, if the membrane moves away from the backplate, the displacement decreases, the electrostatic force is greater than the restoring force and pushes the membrane in A again. It can be concluded that A is a stable equilibrium point.

If the membrane is in B and the membrane moves away from the backplate, the displacement decreases, the restoring force is greater than the electrostatic force and pulls the membrane away from the backplate bringing it in A. On the other hand, if the membrane moves closer to the backplate, the displacement increases, the electrostatic force increases as well but more than the restoring force and the membrane snaps down to the backplate. Thus, B is an unstable equilibrium point.

If the bias voltage is too high, the electrostatic force is always greater than the restoring force, hence the electrostatic force is never counterbalanced, there are not any equilibrium points and the moving membrane collapses directly to the backplate. This phenomenon is called pull-in.

The limit is reached when the electrostatic force is exactly counterbalanced by the restoring force.

$$F_{EL} = \frac{1}{2} \epsilon_0 S_{BP}^E \frac{V_{BIAS}^2}{(x_0 - x_{EQ})^2} = k_D x_{EQ} = F_M \quad (3.8)$$

Where  $k_D$  is the spring constant of the membrane,  $x_0$  is the unbiased air gap and  $x_{EQ}$  is the displacement of the moving membrane at equilibrium.

Looking at figure 3.12, increasing the bias voltage the curve of the electrostatic force moves upwards. The maximum bias voltage level, keeping an stable equilibrium point, is reached when the curve of the electrostatic force is tangent to the line of the restoring force. This means that the spring constant of the moving membrane has the same absolute value of the equivalent electrostatic spring constant:

$$k_D = k_{EL} = \epsilon_0 S_{BP}^E \frac{V_{BIAS}^2}{(x_0 - x_L)^3} \quad (3.9)$$

where  $x_L$  is the displacement of the moving membrane when the bias voltage reaches the maximum value before pull-in occurs.

Substituting  $V_{BIAS}^2$  from (3.9) into (3.8) the displacement at pull-in limit can be calculated:

$$k_D x = \frac{1}{2} \frac{\epsilon_0 S_{BP}^E}{(x_0 - x_L)^2} \frac{k_D (x_0 - x_L)^3}{\epsilon_0 S_{BP}^E} \Rightarrow x_L = \frac{x_0}{3} \quad (3.10)$$

Substituting  $x_L$  given by (3.10) into (3.9) the bias voltage limit before pull-in occurs is

$$V_{PULL-IN} = \sqrt{\frac{8 k_D x_0^3}{27 \epsilon_0 S_{BP}^E}} \quad (3.10)$$

The bias voltage of the microphone has to be always lower than  $V_{PULL-IN}$ , to avoid the moving membrane snap down to the backplate.

### 3.2.12 Package model

Packaging plays a key role in the microphone performance. It is a first shield from dust and mechanical shock, it provides a signal channel and affects the acoustic performance of the microphone, specially at high frequency. Thus, the design of the package is part and parcel of the design of the MEMS microphone.

The package can have different configurations, but the simpler is just a box where the microphone and the relative ASIC are integrated together. This configuration can be considered as a Helmholtz resonator.

A schematic diagram of a conventional Helmholtz resonator is shown in figure 3.13.

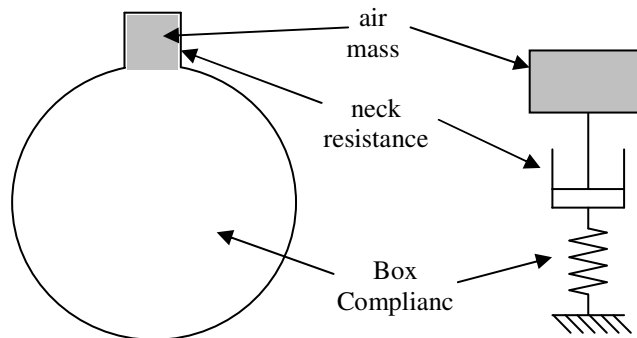


Figure 3.13 Schematic of Helmholtz resonator and its equivalent mechanical circuit

When the acoustic sound pressure forces air into the cavity through the inlet hole of the package, the inside pressure increases. The inside air volume behaves like a spring pushing the air out, but because of the inertial effect of the mass in the inlet hole of the package, the air flowing out is over-compensated and causes a drop pressure in the volume cavity. Such a drop pressure draws the air back into the cavity again, giving rise to an oscillation of the air in the inlet hole of the package. The oscillations are damped by the viscous resistance of the surrounding wall of the inlet hole.

The Helmholtz resonator can be represented by three lumped elements: a mass, representing the air into the inlet hole, a resistance, representing the viscous damping of the wall of the inlet hole and a capacitor, corresponding to the compliance of the volume of the cavity.

The mechanical compliance of the cavity ( $C_{PK}$ ) is calculated in the same way as the backchamber compliance:

$$C_{PK} = \frac{V_{PK}}{\rho c^2}$$

where  $V_{PK}$  is the internal volume of the package excluding the volume occupied by the microphone and the ASIC,  $\rho$  is the air density and  $c$  is the sound velocity.

The mass of a Helmholtz resonator is the mass of air enclosed by the neck of the resonator. However, when the mass moves, it goes outside the height of the thickness of the inlet hole, extending its own effective length. To include this effect, an end correction is applied to the thickness of the package, and its effective length  $t_{PK}^e$  is given by [30]

$$t_{PK}^e = t_{PK} + \frac{0.85d_{PK}}{1 + 0.625 \frac{d_{PK}}{D_{PK}}}$$

where  $t_{PK}$  is the thickness of the package,  $d_{PK}$  is the diameter of the inlet hole and  $D_{PK} = 2\sqrt{\frac{V_{PK}}{\pi h_{PK}}}$

is the equivalent diameter of the volume cavity of the package.

Thus, the mass of air ( $M_{PK}$ ) in the inlet hole of the package with end effect correction is

$$M_{PK} = \rho t_{PK}^e \pi \frac{d_{PK}^2}{4}$$

where  $\rho$  is the air density.

The acoustic damping, due to the viscous resistance in the inlet hole of the package can be approximated as laminar flow in small duct [27]:

$$R_{PK} = 32 \frac{\rho t_{PK}}{\pi d_{PK}^2}$$

### 3.2.13 Schematic

Using the results obtained in the previous sections, an equivalent circuit has been implemented in Simulink to model the MEMS microphone. Figure 3.14 shows a small signal equivalent circuit.

The sound pressure acting on the microphone has been implemented as a controlled voltage source. The overall compliance of the system, that is the compliance of the moving membrane plus the electrostatic contribution, and the air gap impedance are nonlinear because they are function of the moving membrane displacement. A nonlinear element can be implemented as a controlled voltage or current generator. Consider the inductive component of the air gap impedance. The relationship between the current ( $i$ ) and the voltage ( $v$ ) across an inductor ( $L$ ) is expressed by the following equation:

$$i = \int \frac{v}{L} dt \quad (3.11)$$

The relationship between current and voltage across an inductor can be expressed by a differential equation as well, but from the numerical point of view the integral form is better, so that a nonlinear inductor can be represented by a controlled current generator driven by the second member of (3.11). The value  $L$  of the inductor is calculated using a function with the displacement as input.

On the same way, the compliance of the system, which is represented by a capacitor and the air gap resistance are implemented using a controlled voltage generator.

In the electro-mechanic analogy the current represents the velocity so that the position of the moving membrane can be calculated as the integral of the current flowing through the membrane branch. The relative displacement of the moving membrane with respect to the backplate, which characterize the capacitance value of the microphone, is given by the integral of the difference between the current of the moving membrane branch and that one of the backplate branch.

To be noted the resistance in parallel to the inductor representing the air gap mass. The air gap mass has been represented by a nonlinear element with a current generator, and it cannot be connected in series with the inductive component of the flow-by and acoustic holes impedance.

### 3.3. Simulation and experimental results

To tune properly the built model the simulations and the experimental results had been compared. The experimental setup is schematically represented in figure 3.15

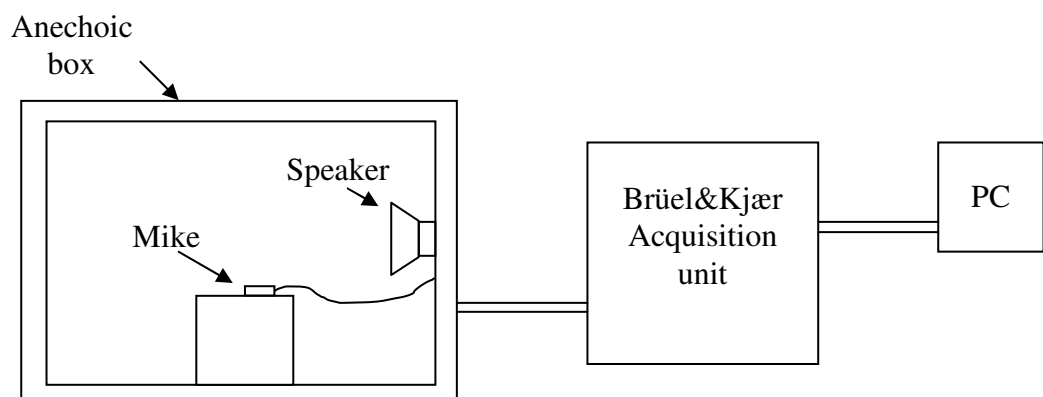


Figure 3.15 Experimental setup to characterize the microphone in Omron

The microphone can be excited in two different ways: in free field or in pressure. Indeed, we have also two different definition of sensitivity: pressure sensitivity, defined as the signal amplitude per unit of pressure the microphone produces when its membrane is hit by a uniform pressure. Free field sensitivity, defined as the signal amplitude per unit of pressure produced by a microphone hit by a travelling wave which is isolated from the boundaries [55]. The latter method is preferable especially for high frequency characterization, even if it has some drawback, such as to be held in anechoic room to isolate the microphone from the external environment and the diffraction phenomenon. To reduce this latter issue, the anechoic box and the internal support are covered by absorbing foam and every hardware inside the box is kept away from, or at least behind the microphone.

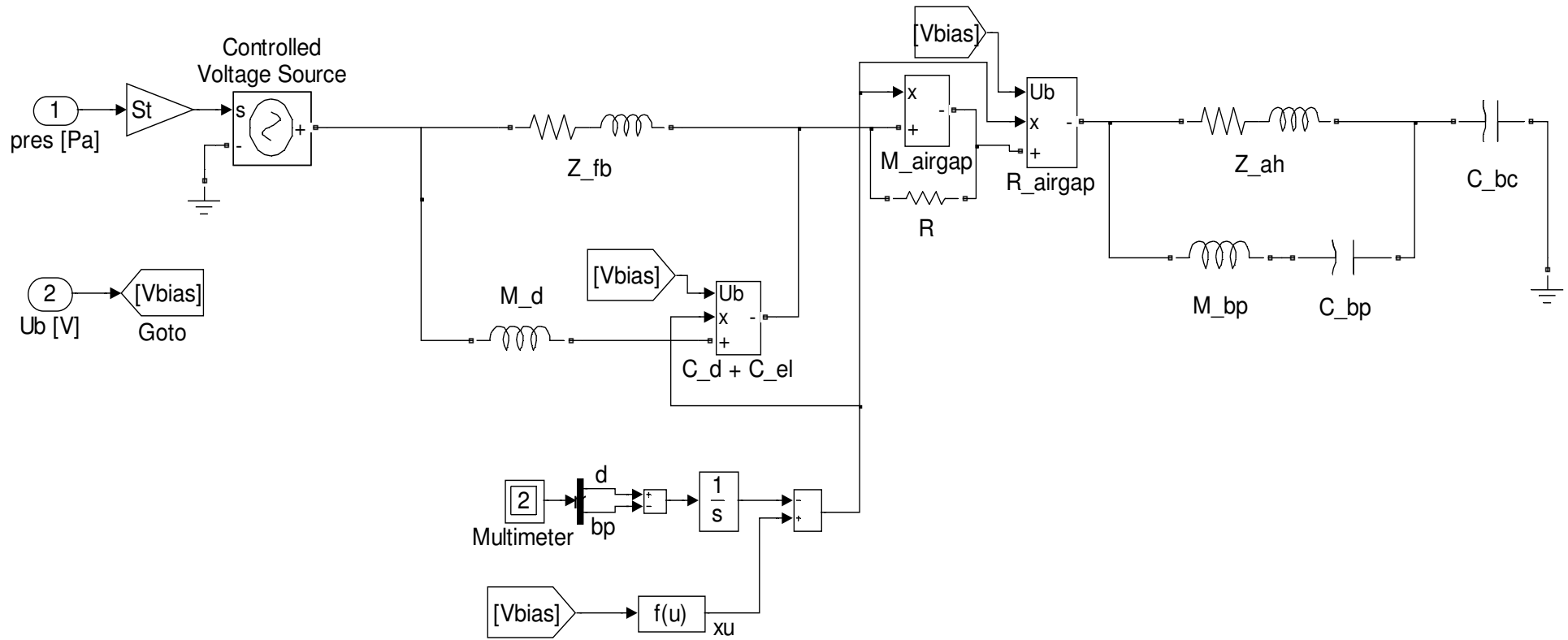


Figure 3.14 Small signal equivalent circuit



Before starting, the setup has to be calibrated. There are two main methods: the simultaneous and the substitution procedures. In the former case, the reference microphone and the microphone under test are checked at the same time. This procedure requires a sound field spatially uniform. The substitution method solves this problem, because the reference microphone and the microphone under test are checked sequentially: first the reference microphone to calibrate the measurement setup and then the microphone under test. The drawback of this system is that the location of the microphones has to be the same, otherwise the sound incident on the microphones will be different, and the sound source has to be stable for a little, because the measure is no longer performed simultaneously.

The simultaneous method has been chosen because it is simpler to realize and the sound source is almost uniform, at least locally around the microphones.

To characterize the microphone under test the first step is to calibrate the sound source emitting 1Pa@1kHz with respect to the output signal of the reference microphone. Afterwards, the system acquires the frequency response of the microphone under test removing the offset due to the frequency response of the speaker. All these operations are automatic and done by the Brüel&Kjær Acquisition unit. All the data are then transferred to the PC for post-processing.

The data acquired had been compared with the simulation results and the model has been tuned accordingly. Figure 3.16 shows the achieved results.

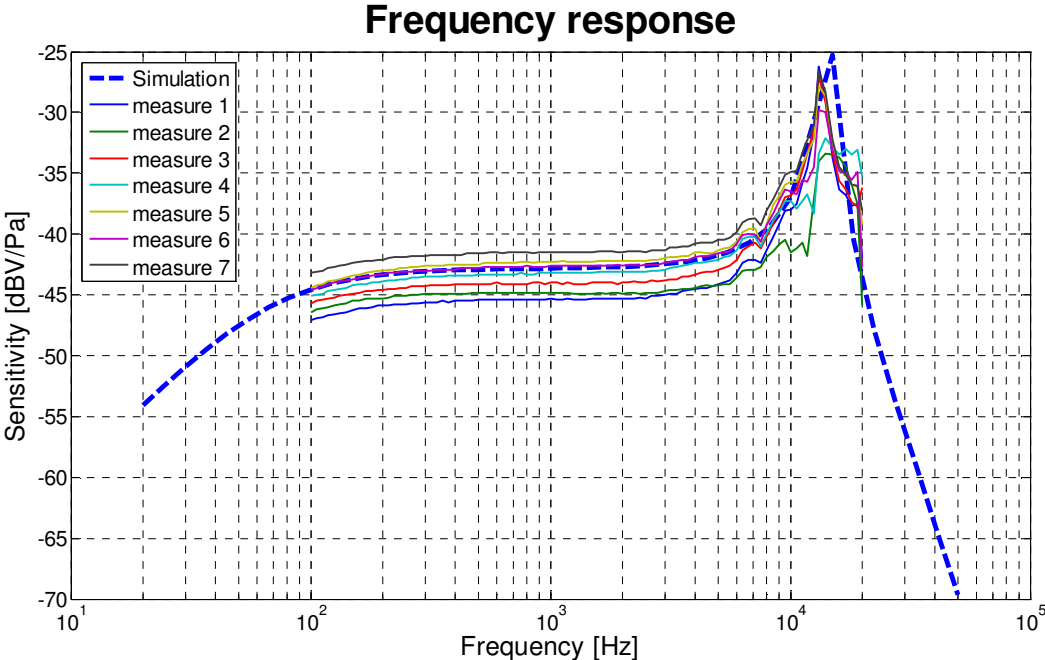


Figure 3.16 Comparison between the acquired data (continuous line) and the simulation results (dashed line) of Omron’s MEMS microphone

From the obtained frequency response it can be recognized the roll-off at low frequency, due to the flow-by impedance and a peak at high frequency, due to the Helmholtz resonance.

The IRST MEMS microphone has been modelled and a first run of microphones has been tested. Figure 3.17 shows the comparison between the simulation and the experimental results.

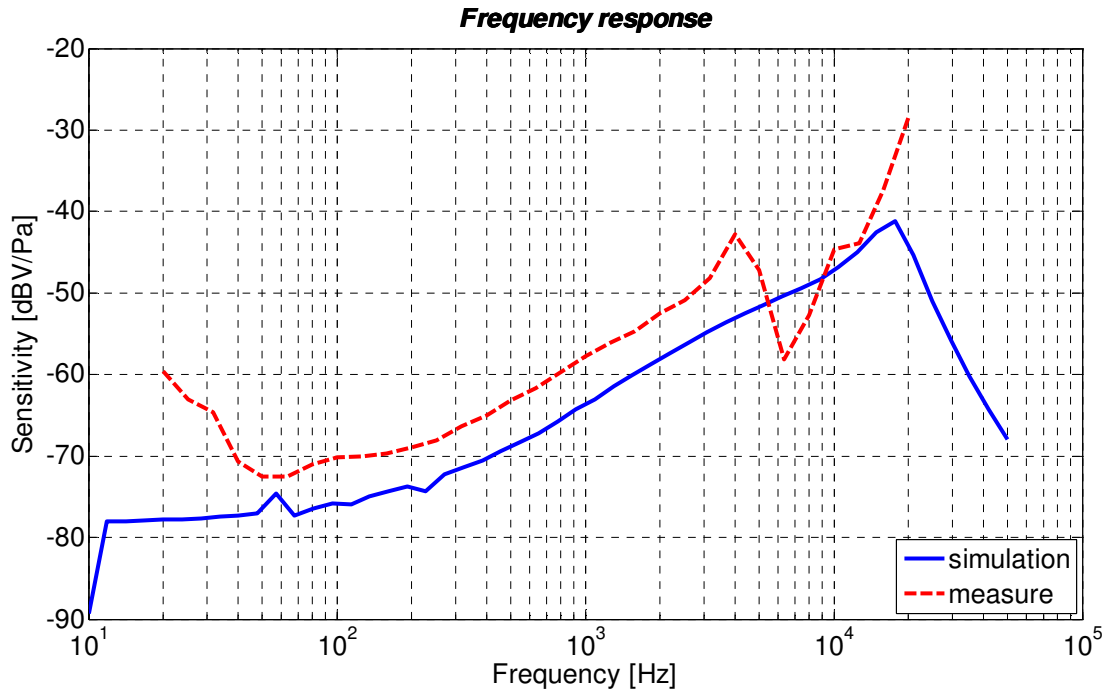


Figure 3.17 Comparison between simulation and experimental results for FBK MEMS microphone

To be noted the model does not include the package model, because its geometry is not known in detail, but can be only roughly estimated.

Figure 3.17 shows a 5dB difference between the simulated and the measured sensitivity. This is due most likely to the value of the parasitic capacitance between the moving membrane and the substrate. Indeed, the sensitivity is given by

$$V_{\text{OUT}} = V_{\text{BIAS}} \frac{\Delta C}{C_T}$$

where  $C_T$  is sum of the capacitance of the microphone and the parasitic capacitance ( $C_p$ ) between the moving membrane and ground. This last value has been measured but it can vary from sample to sample, so that it is possible the  $C_p$  value is slightly lower than the value set in the Matlab simulation file.

Another difference is the peak around 4kHz. At first glance, it could be due to the Helmholtz resonance of the package, but a rough estimation shows us this is not possible. Indeed, the package can be assumed to have a volume of about 30mm<sup>3</sup>, the inlet hole radius of 0.9mm and the thickness of the cover of the package, that is the neck length of a classic Helmholtz resonator, about 1mm, the frequency of resonance of the resonator is given by [30]

$$f_{\text{HELM}} = \frac{c}{2\pi} \sqrt{\frac{S}{VL}} \cong 16 \text{ kHz}$$

which is closer to the high frequency peak, instead of the 4 kHz. However, the produced microphones demonstrate a bending on the membrane at rest, increasing the flow-by slots and changing the designed structure, modifying even the mechanical characteristics of the microphone.

The origin of this peak at 4 kHz is not clear yet, and further investigation are necessary.

The rising trend of the frequency response from the low frequency is clear, and depends on the too low value of the flow-by impedance. Besides, the bending of the moving membrane makes the situation worse, because it increases the dimension of the flow-by slots reducing their impedance furthermore.

### 3.3.1 Noise

Improvements in silicon micromachining technologies allow to build very small and sensitive pressure sensors. In such sensible devices, however, noise becomes a big issue, limiting the minimum detectable sound pressure [32]. There are many sources of noise, both electrical and mechanical, but the main sources are the read-out electronics interface and the Brownian motion from the air surrounding the moving membrane.

As to the former, using classical read-out interfaces, the electrical noise is too high and limits the minimum detectable sound [31]. New interface configurations have been developed [35] to keep down the noise level, so that the performance of the device is only partially limited by the electronics and the thermal noise becomes relevant.

The mechanical noise, on the other hand, depends on the layout of the microphone and it can be often reduced to the detriment of the sensitivity of the device. Thus, a trade-off has to be found in the design process.

The main mechanical noise is due to the Brownian motion caused by the thermal agitation of the molecules of air surrounding the moving membrane. The molecules randomly hit the membrane

causing a local pressure variation. These collisions make the membrane move giving rise to a noise floor which limits the minimum detectable sound pressure. This motion is damped by the dissipating elements present in the device, that is the acoustic resistances.

Supposing the system in thermal equilibrium, the mechanical-thermal noise can be considered as a force generator acting on each dissipative element of the device [33].

Using the Nyquist's relation [50] the spectral density of the equivalent pressure related to each dissipative element is given by [33]:

$$P_B = 4 k_B T R_A \quad (3.12)$$

where  $P_B$  is the power spectral density in  $N^2/Hz$ ,  $k_B$  is the Boltzmann's constant,  $T$  is the absolute temperature and  $R_A$  is the acoustic resistance of the considered dissipative element.

The main source of thermal noise in the microphone is the air gap. Indeed, making small air gap increases the capacitance value and reduces the microphone size as well, but it increases the resistance due to the squeezing of the air film between the moving membrane and the backplate, thus the equivalent noise pressure.

It is possible to keep a small air gap increasing the dimension of the acoustic holes and/or increasing the density of the acoustic holes in the backplate. It is possible to modify the behaviour of the system applying an electromechanical feedback, changing the equivalent damping coefficient to a more suitable value, but in this case the noise level will not decrease, because the noise depends only on the real damping coefficient and not on the equivalent achieved after the feedback control.

The mechanical noise due to the Brownian motion is dependent on temperature and pressure, but is independent of frequency [49]. Like Johnson noise for electrical resistance, the mechanical noise due to the Brownian motion can be represented by a generator of white noise with spectra density expressed by (3.12).

Another more subtle source of mechanical noise is the  $1/f$  noise. In [50] a  $1/f$  component was noticed in the mechanical motion of a vibro-acoustic sensor and [34] confirmed experimentally this presence characterizing the noise properties of some Bruel&Kjaer microphone.

The source of  $1/f$  noise is still not clear. It has been observed in [51] characterizing a thermionic tube to verify the Schottky's formula for the shot noise spectral density, but at low frequency Johnson observed a flicker noise. A first explanation of the outcome was given by Schottky in [52], where the charge trapped on the cathode surface of the tube were released according to an exponential relaxation law which has a  $1/f$  spectral density.

Actually, the flicker noise has a variable spectral density and behaves like  $1/f^\alpha$ , where  $\alpha$  is in range 0.5-1.5 and it has been observed in many physical phenomena such as resistors [53], tides, heart beat rhythms and in many other fields. Nevertheless it is far from being well understood and from finding an univocal law to explain each phenomenon. For the time being for each case an ad hoc model has been developed to explain properly the source of the  $1/f$  noise.

In the specific case of MEMS microphone, a model to explain the presence of  $1/f$  noise component has not been developed yet, but in [34] the experimental results demonstrate with a high level of confidence the presence of the  $1/f$  noise and a strong correlation with the acoustic resistance of the air gap microphone. From the correlation between the acoustic resistance and the  $1/f$  power spectral density a relationship has been achieved:

$$\log_{10}(P_{1/f}) = -22.9847 + 1.76 \log_{10}(R_{\text{AIRGAP}}^A) \quad (3.13)$$

where  $P_{1/f}$  is the power spectral density of the  $1/f$  noise in  $\text{Pa}^2$  and  $R_{\text{AIRGAP}}^A$  is the acoustic air gap resistance. Multiplying the (3.13) by the square of the moving membrane surface the equivalent force of the  $1/f$  noise acting on the moving membrane is obtained.

Once calculated the total power spectral density due to the  $1/f$  component and the Brownian motion it can be design a signal with such a power distribution.

There are several ways to generate white noise representing the Brownian motion and the pink noise. A computationally efficient method to use is the inverse discrete Fourier transform (IDFT) [54].

The idea is to generate a signal in frequency domain with the desired power density behaviour and than apply the IDFT to get a signal  $x(t)$  in the time domain, which can be expressed as

$$x(t) = \sum_{k=1}^n A_F(f_k) \cos(2\pi f_k t + \varphi_k) + i \sin(2\pi f_k t + \varphi_k) \quad (3.14)$$

The amplitude of the signal in the frequency domain is obtained by the sum of the square of the power spectral density of the Brownian motion and the  $1/f$  noise, scaled by the number of the samples:

$$A_F(f_k) = n \sqrt{2 P_{\text{NOISE}}(f_k)} \quad (3.15)$$

where  $A_F(f_k)$  is the amplitude of the signal in frequency domain,  $n$  is the number of samples,  $P_{\text{NOISE}} = P_B + P_{1/f}$  is the total PSD of the noise.

The key issue to generate a different sinusoidal signal for each considered frequency is to apply a random phase  $\phi_k$ . Each frequency is chosen from a uniform distribution in the angle range  $0 - 2\pi$ . It is then possible to apply the IDFT obtaining a signal in the time domain with the desired spectrum behaviour.

A script in Matlab<sup>®</sup> has been written and the following figure plot the power spectrum density generated.

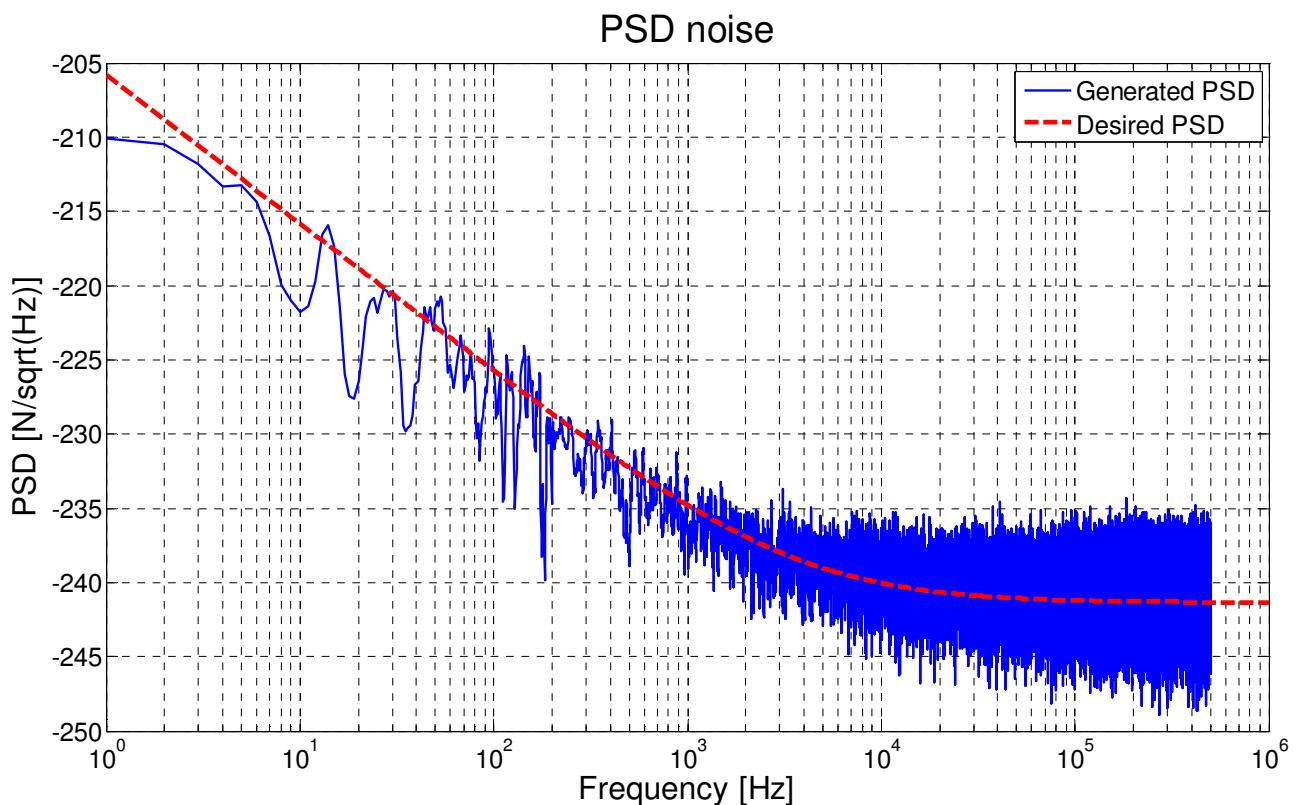


Figure 3.18 Comparison between the desired PSD noise (and the PSD generated using the Matlab<sup>®</sup> script

The dashed line is the desired profile and the continuous one is the generated power spectral density.

### 3.3.2 Experimental setup and results

The characterization of the microphone noise was held in Omron's facilities in Japan, using Omron's MEMS microphone. For this reason the description of the measurement setup and other procedures used to characterize the microphones can not get too much in the detail.

The measures were held inside an anechoic box. Inside there is a support where the microphone is laid on in order to reduce the environment vibration acting on the microphone.

The activity of analysis and acquisition of the microphone output signal is controlled by a Brüel&Kjær Pulse Analyzer Platform. It is composed by a data acquisition unit, which acquires the output signal of the microphone, and a Brüel&Kjær Pulse Electroacoustic software to analyze the acquired data.

Even if the anechoic box is isolated both acoustically and electromagnetically the inlet acoustic hole of the microphone is closed and the device is placed inside a grounded metallic box in order to ensure a better isolation from the external environment noise.

To isolate the noise due to the microphone from that one coming from the electronic read-out and the measurement setup there are two main ways. A method is to measure the noise of the microphone when it is polarized and when it is not. Indeed, when the microphone is not polarized the coupling factor which convert the acoustical signal into electrical one is zero [34], thus the total power measured is just that of the electronic read-out and the measurement setup. The pros of this method is that the measurement setup does not change switching from polarization and not. On the other hand, when the microphone is polarized the air gap is reduced and its acoustical resistance and the capacitance value of the microphone increase. In this case, when the PSD of the unpolarized microphone is subtracted by that one of the polarized device to obtain the PSD of the noise of the moving membrane, a term not depending on the moving membrane will appear, due to the difference of the capacitance value of the microphone in the two different states [34]. Anyway, knowing the difference of the capacitance value, it is possible to compensate such an extra component.

One way to solve this problem is to replace the microphone with a condenser having the same capacitance as the polarized microphone, and this is the second method. In this way, the resulting PSD obtained by the difference of the two noise PSD with the microphone and the capacitor microphone will contain only the noise due to the moving membrane. On the other hand, however, changing the microphone entails that the setup has to be altered and the environment conditions could change.

The second method was used to characterize the microphone noise, because it was not possible to switch off the polarization of the microphone keeping on the read-out electronics.

Figures 3.19(a) and 3.19(b) show the acquired PSD of the noise respectively from the sample with the microphone and that one with the capacitor.

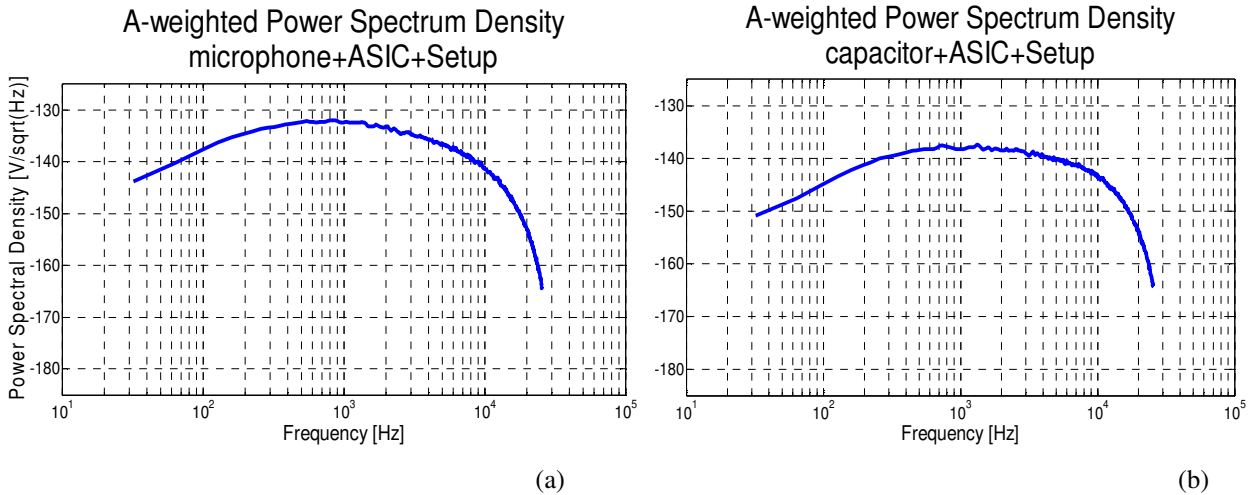


Figure 3.19 (a) noise PSD microphone+read-out (b) noise PSD capacitor+read-out.

The PSD reported in figures 3.19 are A-weighted. Indeed, the ears have a sensitivity which varies with the frequency. This means a noise at one frequency can be heard louder than the same noise at another frequency. To consider this phenomenon the PSD is multiplied by a factor. This operation is called A-weighting. Figure 3.20 shows the A-weighting curve. Even if A-weighting reproduces the real frequency response of human ear, to have a correct estimation of the noise, especially concerning the 1/f component, it is necessary to remove the A-weighting.

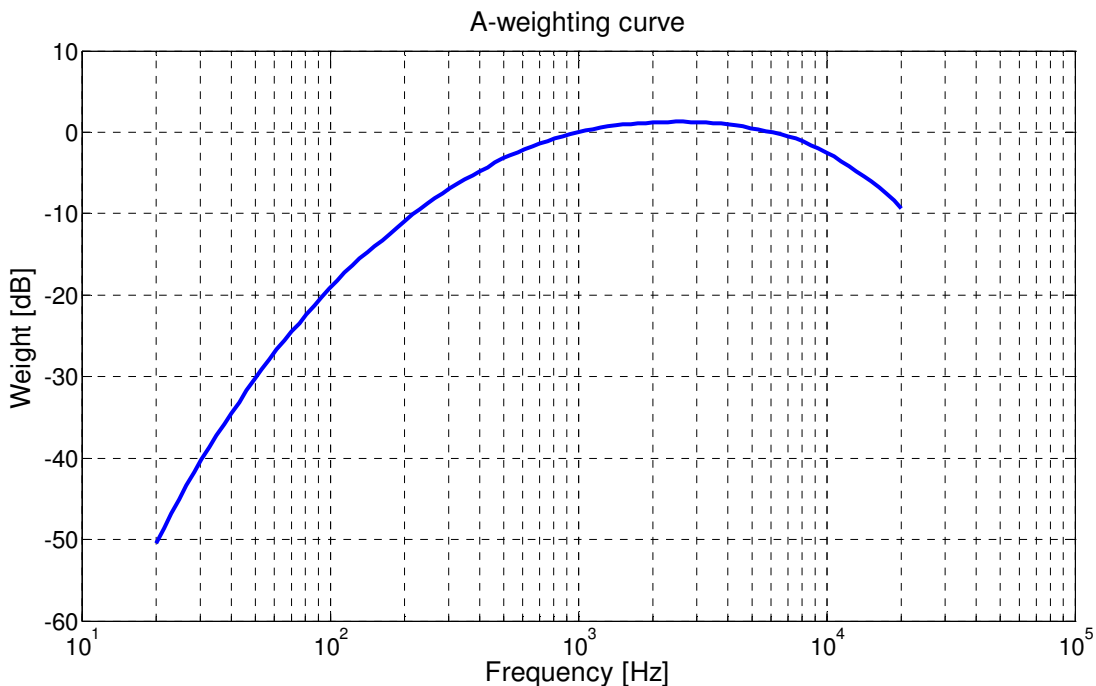


Figure 3.20 A-weighting curve



The PSD of the microphone alone is obtained subtracting the PSD of the read-out electronics with the capacitor from the PSD of the read-out electronic with microphone; then the A-weighting is removed obtaining the PSD shown in the following figure 3.21.

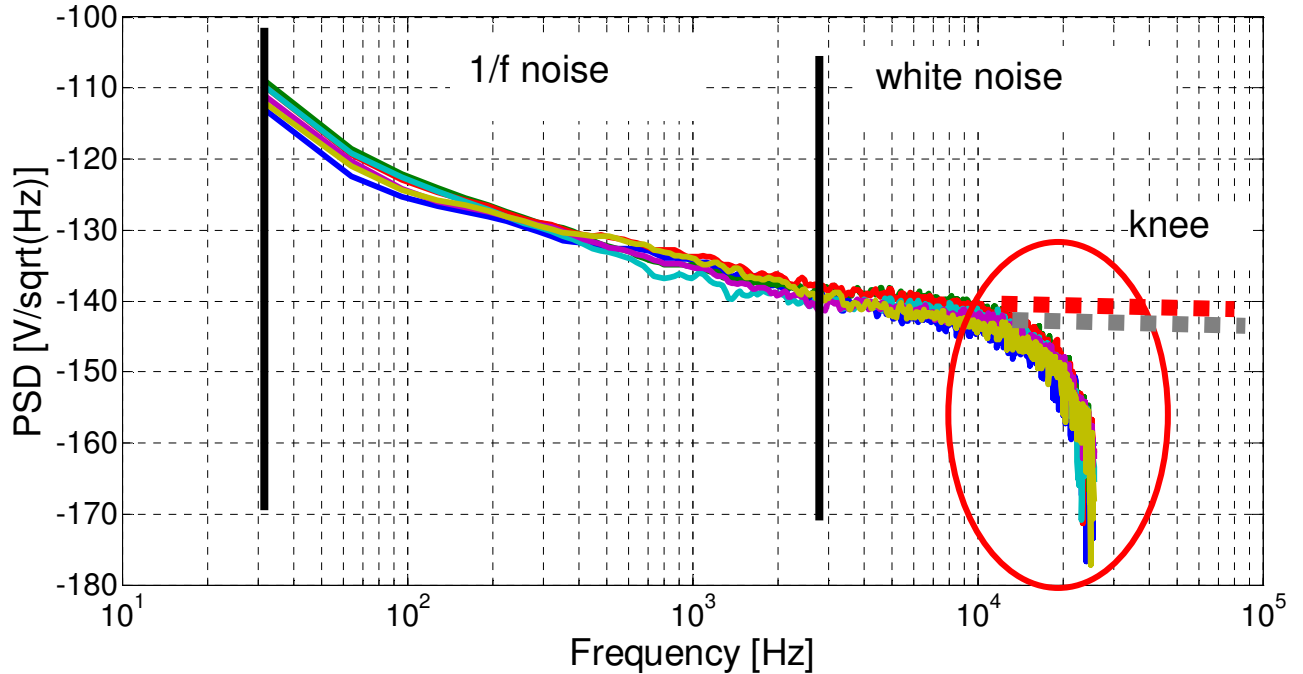


Figure 3.21 PSD of microphone noise of five Omron MEMS microphone.

As stated in the previous section, in figure 3.21 it is possible to identify two regions: from low frequency to about 3kHz, where the noise has a 1/f behaviour; from 3kHz on, where the Brownian noise dominates and the PSD noise tends to be flat. Around 10kHz, however, the PSD sinks, due to the mechanical cut-off frequency of the microphone.

The model used to simulate the noise behaviour of the microphone is different from that one used for the microphone excited from an acoustic pressure, because in this case the source is inside the microphone and acts directly on the moving membrane. The schematic of the noise model is shown in figure 3.22.

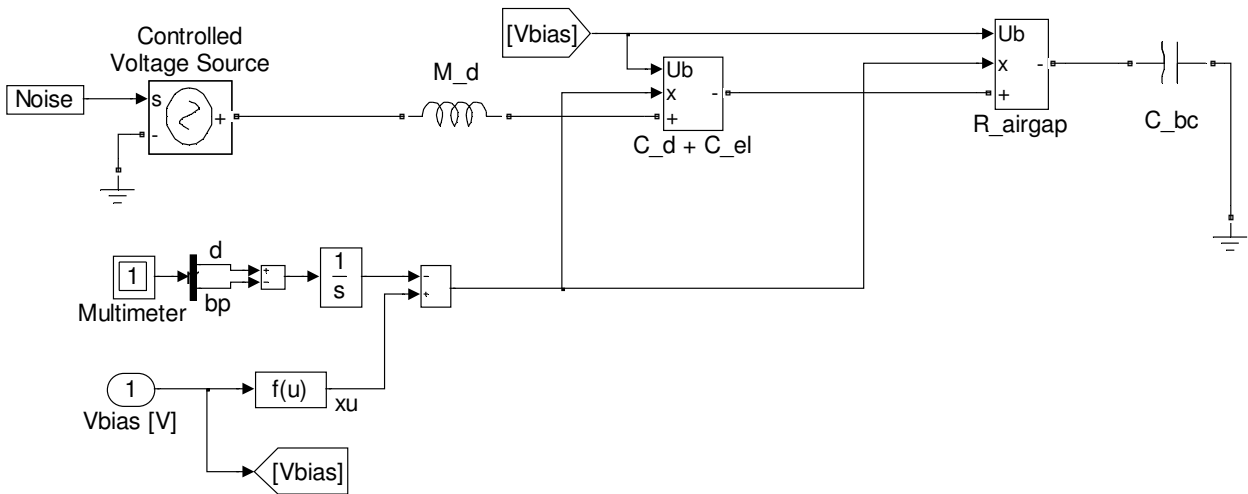


Figure 3.22 Simulink noise model

The noise acts directly on the moving membrane and its displacement is only damped by the resistance of the air gap. The compliance of the system is characterized only by the moving membrane and the backchamber. The backplate displacement can be neglected, because the exciting force is small and its displacement with respect to the moving membrane is negligible. The equivalent circuit is then supplied by the noise generator designed in the previous section. The simulation and the experimental results are compared in figure 3.23.

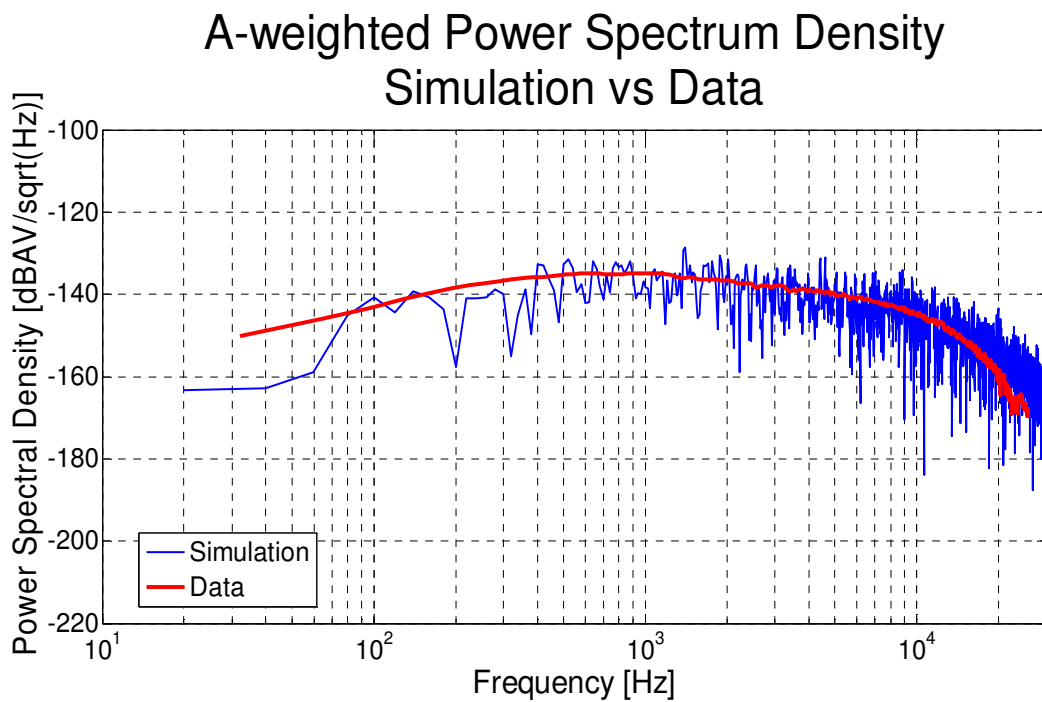


Figure 3.23 Comparison between simulation and experimental results noise PSD

### 3.4. Model Simplification

The model obtained in section 3.2 is almost complete and considers almost all component of a microphone, with their nonlinearities. However, to analyze the microphone coupled to the read-out electronic and its stability in open and closed loop becomes very complicated.

From the simplest point of view, the microphone can be approximated by a second order system mass-spring-dashpot.

With this idea the model can be simplified keeping only the main elements. Using the analogy of the second order system, the mass to move will be the moving membrane mass, whereas mass of the airgap, backplate and flow-by slots can be neglected. The main damping element of the microphone is the air gap resistance, which characterizes the frequency response and the noise of the microphone. The acoustic holes resistance could be considered as well, but their value is usually negligible with respect to the air gap resistance. The spring is the compliance of the moving membrane, considering both the mechanical and the equivalent electrostatic spring constant and the contribution of the backchamber as well. Both air gap resistance and spring coefficient of the microphone depend on the displacement of the moving membrane, so they are nonlinear. The system can be linearized considering their respective values at steady state and making them independent from the moving membrane position.

Figure 3.24 shows the comparison between the frequency response of the complete and simplified model of Omron's microphone.

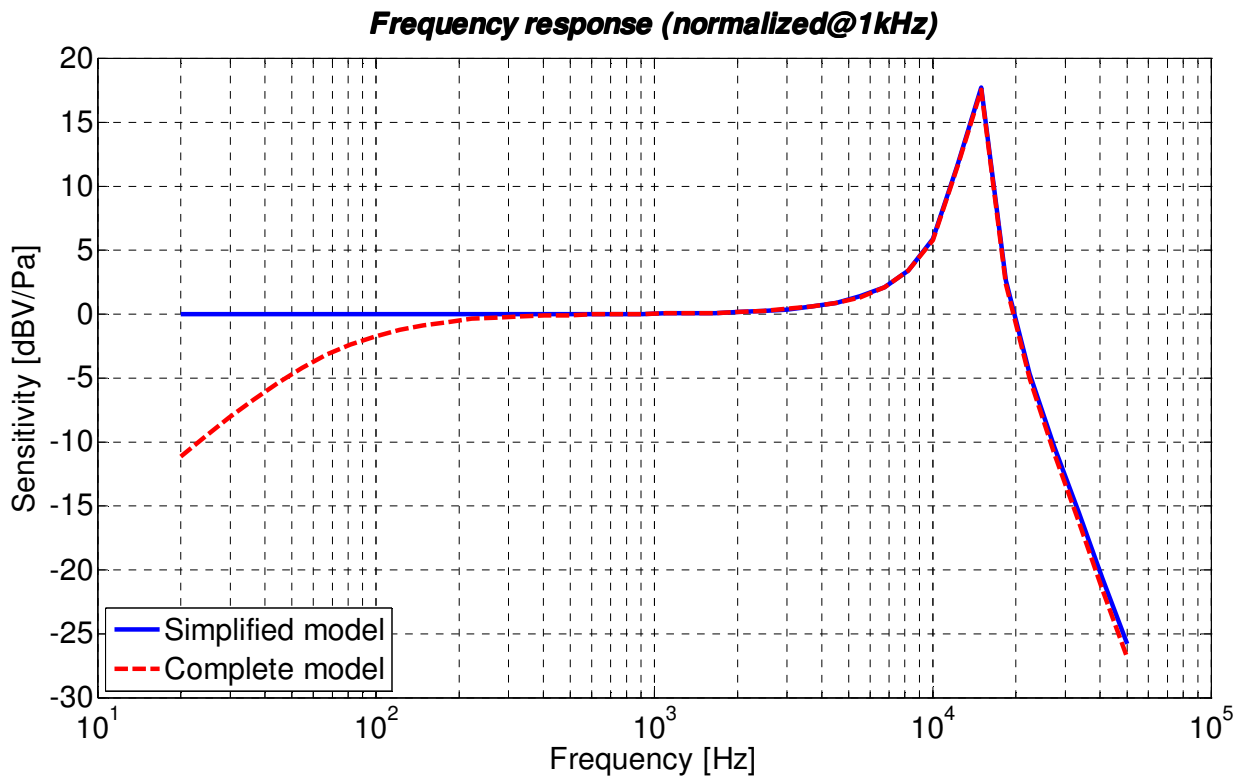


Figure 3.24 Comparison between the complete (dashed) and simplified model (continuous).

As expected, approximating the microphone as a second order system, the roll-off at low frequency due to the flow-by impedance disappears. Except for that, the frequency response of the simplified model has the same behaviour of the complete model and can be used to represent the MEMS microphone in a simpler way.

# Chapter 4

## 4. Microphone Design and Testing

This chapter presents a brief description of the design choices and the main issues arose during the manufacturing process and the relative adopted solutions. From experimental results the main mechanical and electrical characteristics have been estimated and compared with the expected values highlighting some problem in the production process again. Finally the chapter concludes with an acoustical characterization to verify the sensitivity of the microphone.

### 4.1. Microphone Design

The microphone design and the manufacturing process have been developed in IRST, Trento.

The goal was to produce a piston-like capacitive MEMS microphone with high sensitivity, low mechanical noise, flat frequency response inside the audio frequency range, embedded passive elements for the electronic read-out and compact size. The first run was produced to study the feasibility of the process to produce a piston-like membrane and a perforated gold backplate, as well as to evaluate different microphone configurations.

The main advantage in using a piston-like membrane is that almost all the surface of the membrane is used as transducer. Indeed, if the membrane is fully clamped, when a force acts on it, the moving electrode bends and only its central part contributes to the transduction process because its rim is constrained and cannot move and the external regions do not move significantly. Instead, in a piston-like membrane the electrode moves almost parallel to the fixed electrode and all the moving membrane takes part in the transduction (figure 4.1).

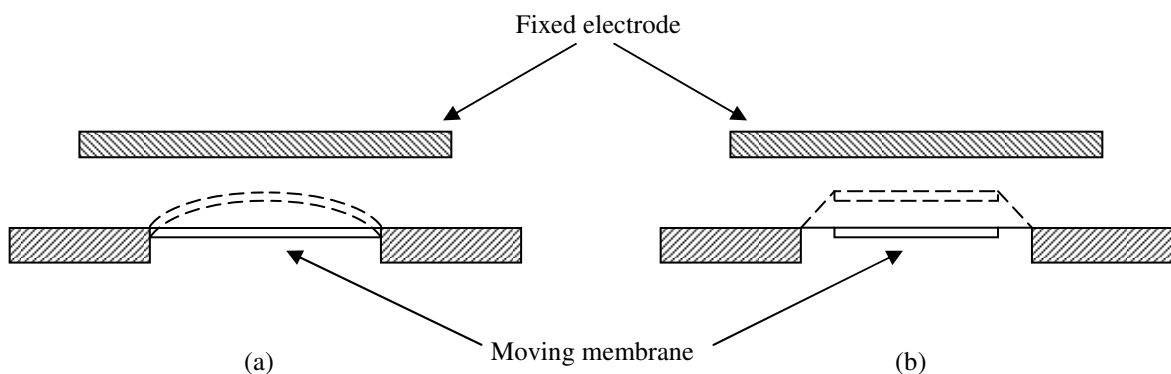


Figure 4.1 Schematic representation and comparison between the displacement of (a) a fully clamped membrane and (b) a piston-like membrane

To obtain a moving electrode with a piston-like displacement, a stiffened membrane suspended by four beams has been designed and produced. To ensure a piston-like behaviour, the moving membrane has to present a rigidity an order higher than the rigidity of the suspending beams, so that when a force acts on it only the flexural beams bends and the moving electrode remains almost parallel to the fixed electrode.

The stiffness of the moving membrane can be increased making the moving membrane thicker. However, the mass increases as well changing the resonance frequency of the microphone. Another way is to apply an array of ribs on the whole surface of the moving membrane but the supporting beams. The applied ribs counteract the bending moment of the moving membrane when a force acts on it. The achieved rigidity with ribs is lower than that one reached increasing the thickness of the same height of the ribs, but on the other hand the mass does not increase too much, thus the system resonant frequency does not change significantly. These ridges are applied on the whole surface but the supporting beam, which have to guarantee a desired compliance.

Ridges are present at the surrounding frame as well to anchor it to the substrate. Figure 4.2 shows a rear view of the moving membrane. Over the membrane and the surrounding frame we can see a black grid, which is the array of ridges used respectively to stiffen the membrane and fasten the frame to the substrate. At the corners of the membrane there are flexural beams, which support the moving electrode and they are the only part of the membrane not covered by the ridges because they have to be flexible and guarantee the desired compliance.

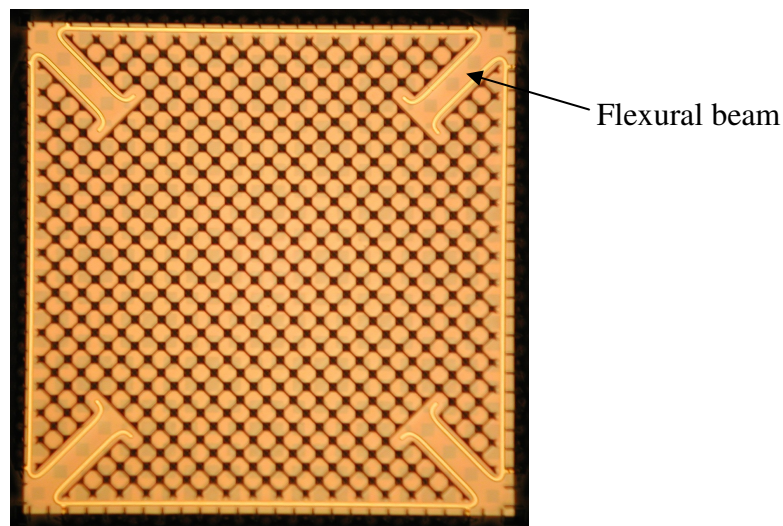


Figure 4.2 Rear view of the manufactured moving membrane

The first run contained different configurations in order to investigate the influence of different geometrical parameters. The main parameters considered are the air gap, the membrane size and the dimension of the supporting beams. The air gap considered are  $3\mu\text{m}$  and  $6\mu\text{m}$ , and the length of the moving membrane side is 1, 1.8 and  $2.2\mu\text{m}$ . Different configurations have been taken into account for the acoustic holes of the backplate as well, in order to investigate the damping effect of the squeezing of the air film in the air gap, but keeping constant the ratio between the surface of the backplate and the surface of acoustic holes. Furthermore two different layouts have been designed for the supporting beams: radial, as shown in figure 4.2, and tangential.

The fabrication process ran into several problems, partially solved during the manufacturing process.

The main problems are here briefly summarized but other issues and their extensive treatment can be found in [45,60,61]:

- The fabrication of trenches into the silicon substrate to produce the ridges were not well defined,
- Removing of the mould for the gold backplate turned out to be very difficult,
- Problems on etching the cavities behind the moving membrane due to a lower anisotropy factor than expected.
- Issues concerning the stability of the moving membrane because of the high internal compression stress of the silicon dioxide remained around the ridges which causes a bending of the membrane as well [61].

Despite the problems arose during the fabrication process, the first run showed the feasibility of the designed structure and gave important information about adjustment and improvement of the manufacturing process. The main corrections are about the mould for the gold plate, changing the material used to make it, and the tuning of the etching process to get the expected anisotropy factor for the bulk silicon etching.

To solve the problem of the stability of the membrane, a layer of silicon nitride has been added on the top of the moving membrane to balance the compressive stress of the silicon dioxide. This solution has also another advantage. The maximum bias voltage is limited by the pull-in voltage, as shown in section 3.2.11, but by the breakdown voltage of air as well. Indeed, the dry air breakdown voltage is  $33\text{kV/cm}$ . Actually this is an upper limit, because usually the microphone will work in humid environment, lowering that value. Considering the two configurations of  $3\mu\text{m}$  and  $6\mu\text{m}$  they have respectively  $9.9\text{V}$  and  $19.8\text{V}$  as upper limit. The silicon nitride layer, even if just  $50\text{nm}$  thick, increases the breakdown voltage to  $50\text{V}$ , so that the limit on the bias voltage is only due to the pull-in instability. On the other hand, adding the silicon nitride layer is equivalent

to add an capacitor in series to the air gap capacitance, lowering its value. However, the added layer is very thin and the change of the capacitance for the  $3\mu\text{m}$  air gap condenser can be estimated in 0.2% [60] therefore negligible.

This first run highlights also some issues about the different configurations of the microphones. It turned out that the radial spring configuration is more reproducible then the tangential, and that small membrane and air gap microphones where the most reliable [60].

In the second run the main manufacturing problems were solved and samples were available for experimental tests. The microphones had been characterized measuring and estimating mechanical and electrical parameters, as reported in the following section.

## 4.2. Microphone Testing

### 4.2.1 CV characteristic

The CV characteristic is one of the main way to characterize the principal features of a microphone. It allows to see in a glance if a sample can work or not, giving important information about the critical aspects of the design and fabrication process.

The CV characteristic gives the capacitance value of the microphone as a function of the bias voltage. Modelling the capacitance of the microphone as a parallel plate capacitor and fitting its data, it is possible to estimate the air gap height when the microphone is not polarized, the spring constant of the supporting beam of the moving membrane and the pull-in voltage as well.

The measurement setup is composed by a Probestation Karl Suss PM8 which allows to perform measures directly at wafer level, avoiding the main parasitic components due to a package, and an impedance analyzer HP 4192A connected to a PC which collects the data. The impedance analyzer is set to measure impedance having as equivalent circuit a parallel between a resistor and a capacitance. The capacitance represents the searched value, whereas the resistance is a parasitic parameter of device. The CV characteristic is obtained applying a static bias voltage with an oscillating component between the backplate and the moving membrane. The oscillating component has to have a frequency far beyond the expected resonant frequency of the microphone, to avoid to affect the capacitance measure. Indeed, if the frequency falls in band, the moving membrane will have a constant displacement, due to the fixed component and moves according to the oscillating component as well, making unreliable the measurement of the capacitance. Thus, the oscillating component is a sinusoid with amplitude 1V and frequency 1MHz.



The expected pull-in voltage is about 3.5V, so that the bias voltage sweeps from 0 to 4V with voltage step of 0.1V. The schematic of the measurement setup is shown in figure 4.3.

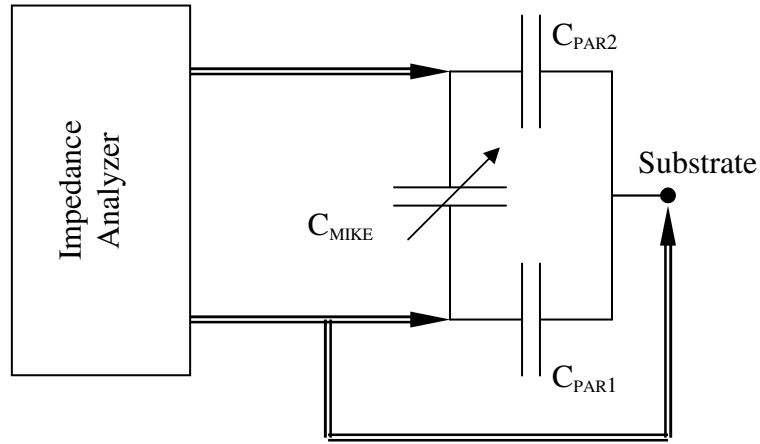


Figure 4.3 Schematic of the measurement setup to acquire CV characteristic

The Impedance Analyzer applies the polarization voltage to the backplate and moving membrane terminals. All connections are made using coaxial cable, to minimize the noise and the measures had been held in a dark and closed environment. Besides, in order to minimize the effect of the parasitic capacitance between the polysilicon and the substrate, the latter is connected to ground. The measures were held in quasi-static state, then at equilibrium the restoring force of the supporting beam is equal to the electrostatic force:

$$k_D x = \frac{1}{2} \epsilon_0 S_{BP}^E \frac{V_{BIAS}^2}{(x_0 - x)^2} \quad (4.1)$$

where  $k_D$  is the spring constant of the supporting beam,  $S_{BP}^E$  is the active electrical surface of the backplate  $V_{BIAS}$  is the polarization voltage,  $x_0$  and  $x$  are respectively the air gap without any biasing and the displacement of the moving membrane due to the biasing.

The equilibrium distance is given by the solution of the (4.1) with respect to  $x$ :

$$x^3 - 2x_0 x^2 + x_0^2 x - \frac{1}{2} \frac{\epsilon_0 S_{BP}^E}{k_D} V_{BIAS}^2 = 0 \quad (4.2)$$

The solution of the (4.2) gives the displacement of the moving membrane as function of the spring constant, the active electrical backplate surface and the bias voltage. Only one of the three solution of (4.2) is valid, and it can be easily selected choosing the solution which respects the following physical constraints: it has to be real and less than  $x_0$ . Once calculated the equilibrium distance between moving membrane and backplate, supposing a parallel plate model for the microphone, its capacitance can be estimated as

$$C_{MIKE} = \frac{\epsilon_0 S_{BP}^E}{x(V_{BIAS}, x_0, S_{BP}^E)} + C_F \quad (4.3)$$

where  $C_p$  is the fixed contribution mainly due to the frame of the polysilicon of the moving membrane which is covered by the backplate. The expression (4.3) was used to fit the experimental data acquired through the CV characterization and using a least squares method an estimation of  $C_F$ ,  $x_0$  and  $k_D$  is obtained. Figure 4.4 shows a typical set of measured data and the resulting fitting.

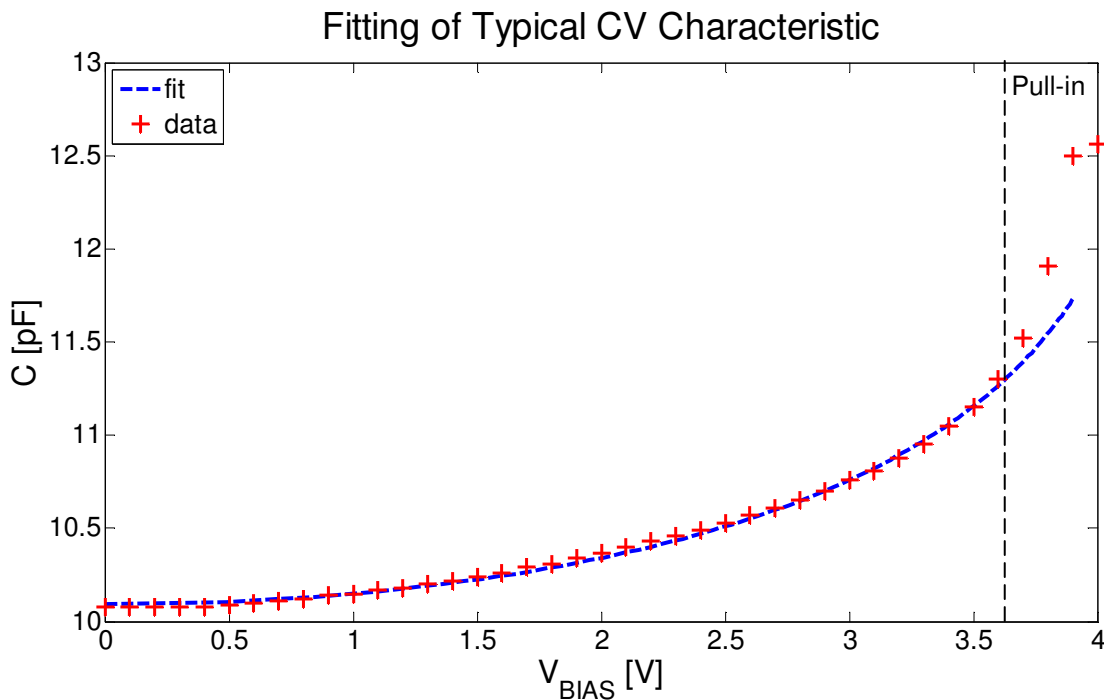


Figure 4.4 Fitting of a typical CV characteristic

The fitting of the data is extended till the pull-in limit. Indeed, after that voltage level, the electrostatic force overcomes the restoring force of the supporting beam and the equality (4.1) is no longer valid.

Measurements were performed over several microphones of the same wafer in order to characterize it. The following table compares the expected values with those estimated by the fitting of the CV characteristics:

	Expected	Fitting
Capacitance at zero bias	6.4pF	$10.76 \pm 0.62$ pF
Fixed capacitance	1.6pF	$4.8 \pm 0.79$ pF
Air gap	1.6 $\mu$ m	$1.41 \pm 0.13$ $\mu$ m
Spring constant	160N/m	$214.8 \pm 17.32$

Table 4.1 Comparison between expected value and the values obtained fitting the experimental data

As shown in table 4.1 the dimension of the air gap is close to the expected value, even if slightly lower. This difference could be due to the stress on the surface of the moving membrane which bends the membrane itself toward the backplate and gives rise to a bump. The estimation of the air gap was performed supposing a parallel plate capacitance, thus estimating an equivalent average distance between moving membrane and backplate. The bump decreases the average distance between them, thus the estimated air gap results lower than expected.

The estimated spring constant is also higher than expected. This high value is likely due to the superficial stress of the moving membrane again. Indeed, when the membrane bends, it pulls the supporting beams increasing their stiffness thus making the springs more rigid.

The capacitance values are higher as well, both the capacitance at zero bias voltage and the fixed component. The fixed capacitance is due to the fixed part of the polysilicon layer used to make the moving membrane, that is it is mainly due to the membrane frame. Comparing the expected value of the fixed part of the capacitance with that one estimated we can see a difference of about 3.2pF. If we subtract this value to the capacitance at zero voltage, the estimated value is close to the expected value. This means the difference is due to the fixed part.

In the new design, to reduce the fixed component, the frame has been divided as shown in figure 4.5.

The edges of the frame are separated from the corners, where there are the flexural beams which support the moving membrane. Each edge is connected to each other. In this configuration it is possible to connect the backplate to the edges of the frame. In this way both backplate and the edges of the frame have the same potential so that the capacitance between them is almost short-circuited and the fixed part of the microphone capacitance is reduced.

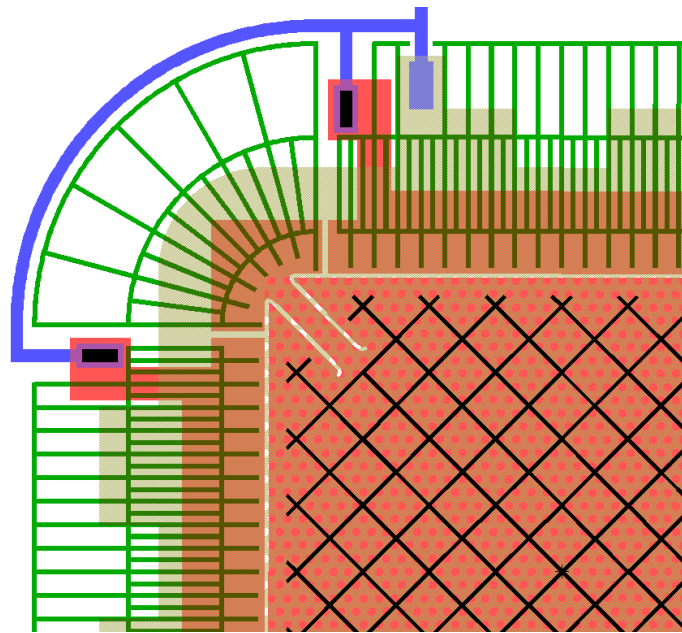


Figure 4.5 Detail of the divide frame of the moving membrane in the new desing.

### 4.2.2 Integrated resistances

A common read-out interface for a MEMS microphone is shown in figure 4.6.

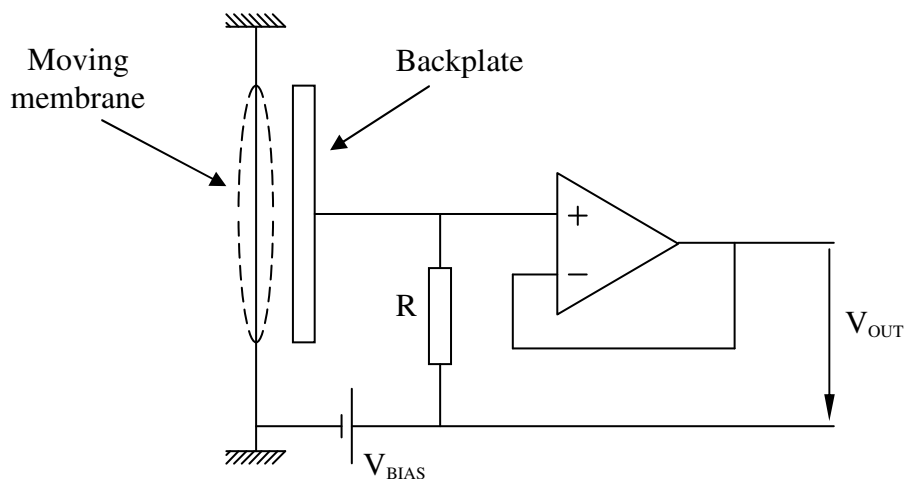


Figure 4.6 Schematic of common read-out interface for a condenser MEMS microphone

The capacitive microphone is charged by an external biasing voltage. When a sound pressure acts on the microphone, the moving membrane moves and the follower at the output of the microphone allows to measure the voltage drop across the resistor R. To avoid output voltage degradation, it is important the follower has input capacitance as small as possible. The best would be to have the read-out electronic embedded in the chip, but as first stage to test the microphone we used an external JFET in follower configuration, as shown in figure 4.7.

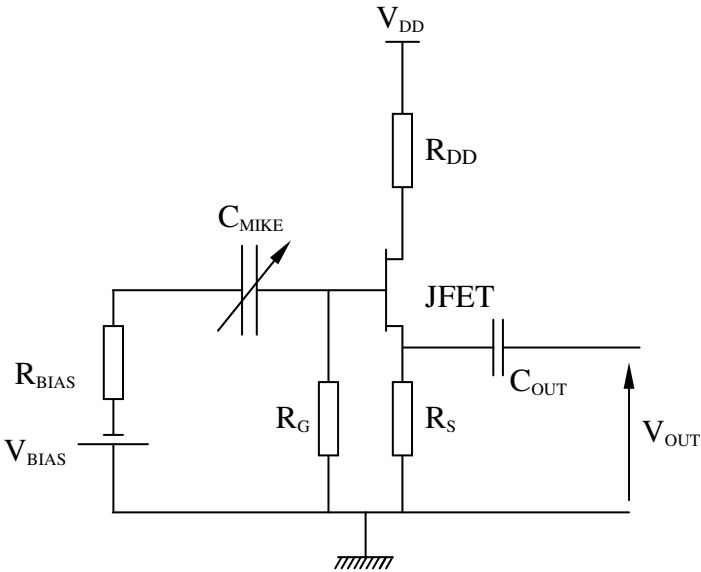


Figure 4.7 Simple microphone read-out electronics with a JFET in follower configuration

Anyway, even if the JFET is not embedded in the chip, to keep down the number of elements to be packaged along with the microphone, the gate and source resistors are embedded into the microphone chip, as shown in the layout of the microphone in figure 4.8

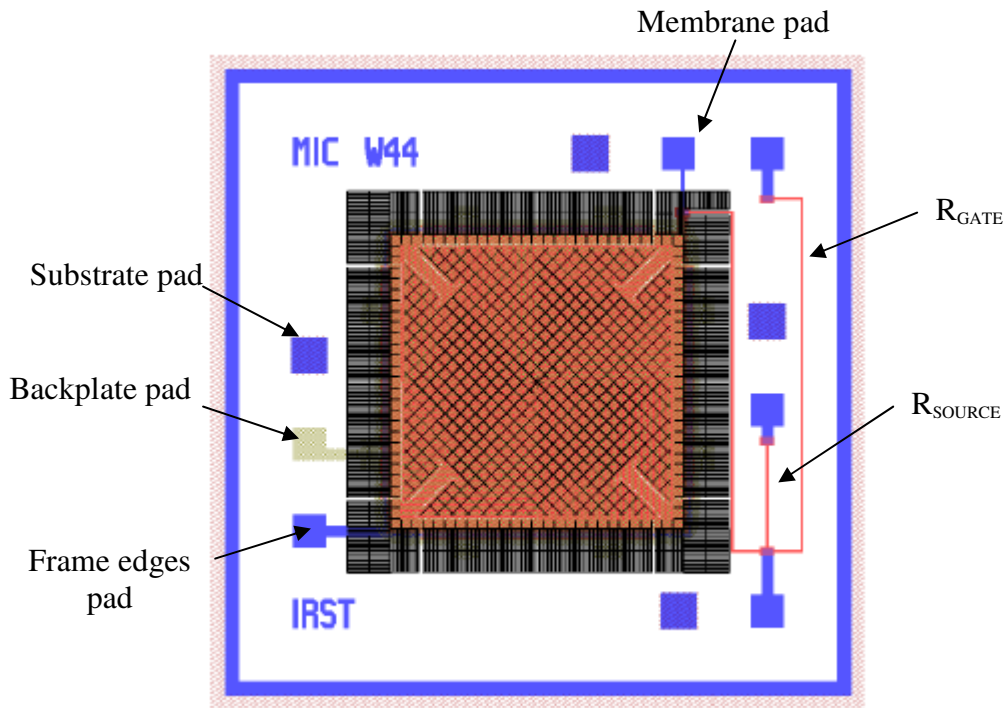


Figure 4.8 Layout of the FBK MEMS microphone with the gate and source resistors embedded in the microphone chip

In the first run it was impossible to test the embedded resistances because the difficulties we ran into due to the wrong anisotropy factor during production process which dissolved metal lines connecting pads as shown in figure 4.9 where we can see just its trace.

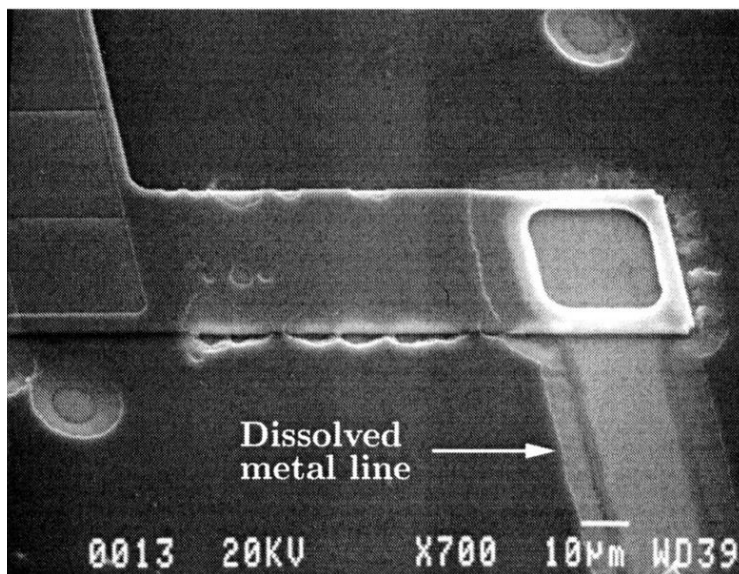


Figure 4.9 Dissolved metal line due to the wrong anisotropy etching

Due to the impossibility to perform some characterization of the embedded resistances, an additional run has been made to produce only the embedded resistors. The process uses the same masks as the main process, and the only difference was different implantation level for different produced resistors. In this way, characterizing the resistance value as function of the doping level it is possible to tune the manufacturing process in order to achieve the desired resistance value [45].

In the second run all main process problems have been solved and almost all microphones have a correct connection between pads. Thus, it was possible to measure and characterize the embedded resistances.

Measurements have been performed at the wafer level by means of Probestation Karl Suss PM8 and the semiconductor parameter analyzer HP4145. A schematic of the measurement setup is shown in figure 4.10.

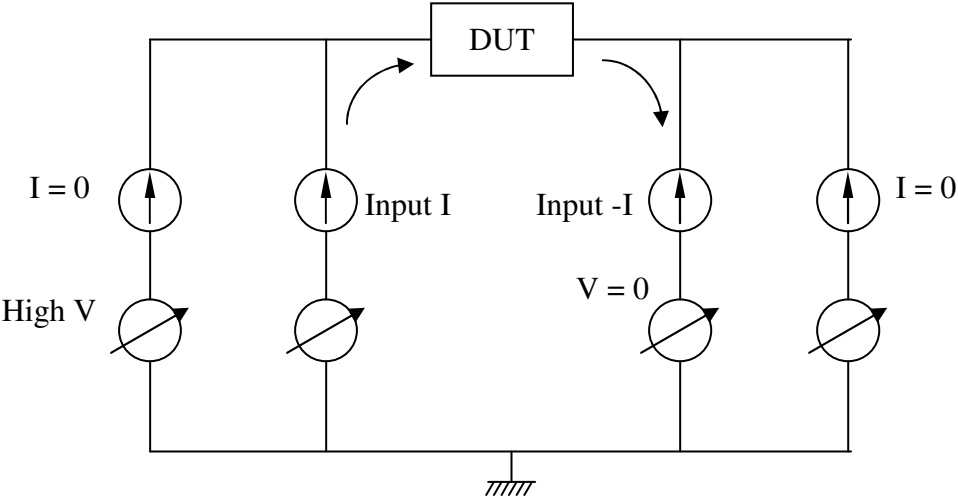


Figure 4.10 Schematic of the measurement setup to measure the embedded resistances

To measure the embedded resistances we used a four terminals configuration. Indeed, the probe station has four probes and each of them can be set as an ideal voltage or current source with respect to ground. In this way each terminal is connected by two probes. As depicted in the schematic of figure 4.10, two probes are used as voltage generators to set the voltage drop across the device under test (DUT), and the remaining two probes are used to measure the current flowing through the DUT. The forced voltage sweeps in the range  $\pm 4V$  for the gate resistance and  $\pm 1V$  as to the source resistance.

Figures 4.11 and 4.12 plots a typical I-V characteristics of microphones coming from the same wafer.

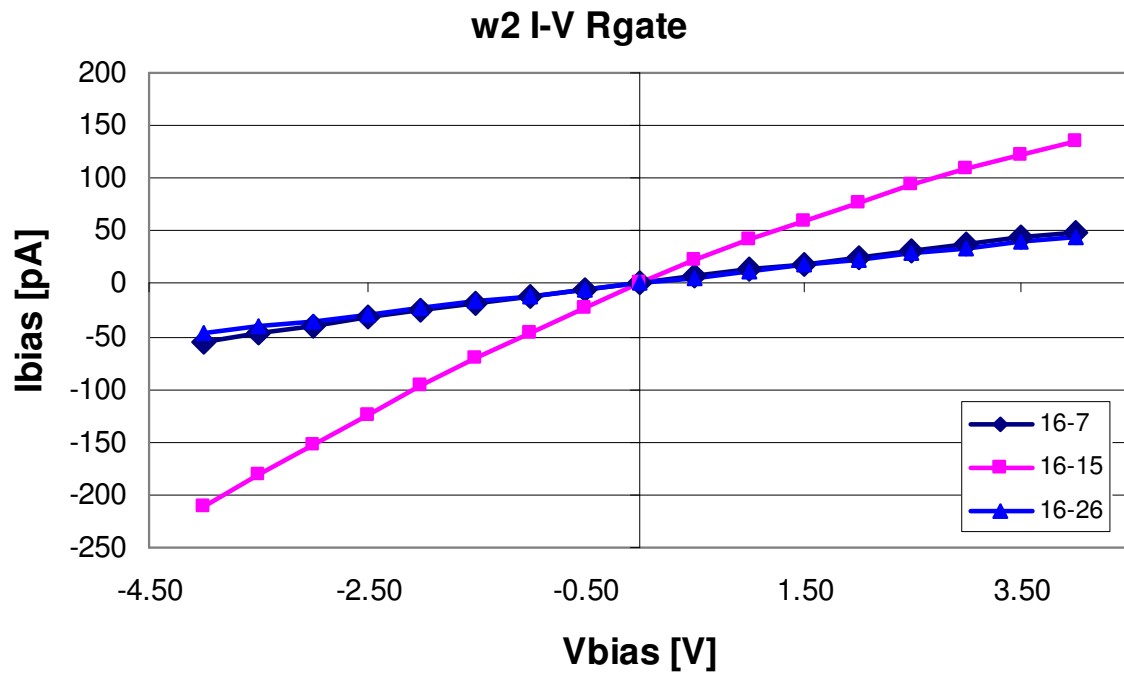


Figure 4.11 I-V characteristic of the embedded gate resistance

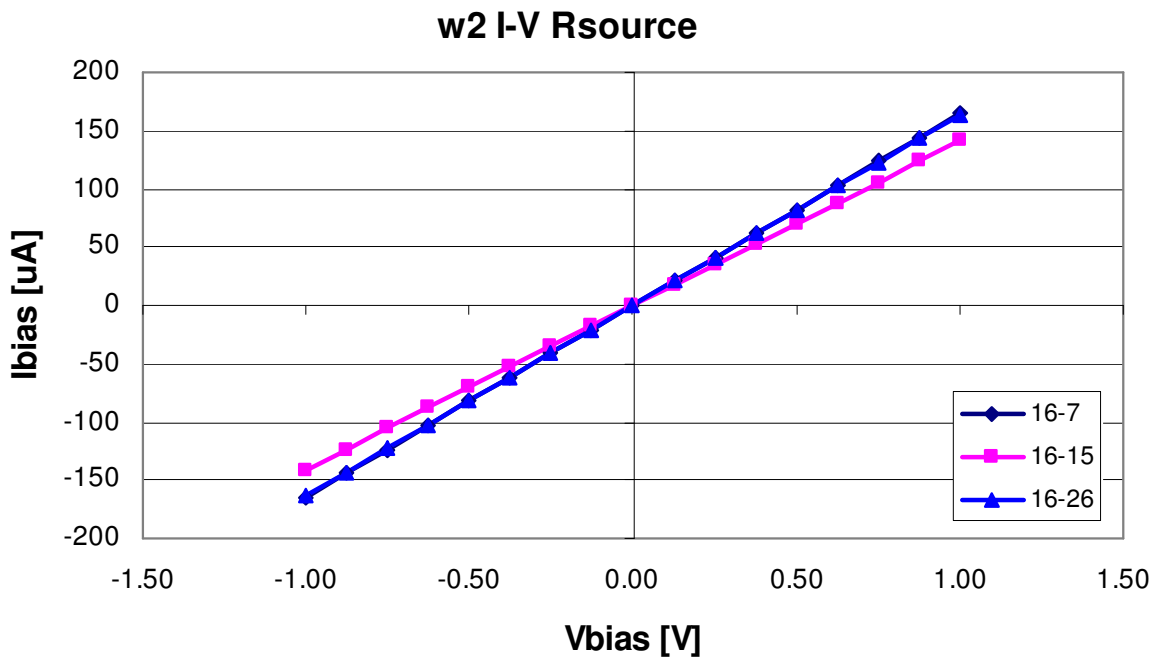


Figure 4.12 I-V characteristic of the embedded source resistance

Table 4.2 summarizes the resistance values of the embedded resistances plotted in the previous figures calculated as the reciprocal of slope of the acquired characteristics.



mike	$R_{\text{GATE}}$ [ $\text{G}\Omega$ ]	$R_{\text{SOURCE}}$ [ $\text{k}\Omega$ ]
w216_7	77.8	6.06
w216_15	23.0	7.09
w216_26	87.4	6.11

Table 4.2 Embedded gate and source resistances

The expected value of the gate and source resistance is about  $10\text{G}\Omega$  and  $30\text{-}50\text{k}\Omega$ . However, the experimental results show completely different values. About the gate resistance, the measured values are much higher, whereas as to the source resistances are much lower than expected, even though the additional tuning run to calibrate the doping process. Further tests and additional runs were not performed, even if it would be necessary to get a better tuning of the doping and annealing process, because the next microphone generation the embedded resistances are no longer present. Indeed, all the read-out electronics will be developed externally integrated in a chip different from the microphone chip.

### 4.2.3 Parasitic capacitances

Parasitic capacitances affect microphone performances and it is important to keep them as small as possible. Figure 4.13 shows a schematic of the microphone with the main parasitic capacitance.

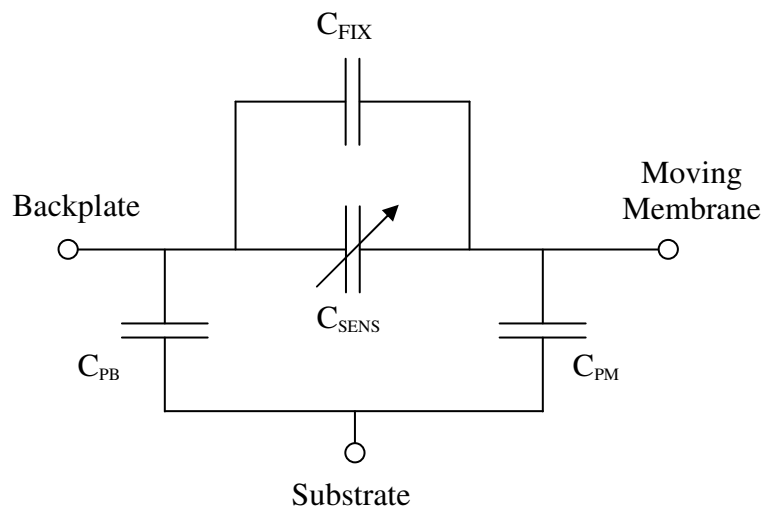


Figure 4.13 Schematic of the microphone with the main parasitic capacitance

$C_{\text{FIX}}$  and  $C_{\text{SENS}}$  are respectively the fixed and the variable part of the microphone capacitance, whereas  $C_{\text{PB}}$  and  $C_{\text{PM}}$  are the parasitic capacitance at the backplate and the moving membrane respectively. The main issue is  $C_{\text{PM}}$ . Indeed, it represents a partition voltage for the output signal, so that it is necessary to keep it as small as possible, in order to be as close as possible to the open circuit sensitivity.

All the measurements have been performed at wafer level using the Probestation Karl Suss PM8 and the impedance analyzer HP 4192A. The substrate has been connected to ground through a probe, whereas the other microphone pads are left floating but the pad of the DUT, which is connected to the other probe. To avoid the displacement of the moving membrane, to sense the capacitance a signal of amplitude 0.1V at 1MHz has been applied across the DUT. The oscillating signal is biased with a voltage which sweeps in the range 0 - 2.5V.

Figures 4.14 and 4.15 show typical CV characteristics of the two aforementioned parasitic components of the microphone.

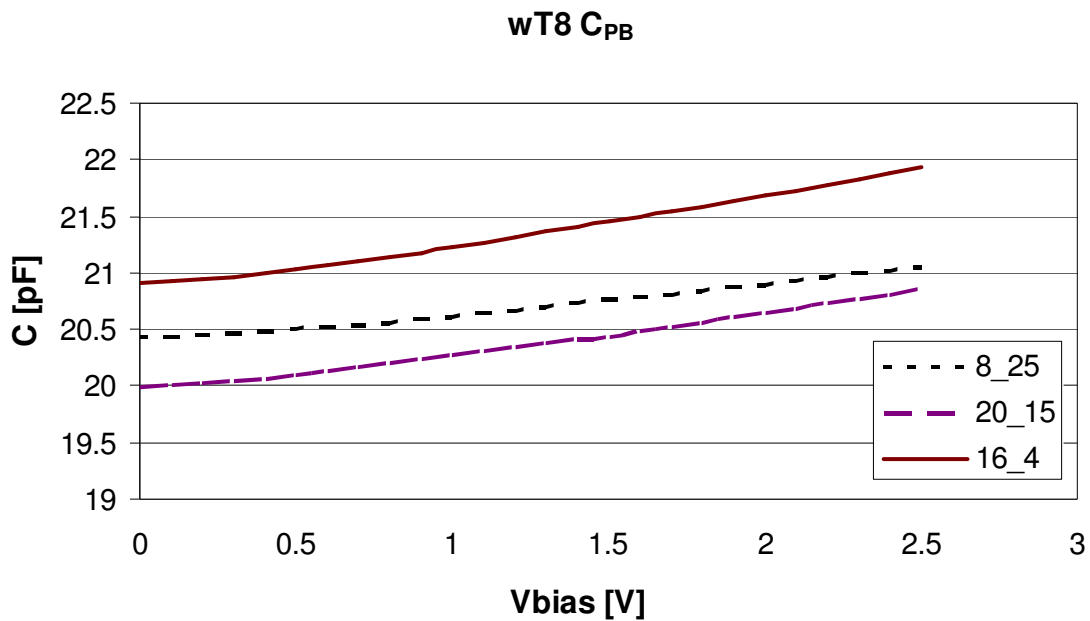


Figure 4.14 Typical C-V characteristic of the parasitic capacitance between the backplate and the substrate

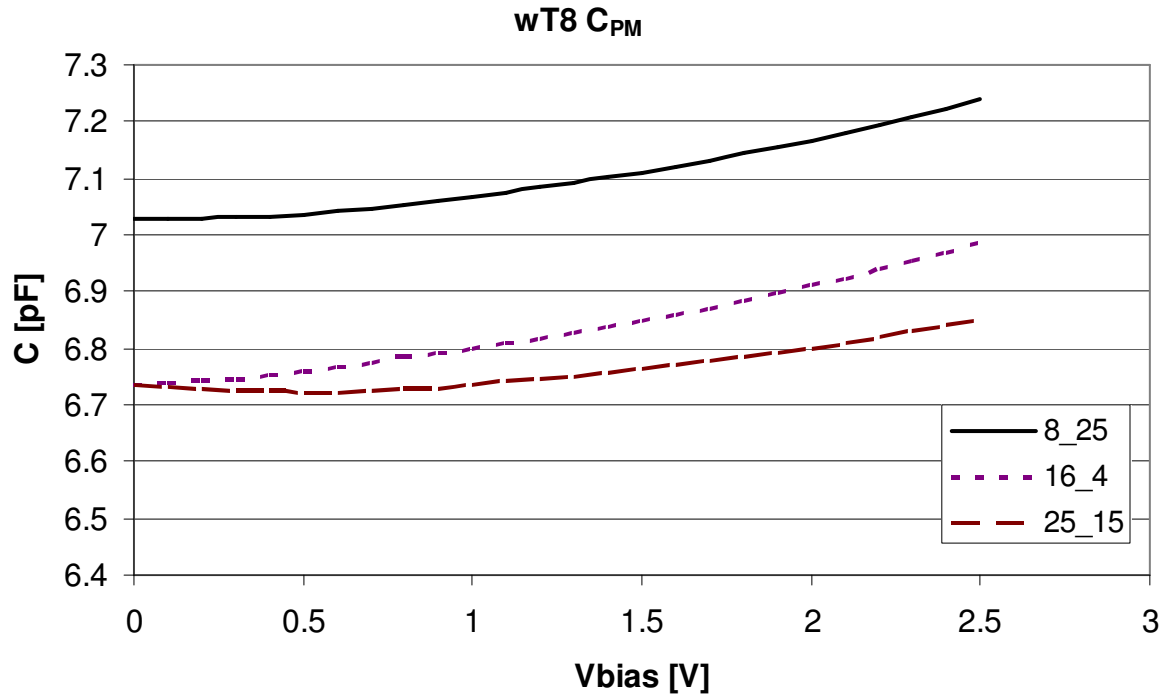


Figure 4.15 Typical C-V characteristic of the parasitic capacitance between the moving membrane and the substrate

Both the characteristics presents a small increasing trend as the bias voltage increases likely due to the inducted polarization of the moving membrane and the backplate which moves the membrane. This effect is however negligible and we can consider the parasitic elements constant with respect to the bias voltage. What is a little concerning is the value of the parasitic capacitance between the moving membrane and the substrate. Indeed, it presents a value slightly lower then the sensing capacitance, which means the signal is reduced because of the voltage partition.

To reduce this effect  $C_{PM}$  has to be reduced modifying the layout, otherwise it can be compensated through a feedback coming from the read-out electronics using a bootstrapping configuration, as reported in section [35]. However, applying such a technique, some strange effects occurred and further investigation on the parasitic components were performed.

Some devices showed a non-negligible resistance component in parallel to the parasitic capacitance. With the aim to estimate the resistive component an I-V characterization has been performed with the same setup used to characterize the embedded resistances. Figure 4.16 shows a typical I-V characteristic of microphones coming from the same wafer.

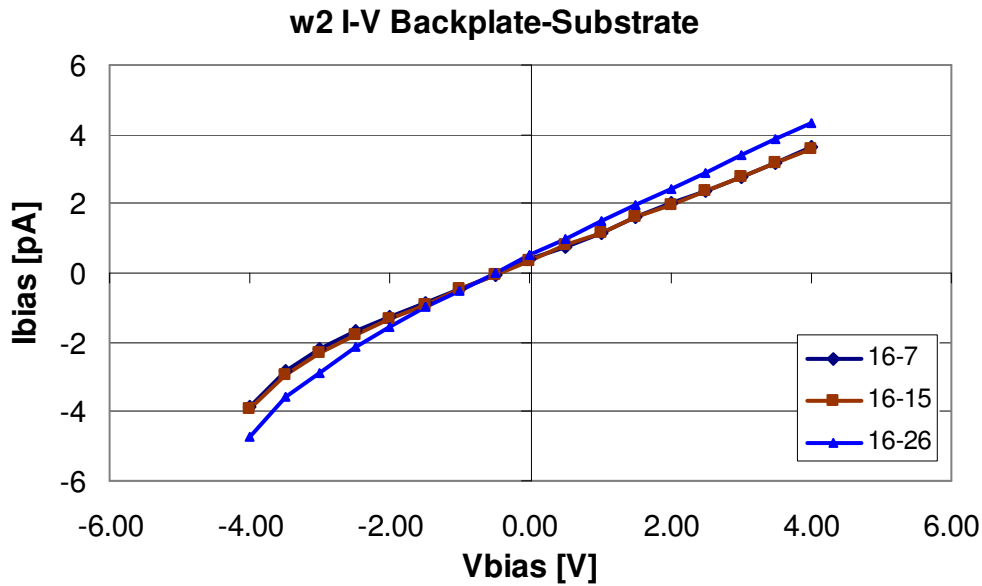


Figure 4.16 Typical I-V characteristic of the parasitic element between the backplate and the substrate

Table 4.3 reports some values of parasitic resistance estimated as the reciprocal of the slope of the I-V characteristic. w2 and w16 are internal label for different wafer.

mike	w2		w16	
	$R_{PB}$ [G $\Omega$ ]	$R_{PM}$ [G $\Omega$ ]	$R_{PB}$ [G $\Omega$ ]	$R_{PM}$ [G $\Omega$ ]
16_7	1225	1197	188	654
16_15	1206	1151	544	1030
16_26	1011	1021	780	966

Table 4.3 Some characteristic value of the parasitic resistance between the substrate and respectively the backplate and the moving membrane

The estimated values highlight as the wafer w2 has a parasitic resistance both at the backplate and the moving membrane about tera-ohm, but the wafer w16 has lower values, just hundreds giga-ohm. In this latter case there is a resistive path due to some lack of isolation. A visual inspection of the microphone at the electronic microscope (SEM) reveals that the polysilicon and the substrate are not properly isolated as shown in figure 4.17. The silicon dioxide used to isolate should cover all the surface of the polysilicon but because of the over-etching action of the wet solution used to remove the sacrificial layer behind the moving membrane, the silicon dioxide is slightly removed from the fixed frame as well, reducing the isolation.

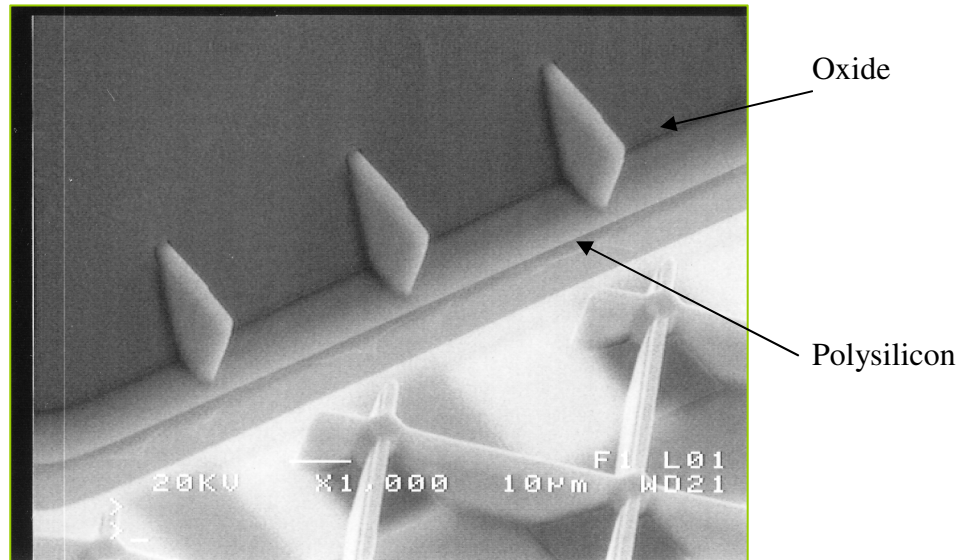


Figure 4.17 Image for SEM of a microphone with a bad isolation because the isolation oxide does not cover completely the polysilicon.

This lack of isolation has been observed from the frequency characterization of the parasitic capacitance as well. The measurement has been performed at wafer level using the Probestation Karl Suss PM8 and the impedance analyzer HP 4192A. An oscillating signal has been of amplitude 0.1V with frequency sweeping from 1kHz to 1MHz. The measures were done for two values of bias voltage to verify if the frequency behaviour of the parasitic element could depend on the bias voltage as well. Figure 4.18 shows the frequency behaviour of the parasitic capacitance of the backplate to the substrate.

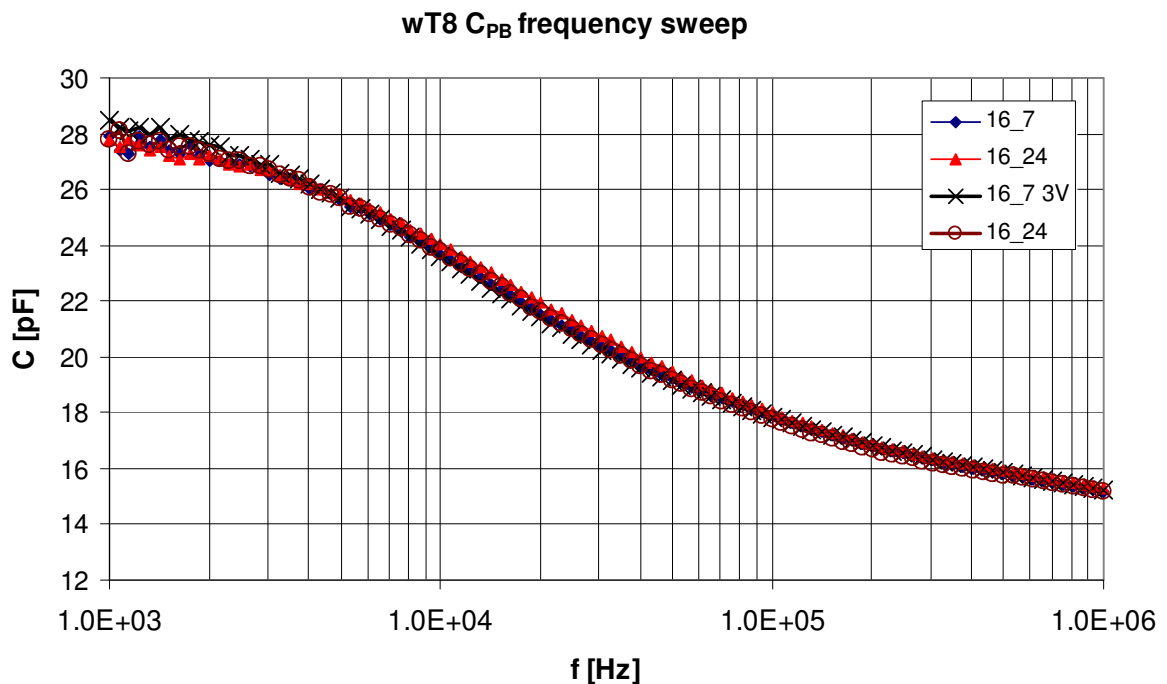


Figure 4.18 Frequency characteristic of the parasitic capacitance between the backplate and the substrate

The figure does not show any resonance peak, so that the model of the parasitic element of a capacitance in parallel to a resistor can be considered valid. The variation of the capacitance value can be due to the dielectric relaxation phenomenon.

The dielectric relaxation is due to the delay of the molecular polarization with respect to the applied electric field in a dielectric medium. In the hypothesis of having a spherical molecular dipoles and that there are not any interaction dipole-dipole, the system can be described by the Debye equation. This model describe the dynamic of the polarization as a first order system with time constant  $\tau$  defined as [62]

$$\tau = \frac{4\pi\eta R_D^3}{kT} \quad (4.4)$$

where  $\eta$  is the viscosity of the material and  $R_D$  is the radius of the dipole,  $k$  is the Boltzmann constant and  $T$  is the absolute temperature. Usually the relaxation is described as a function of frequency expressing the polarization by the Fourier transform. Thus, the polarization can be expressed as [62]

$$P_{REL}(\omega) = \frac{P_{REL}^S}{1 + i\omega\tau} \quad (4.5)$$

where  $P_{REL}$   $P_{REL}^S$  is the polarization due to the relaxation,  $P_{REL}^S$  is the expected polarization in steady state and  $\omega$  is angular frequency of the applied oscillating electric field. The polarization at steady state can be expressed as a function of the applied electric field:

$$P_{REL}^S = \epsilon_0(\epsilon_s - \epsilon_\infty)E \quad (4.6)$$

where  $E$  is the electric field,  $\epsilon_0$  is the vacuum permittivity,  $\epsilon_s$  is the medium permittivity in steady state, which represents the response of the medium to a static electric field, and  $\epsilon_\infty$  is the unrelaxed permittivity caused by the distortion of the electronic cloud and the position of the nuclei of the atoms by the effect of the electric field [63]. The electric displacement field is defined as  $D = \epsilon_0\epsilon_r E$ , but it can be also expressed as a function of the electric field, the polarization and the unrelaxed permittivity [63]:

$$D = P_{REL} + \epsilon_0 \epsilon_\infty E = \epsilon_0 \epsilon_r E \quad (4.7)$$

Substituting (4.5) and (4.6) into (4.7) we achieve the frequency representation of the relative permittivity:

$$\epsilon_r(\omega) = \frac{\epsilon_s - \epsilon_\infty}{1 + i \omega \tau} + \epsilon_\infty \quad (4.8)$$

The complex relative permittivity (4.8) can be divided into its real and complex part:

$$\epsilon' = \frac{\epsilon_s - \epsilon_\infty}{1 + \omega^2 \tau^2} + \epsilon_\infty \quad \epsilon'' = \frac{\epsilon_s - \epsilon_\infty}{1 + \omega^2 \tau^2} \omega \tau \quad (4.9)$$

These are equations are the so-called Debye equations. The real part  $\epsilon'$  is the measure of the energy stored in the oscillations of the dipolar units. The imaginary part  $\epsilon''$  is called dielectric loss, because it represents the energy dissipated in the medium due to internal frictions.

To characterize the behaviour of our capacitance due to dielectric relaxation we are interested in the first of the Debye equations. Using this relation and estimating the geometrical parameter of the parasitic capacitance of the microphone a model has been built and used to fit the experimental data [61]. Figure 4.19 shows the obtained fitting.

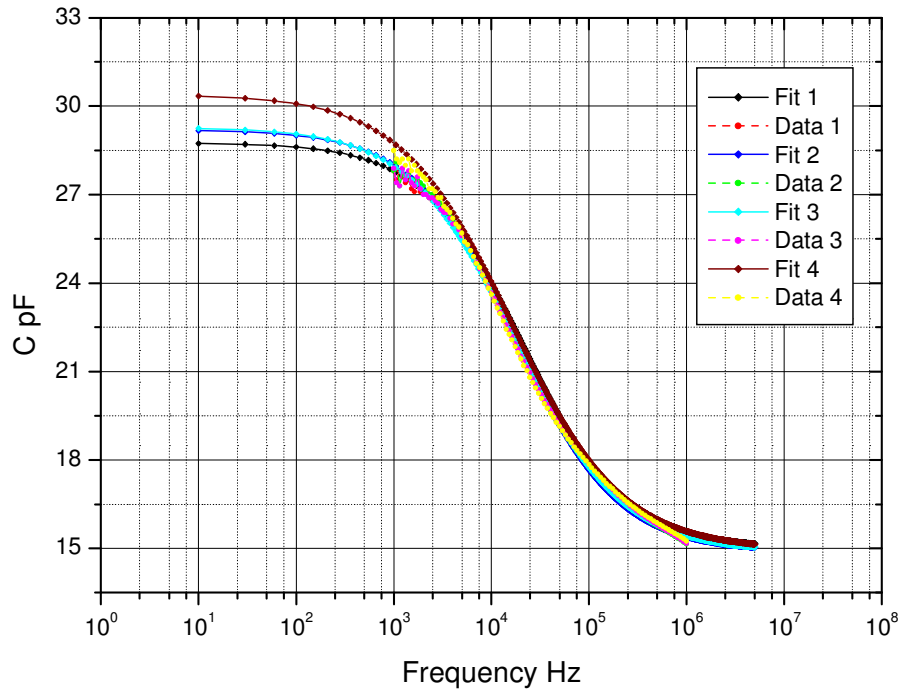


Figure 4.19 Fitting of the experimental data of the frequency characteristic of the parasitic capacitance using a Debye model

Both the issue of the resistive path and the dielectric relaxation can be explained by the lack of isolation between the polysilicon and the substrate. The problem will be solved coating the oxide with a thin layer of silicon nitride over the fixed part of the polysilicon. Indeed, the wet etching will remove the silicon oxide but it will not remove the silicon nitride, which shields the isolating oxide of the fixed part of the polysilicon.

#### 4.2.4 Acoustic Test

The microphone has been characterized acoustically measuring its sensitivity at 1kHz at different bias voltage and different acoustic pressure, in order to check the linearity of the device as well. Acoustic measurements have been performed in a pseudo-anechoic box. Inside the box there is a speaker which generates the desired sound wave and a holder where the device under test (DUT) and the reference microphone are fixed. All the internal walls of the box are coated with a foam to reduce as much as possible the occurrence of sound reflection. The wooden box lays inside a metallic box in order to shield the measurement environment from external EMI disturbances. Figure 4.20 shows the pseudo-anechoic box.

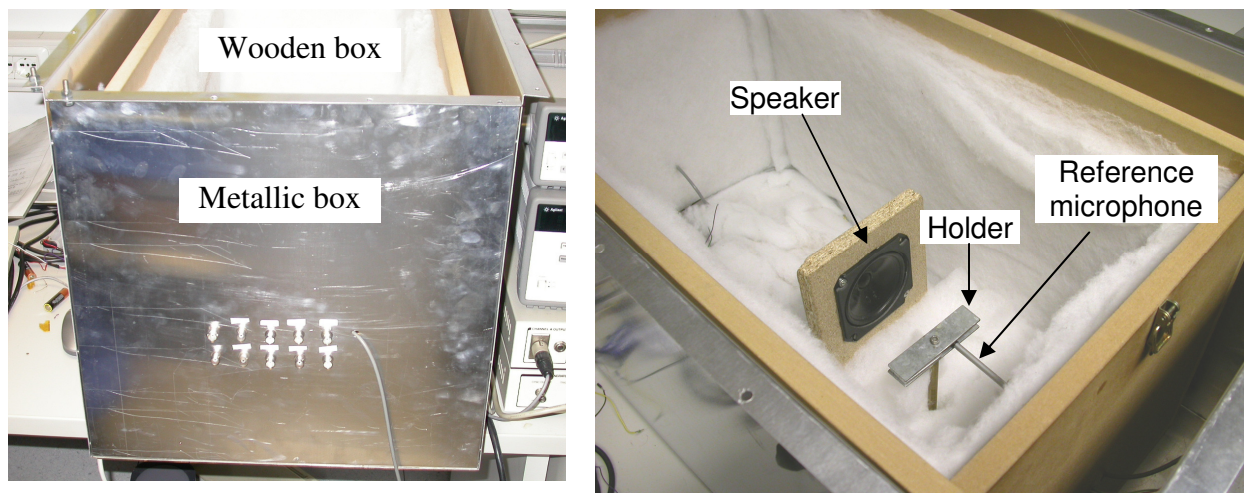


Figure 4.20 Pseudo-anechoic box

The internal speaker is driven by an Audio Precision (AP) System One audio analyzer, shown in figure 4.21. Generators of the AP can generate a sine wave in the band 10Hz – 120kHz with a flatness of 0.3dB, accuracy 0.5% and resolution 0.02%, which allows to drive properly the speaker. The input channels have an accuracy of  $\pm 0.2\%$  and a response flatness of 0.2dB in the



range 10Hz - 50kHz. Most of all, the AP system can acquire two signals at the same time, allowing to perform the simultaneous measurement method.



Figure 4.21 Audio analyzer Audio Precision System One. Acquire data from DUTs and it can generate signals

The sound wave is generated by a Ciare HX100 driven by AP. It is a full range speaker with 50W as maximum power and an input impedance of 8Ω. To calibrate the speaker, a reference microphone is used. It is a Brüel&Kjær 4939-A-001, which guarantees a frequency response of ±2dB in the band 4 – 100kHz along with the conditioning amplifier Nexus 2690--0S.

To characterize the microphone a read-out interface is necessary to avoid to load its output.

Two set of packaged microphones were available: one package type contains only the microphone, the other type, along with the microphone, has a JFET in follower configuration directly connected to the microphone in order to minimize the parasitic capacitance. Unfortunately, the microphones with JFET did not work because of issues due to bonding operations, so that we used the microphones without electronics with an operational amplifier (Opamp) in follower configuration at its output. Figure 4.22 shows the schematic of the microphone connected to the Opamp.

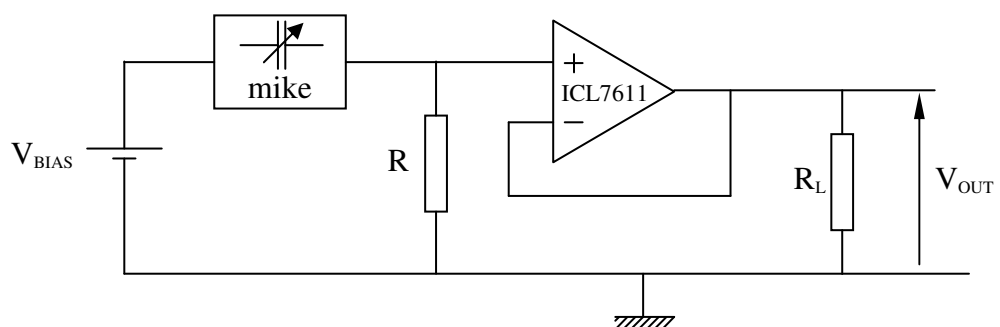


Figure 4.22 Schematic of the read-out interface used to characterize acoustically the microphone

In this configuration, however, the parasitic capacitances at the output of the microphone are greater than those of the configuration with the embedded JFET. To characterize the partition ratio at the output of the microphone due to the extra parasitic capacitances, a brief electric test has been performed: for different polarization voltage, a sinusoidal signal at 1kHz and different amplitudes has been applied at the backplate of the microphone and then the output voltage of the follower has been measured. Table 4.4 reports the measured values.

	$V_{BIAS} 0V$		$V_{BIAS} 3V$		$V_{BIAS} 3.5V$	
$V_{IN}$ [mV]	$V_{OUT}$ [mV]	$V_{OUT}/V_{IN}$	$V_{OUT}$ [mV]	$V_{OUT}/V_{IN}$	$V_{OUT}$ [mV]	$V_{OUT}/V_{IN}$
99.16	11.84	0.1194	11.95	0.1205	12.08	0.1218
198.4	23.76	0.1197	23.97	0.1208	24.21	0.1220
297	35.63	0.1200	35.85	0.1207	36.22	0.1219
396.6	47.54	0.1199	47.76	0.1204	48.25	0.1217
	Average	0.1197	Average	0.1206	Average	0.1218

Table 4.4 Electric characterization of the system microphone + follower.

The table shows an average attenuation of the input signal of about 88% and slightly increasing with the bias voltage, but this effect can be neglected. This attenuation will be considered when will be estimated the open-circuit sensitivity increasing the measured signal of the same ratio.

Both microphones, the reference one and the DUT are placed in the holder close each other, so that both microphones are lighted by almost the same sound pressure.

The speaker is calibrated at 1Pa at 1kHz controlling its supply voltage by the Audio Precision and measuring the emitted sound pressure using the reference microphone.

The table 4.5 reports the different output voltage acquired from the DUT for different pressure and polarization voltage values.

$V_{BIAS}$ [V]	$V_{OUT@1Pa}$ [mV]	$V_{OUT@2Pa}$ [mV]	$V_{OUT@3Pa}$ [mV]	$V_{OUT@3.5Pa}$ [mV]
0	0.2754	0.5478	0.8219	0.8889
0.5	0.3093	0.6173	0.9246	0.9997
1	0.3456	0.6886	1.0329	1.1080
1.5	0.3837	0.7606	1.1393	1.230
2	0.4226	0.8382	1.258	1.3491
2.5	0.4664	0.9240	1.4022	1.4649
3	0.5152	1.0204	1.5400	1.5901
3.5	0.5734	1.1268	1.8467	1.9281

Table 4.5 Acoustic characterization of the system microphone + follower

Assuming that the electrical charge in the microphone is constant and the displacement of the moving membrane is small with respect to the air gap height, the open-circuit output voltage ( $V_{OUT}$ ) can be expressed as [47]

$$V_{OUT} = \frac{\Delta C}{C_{BIAS}} V_{BIAS} \quad (4.10)$$

where  $C_{BIAS}$  is the capacitance value of the biased microphone without any acoustic load,  $V_{BIAS}$  is the polarization voltage and  $\Delta C$  is the amplitude of the oscillating component of the microphone capacitance when it is loaded by a sound wave.

The open-circuit sensitivity, in [F/Pa], is defined as:

$$S_0^C = \frac{\Delta C}{P} \quad (4.11)$$

and substituting (4.10) into (4.11) and compensating the partition voltage at the output of the microphone, we obtain the following open-circuit sensitivity.

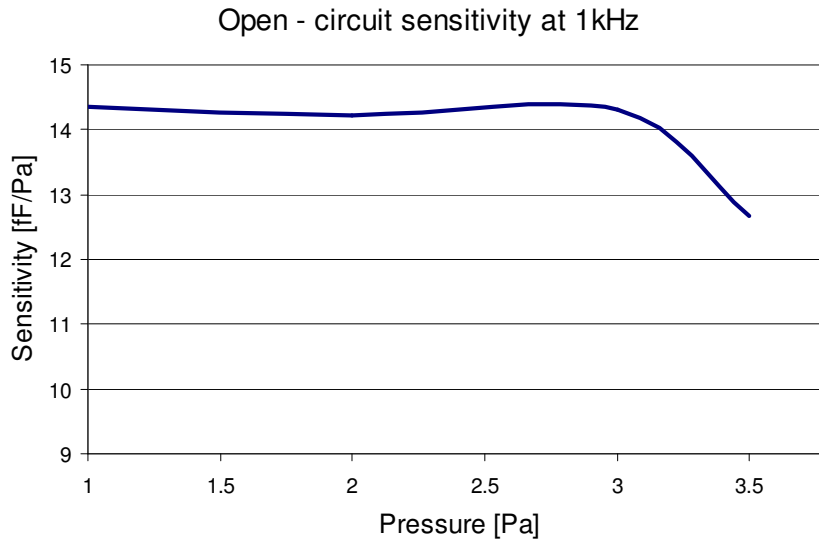


Figure 4.23 Acoustic open-circuit sensitivity of the microphone with  $V_{\text{BIAS}} = 3\text{V}$  and acoustic pressure at 1kHz.

The expected sensitivity for this microphone was 40fF but the experimental one is quite far from it. This difference is caused by two main reasons: the first is the mechanical characteristic of the microphone under test. From its C-V characteristic it was estimated an air gap at zero bias of  $1.73\mu\text{m}$  and a spring constant of about 221N/m. The air gap is quite close to the expected value of  $1.6\mu\text{m}$ , but the spring constant is rather high, making the system stiffer and thus reducing the sensitivity. The second reason is the extra parasitic capacitances, especially at the output of the microphone. Using an external Opamp as read-out interface introduces load capacitances which degrades the microphone output signal. Even if we tried to take them into account and reduce their effect estimating the partition voltage at the output of the microphone, they are not completely compensated because the compensation is based on the electric characterization which considers only the parasitic capacitance at the output and not that one at the backplate side.

The characterization is limited at 3.5Pa, because this is the maximum value the speaker can reach keeping a distortion level lower than 30%. Anyway, the loudness of the sound is enough for the microphone under test to enter into its nonlinear region, as we can see from the knee of the curve around 3Pa, which is equivalent to  $103.5\text{dB}_{\text{SPL}}$ .

# Chapter 5

## 5. Control Applications

In this chapter we will deal with two control laws applied to the MEMS microphone in order to improve its performance: the force feedback and the optimization of the microphone polarization voltage to tune its resonant frequency.

As to the force feedback, a digital readout interface has been designed with force feedback functionality [35]. The stability of the sigma delta modulator (SDM) will be considered and evaluated using the root locus method. Defined the stability limits of the SDM an analysis of the closed loop system microphone + SDM will be considered.

The second control issue is the tuning of the microphone resonant frequency. This property can be useful to maximize the response exploiting the spring softening due to the electrostatic force and using the bias voltage to control the electrostatic force. The polarization voltage will be adjusted using an extremum seeking controller.

### 5.1. Force Feedback analysis

A force feedback is a well-known technique used in many applications such as gyroscopes and accelerometers, and used to improve their performances. The aim of this configuration in a MEMS microphone is to counterbalance the acoustic force, which turns out in reducing the displacement of the moving membrane, thus improving the linearity of the system. Furthermore, introducing the MEMS microphone inside the loop of the SDM improves the noise performance because it increases the equivalent order of the SDM. Indeed, in feedback configuration the noise is filtered twice: by the SDM, which performs a noise shaping, and by the MEMS microphone, which filter the noise in the band. On the other hand, increasing the relative degree of the SDM could lead to instability.

To study the stability of the closed loop electro-mechanical SDM, namely the microphone + SDM, we shall first consider the SDM separately, to analyze its behaviour, and afterward we will consider the whole system.

### 5.1.1 SDM stability

As said in section 2, the SDM is strongly nonlinear because of the quantizer. Among the several ways to deal with this issue we use the quasi-linear method, which was found useful to model and analyze high order SDMs [64]. In this method, the quantizer is modelled as a linear gain and an additive noise source, so that standard linear system theory can be used to predict the stability of the modulator.

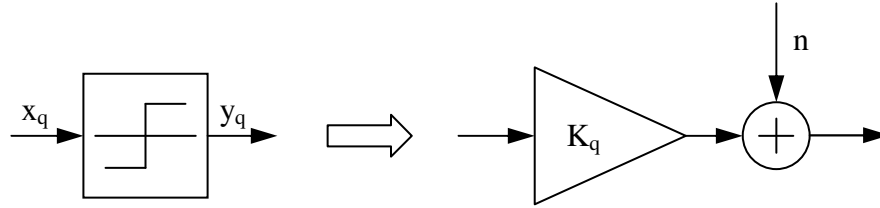


Figure 5.1 Representation of the quantizer using the quasi-linear model

The gain of the quantizer can be defined as [65]

$$K_q = \frac{|y_q|}{|x_q|} \quad (5.1)$$

where  $x_q$  is the input of the quantizer and  $y_q$  is its output. With this definition, the gain can be defined knowing only the signal amplitude at the input and output, and it ranges from zero to infinity, even if in practical implementation there are limitation on both extremes. The system is thus thoroughly described by two transfer functions: the signal transfer function (STF) and the noise transfer function (NTF). The stability of the system and the presence of limit cycles can be estimated from the root locus parameterized with respect to the equivalent gain  $K_q$ .

In this representation, our SDM has the following STF:

$$\frac{Y(z)}{X(z)} = \frac{0.08 K_q}{z^3 - 3z^2 + 3z - 1 + K_q (0.6z^2 - 1.1z + 0.504)} \quad (5.2)$$

and its root locus with respect to  $K_q$  is drawn in figure 5.2.

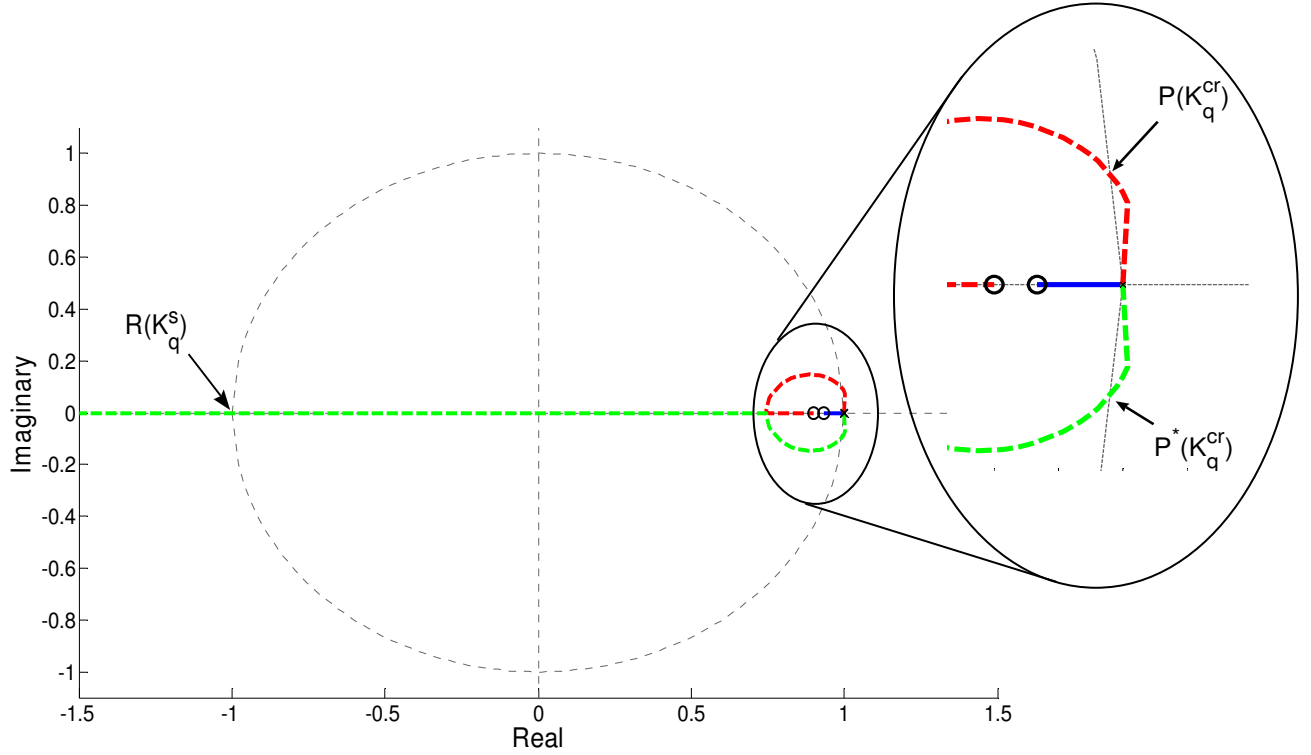


Figure 5.2 Root locus of the quasi-linear model of the SDM

The SDM root locus has been drawn using the equivalent auxiliary transfer function:

$$TF_{AUX} = K_q \frac{(0.6z^2 - 1.1z + 0.504)}{z^3 - 3z^2 + 3z - 1} \quad (5.3)$$

which has the same root locus of the STF of our SDM.  $TF_{AUX}$  has a relative degree 1, thus at least one branch of the root locus tends to infinity as the equivalent gain  $K_q$  tends to infinity, that is for  $K_q > K_q^S$  the pole of the auxiliary transfer function goes out of the unit circle and becomes unstable. The other two branches tend to the two zeros of  $TF_{AUX}$  as  $K_q$  tends to infinity, but before reaching the zeros both branches are out of the unit circle, that is unstable. This means there exist a minimum value  $K_q^{cr}$  so that if  $K_q < K_q^{cr}$  the system is unstable. Anyway, the behaviour of such three critical points is different. In  $R(K_q^S)$ , when the gain is higher than  $K_q^S$ , it means that there is a small signal at the input of the quantizer and the pole is outside the unit circle. In this situation, the input of the quantizer ( $x_q$ ) tends to increase, reducing  $K_q$  and bringing back the pole inside the unit circle. This decreases  $x_q$  and increases the gain again, pushing the pole out of the unit circle. This process repeats and gives rise to a stable limit cycle.

On the other side, in  $P(K_q^{cr})$  and  $P^*(K_q^{cr})$ , if  $K_q$  is less than  $K_q^{cr}$  it means that  $x_q$  is high and the poles are outside the unit circle. In this situation,  $x_q$  tends to further increase, reducing the gain and keeping the poles outside the unit circle. This causes the integrators to saturate, establishing a low frequency oscillation. This process gives rise to a saturation limit cycle [65]. In our case the critical gain is  $K_q^{cr} = 0.083$ . The system is thus conditioned stable, with  $K_q \in [K_q^{cr}, K_q^S]$ . The equivalent gain is related to the input signal amplitude, which means the constraint on the equivalent gain can be expressed for the input. Unfortunately there is not any mathematical relationship between the input amplitude of the system and the equivalent gain  $K_q$  of the quantizer, and we can only conclude qualitatively that the input cannot be neither too much large or too much small, and stability verification can be preformed qualitatively through simulations. To test the stability of the designed SDM, we simulated the open-loop system microphone + SDM at the maximum considered sound pressure, 20Pa@1Pa. Figure 5.3 shows the SDM output voltage, whereas figure 5.4 shows the filtered SDM output voltage using a low pass with a cut-off frequency of 10kHz and figure 5.5 shows the quantizer gain defined as the ratio between the output signal of the quantizer with respect to its input.

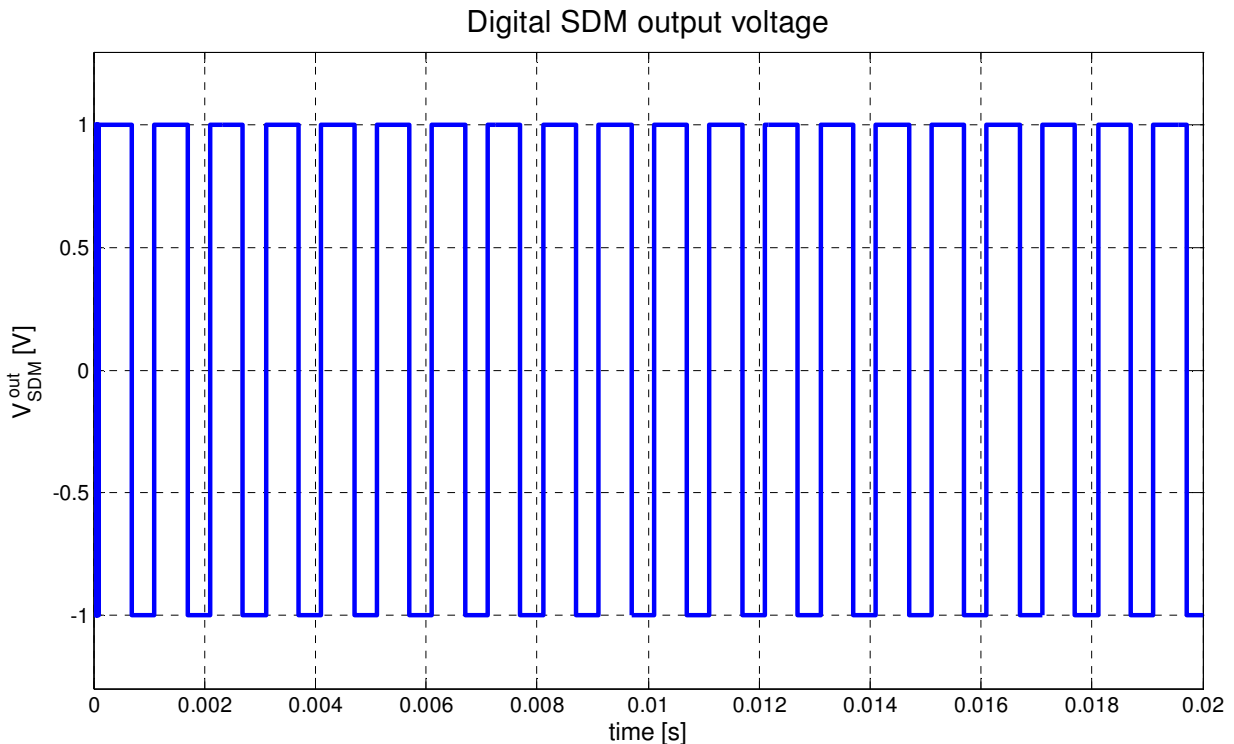


Figure 5.3 Digital output voltage of the SDM with 20Pa@1kHz as microphone input



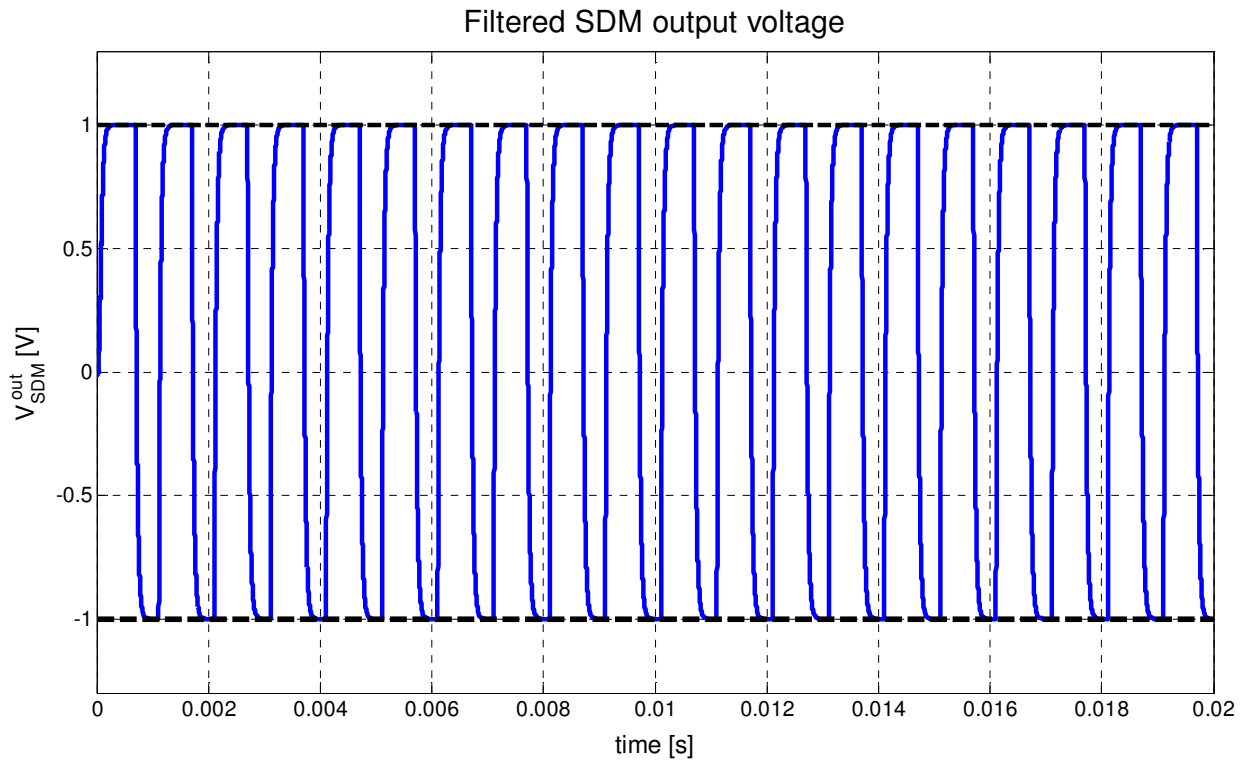


Figure 5.4 Filtered SDM output voltage with 20Pa@1kHz as microphone input

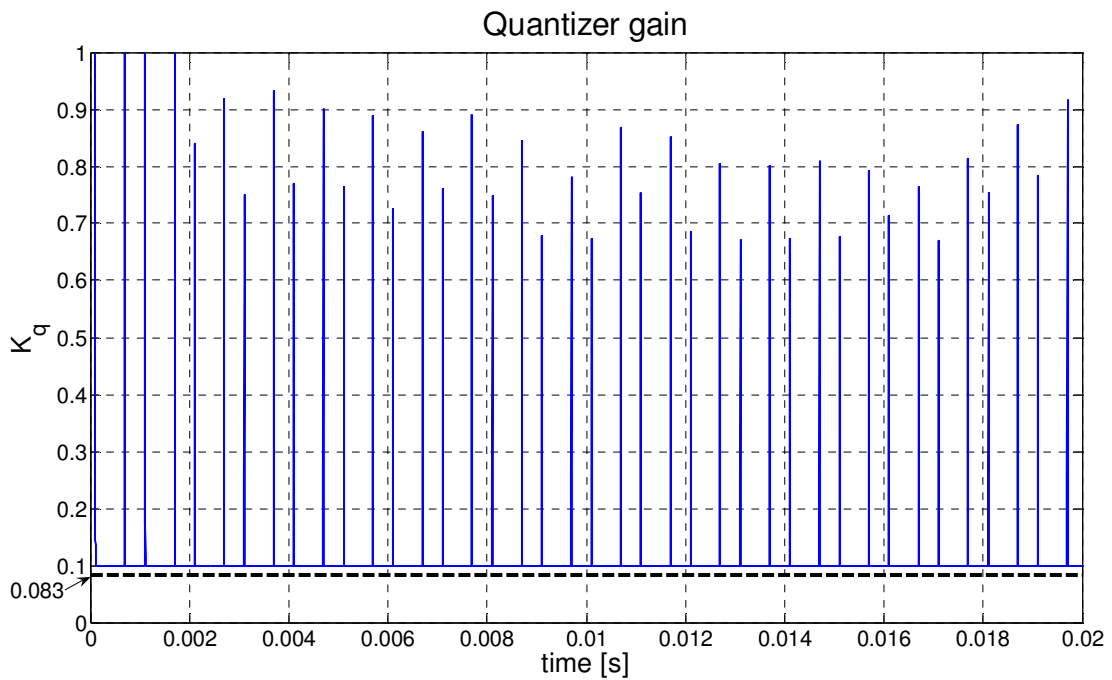


Figure 5.5 Quantizer gain during the simulation of the whole system with 20Pa@1kHz

The SDM is stable, as we can see from the figure 5.3, even if it reaches its saturation limit clipping the output signal, as shown in figure 5.4. The quantizer gain during the simulation is never lower than the threshold of stability, and it guarantees the stability of the SDM.

### 5.1.2 SDM + microphone stability

To study the stability of the electromechanical sigma-delta modulator we will use the quasi-linear model of the SDM again and evaluate the root locus of the whole closed loop system. In the previous section we saw the SDM was stable, so that we can fix the quantizer gain to 1 and draw the root locus of the whole system function of the  $K_{FB}$ .

The microphone is approximated by a second order system characterized by its mass, compliance and damping coefficient due to the air gap resistance. Both air gap resistance and the compliance of the microphone depends on the polarization voltage and the displacement of the membrane, To linearize the system they will be set to their steady state value at working point when there is not any acoustical pressure acting on the moving membrane. The system is then discretized using the bilinear transformation and a sample frequency ( $f_s$ ) of 2.5MHz. Due to the discretization,  $G_{MIKE}^d(z)$  has two zeros at  $f_s/2$ , and the digital transfer function of the microphone is then:

$$G_{MIKE}^d(z) = 10^{-5} \frac{2.09z^2 + 4.179z + 2.09}{z^2 - 1.988z + 0.9904} \quad (5.4)$$

A generic schematic of the electromechanical SDM is shown in figure 5.6 [66].

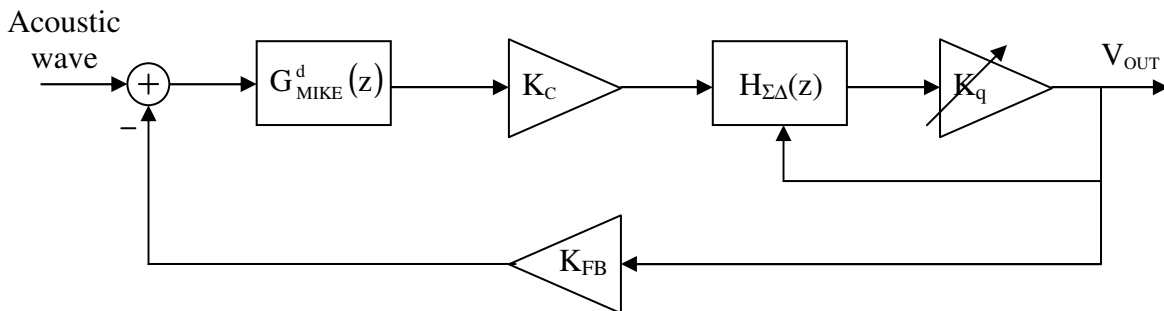


Figure 5.6 Generic schematic of an electromechanical SDM

where  $K_C$  is the gain of the electronic read-out which converts the displacement of the moving membrane to a voltage signal,  $H_{\Sigma\Delta}(z)$  is the electronic filter of the SDM,  $K_q$  is the variable gain, in accordance to the quasi-linear model of the quantizator, and  $K_{FB}$  is the gain which converts the electric output voltage to the electrostatic feedback force.

The signal transfer function, with respect to the schematic of figure 5.6, is given by

$$W(z) = \frac{G_{MIKE}^D(z)K_C H_{\Sigma\Delta}(z)K_q}{1 + M(z)} = \frac{G_{MIKE}^D(z)K_C H_{\Sigma\Delta}(z)K_q}{1 + K_{FB}G_{MIKE}^D(z)K_C H_{\Sigma\Delta}(z)K_q} \quad (5.5)$$

The stability of  $W(z)$  can be studied using the root locus of the equivalent auxiliary function  $M(z)$  in (5.5) and considering the product  $K_{FB}$  and  $K_q$  as a single gain. Figure 5.7 shows the root locus of  $M(z)$ .

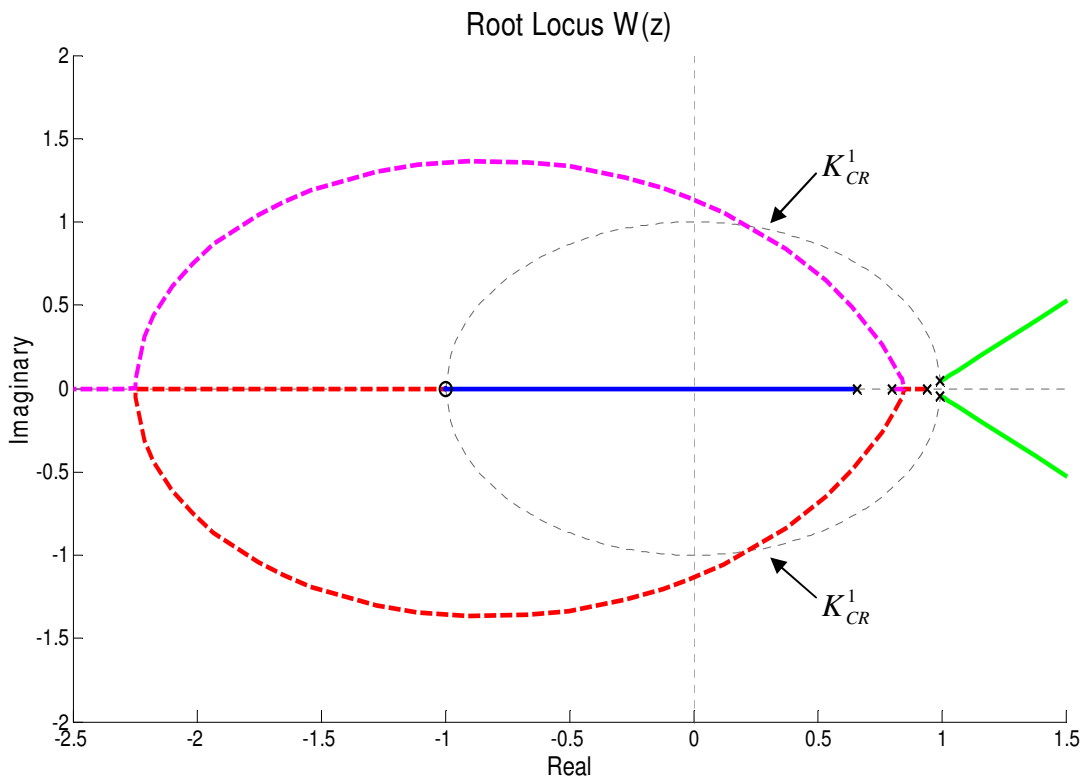
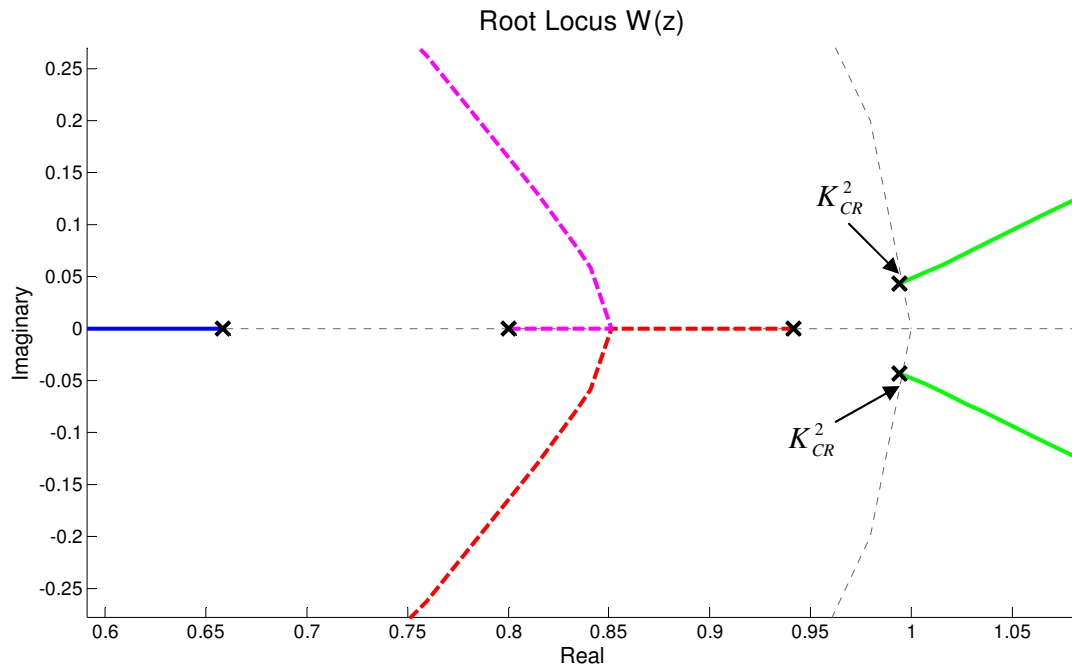


Figure 5.7a Root locus of the whole system microphone + SDM.

Figure 5.7b Inset of the root locus of  $W(z)$ 

The relative degree of  $W(z)$  is 3, so that the root locus has three branches which tend to infinity. Figure 5.7a shows that there are four points where the root locus get out from the unit circle, for  $K_{CR}^1 = 1.28$  and  $K_{CR}^2 = 8.79 \cdot 10^{-7}$ . The feedback force is due to electrostatic force, which has a proportional constant to the square of voltage of about  $4.62 \cdot 10^{-7} \text{ N/V}^2$ . Scaling the critical gains we obtain  $K_{CR}^2 = 1.9$ . This means the feedback voltage has to have an absolute value less then 1.38V.

### 5.1.3 Experimental measurements

To test the effectiveness of the proposed configuration, a deep characterization of each component of the digital readout interface has been performed [35]. Unfortunately there was not any microphone to test with the readout interface, so that the microphone has been emulated using a low pass filter with a corner frequency at 20kHz. In this way, we can at least verify the stability of the whole system and the extra shaping due to the presence of the low pass filter. Figure 5.8 shows the noise spectrum with and without the low pass filter, namely with or without the feedback.

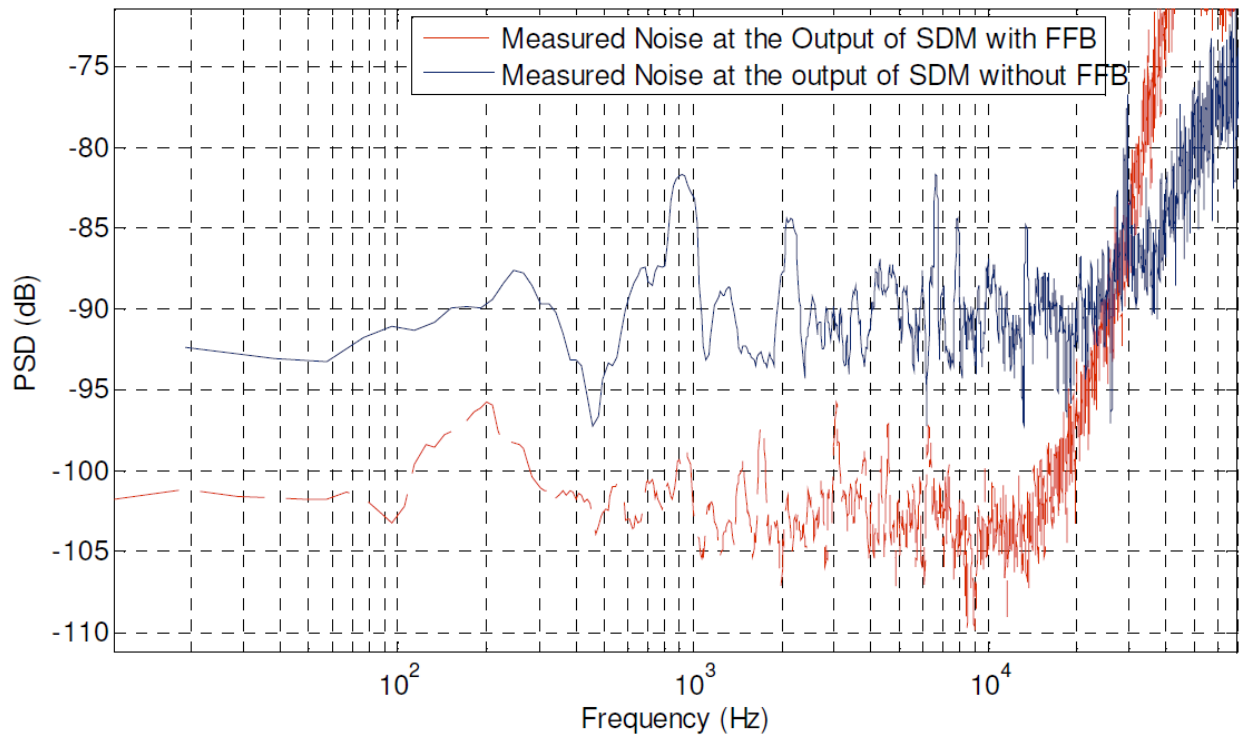


Figure 5.8 Comparison between the noise spectrum with and without force feedback applied to the low pass filter

Figure 5.8 shows the improvement on the noise shaping: the noise in band is reduced because the low pass filter attenuates the quantization noise. The integrated A-weighted noise in the band 20Hz-20kHz is -63dBA without the low pass filter and -73dBA in closed loop configuration.

## 5.2. Frequency tuning

The aim of this control application is to maximize the microphone output at a given frequency. A microphone can be approximated by a second order system as shown in figure 5.9

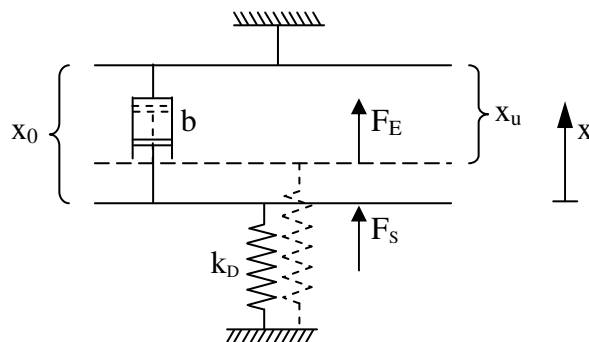


Figure 5.9 Schematic of the reduced model of the microphone

The dynamic of the system is described by the following equation:

$$m_D \ddot{x} + b \dot{x} + k_D x = F_E(x) + F_S \quad (5.6)$$

where  $m_D$  is the mass of the moving membrane,  $b$  is the damping coefficient due to the air resistance in the air gap,  $F_E$  is the electrostatic force due to the bias voltage and  $F_S$  is the force of the acoustic wave.

When the microphone is polarized, at steady state the membrane moves toward the backplate and reaches an equilibrium point ( $x_u$ ), which will be the working point of the microphone.

For small displacements of the moving membrane, the electrostatic force can be approximated by a first order linearization around the working point:

$$F_E(x) = \frac{1}{2} \varepsilon A \frac{V_{BIAS}^2}{(x_0 - x)^2} \approx \frac{1}{2} \varepsilon A \frac{V_{BIAS}^2}{x_u^2} + \varepsilon A \frac{V_{BIAS}^2}{x_u^3} [x - (x_0 - x_u)] \quad (5.7)$$

Furthermore, at the equilibrium  $k_D(x_0 - x_u) = \frac{1}{2} \varepsilon A \frac{V_{BIAS}^2}{x_u^2}$  and substituting in (5.6) we obtain

$$m_D \ddot{x} + b \dot{x} + \left( k_D - \varepsilon A \frac{V_{BIAS}^2}{x_u^3} \right) [x - (x_0 - x_u)] = F_S \quad (5.8)$$

Defining  $p = x - (x_0 - x_u)$ , the (5.8) can be written as

$$\ddot{p} + 2\xi \omega_m \dot{p} + \omega_m^2 p = F_S \quad (5.9)$$

with  $\omega_m^2 = \frac{1}{m_D} \left( k_D - \varepsilon A \frac{V_{BIAS}^2}{x_u^3} \right)$  and  $2\xi \omega_m = \frac{b}{m_D}$

To maximize the output of the microphone with respect to an incoming acoustic wave, we have to match the resonance frequency of the microphone with that one of the sound wave. Indeed, if the acoustic input has angular frequency  $\omega_s$ , the gain of the microphone is given by

$$G(\omega_s, V_{BIAS}) \approx \frac{1}{\sqrt{(\omega_m^2 - \omega_s^2) + (2\xi \omega_m \omega_s)^2}} \quad (5.10)$$

and the gain is maximized if the frequency of the system  $\omega_m$  matches the frequency of the input sound wave  $\omega_s$ .

However, (5.8) shows that the electrostatic force acts on the system softening the spring constant. Therefore, we can only decrease the resonant frequency of the microphone. This means that to maximize the microphone output adjusting the bias voltage, the resonance frequency of the microphone has to be designed higher than the frequency of the input sound wave.

### 5.2.1 Extremum seeking control

The extremum seeking control is a particular kind of adaptive control law which, given a parameterized function, can adapt those parameters in order to keep the function to its extremum value. There are many schemes to implement an extremum seeking controller, based on different operating principles, but the most popular and effective is the perturbation method [67].

The main idea of the extremum seeking controller is to estimate the gradient of a parameterized function we want to maximize or minimize with respect to that parameter. Then this parameter is updated to the value where the local gradient of the function is zero. To sense the gradient of the function, a perturbation is applied to the system and the parameter adjusted accordingly.

To understand the working principle of the extremum seeking control let us consider the following schematic as in [67, 68]

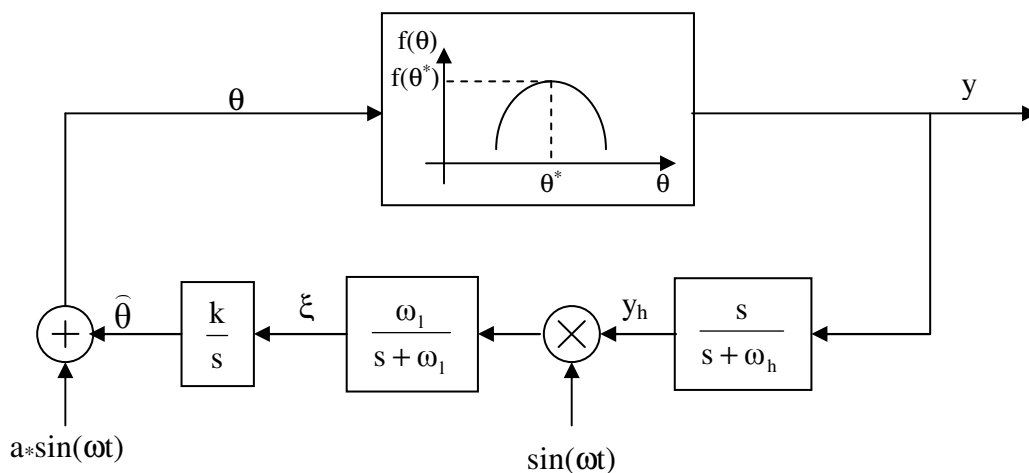


Figure 5.10 Schematic of a classical extremum seeking controller

Let be  $\theta$  the tuneable parameter and  $f(\theta)$  a static map. We assume there exists a value  $\theta^*$  of  $\theta$  such that  $\partial f(\theta^*)/\partial\theta = 0$  and  $\partial^2 f(\theta^*)/\partial\theta^2 < 0$  or  $\partial^2 f(\theta^*)/\partial\theta^2 > 0$ . In other words, we assume that the function  $f(\theta)$  has a local maximum or minimum in  $\theta = \theta^*$ .

Let consider  $f(\theta)$  has a maximum in  $\theta^*$ . Similar consideration can be done in case of a minimum. Intuitively, when the perturbation  $a \sin(\omega t)$  is applied to the input  $\theta$ , it gives rise to an oscillating output signal  $y$  that will be in phase or out of phase with the perturbation signal. Indeed, the function  $f(\theta)$  evaluated in  $\hat{\theta}$  and perturbed by the signal  $a \sin(\omega t)$  can be approximated by the first order Taylor expansion:

$$f(\hat{\theta} + a \sin(\omega t)) \approx f(\hat{\theta}) + \left. \frac{\partial f(\theta)}{\partial \theta} \right|_{\theta=\hat{\theta}} a \sin(\omega t) \quad (5.11)$$

where the oscillating term is in phase with the perturbation if  $\hat{\theta} < \theta^*$  and out of phase if  $\hat{\theta} > \theta^*$ . The high pass filter and the following demodulation retrieve this information. The high pass filter removes the DC components to keep the oscillating component

$$y_h \approx \left. \frac{\partial f(\theta)}{\partial \theta} \right|_{\theta=\hat{\theta}} a \sin(\omega t) \quad (5.12)$$

which is proportional to the gradient of the function in  $\hat{\theta}$ . Demodulating the output of the high pass filter with the same signal used to perturb the system and filtering with a low pass filter, we can retrieve the value of the gradient of  $f(\theta)$  in a neighbourhood of  $\hat{\theta}$ . Indeed,  $\xi$  is given by

$$\xi = \sin(\omega t) y_h = \left. \frac{\partial f(\theta)}{\partial \theta} \right|_{\theta=\hat{\theta}} a \sin^2(\omega t) = \frac{1}{2} a \left. \frac{\partial f(\theta)}{\partial \theta} \right|_{\theta=\hat{\theta}} - \frac{1}{2} a \left. \frac{\partial f(\theta)}{\partial \theta} \right|_{\theta=\hat{\theta}} \cos(2 \omega t)$$

where we have exploited the trigonometric formula  $\sin^2(\omega t) = (1 - \cos(2\omega t))/2$ . The low pass filter extracts the continuous component retrieving a gradient estimation:

$$y_l \approx \frac{1}{2} a \left. \frac{\partial f(\theta)}{\partial \theta} \right|_{\theta=\hat{\theta}} \quad (5.13)$$



Finally,  $\hat{\theta}$  is given by the integral of the estimated gradient, which defines the following updating rule:

$$\dot{\hat{\theta}} = \frac{1}{2} k a \frac{\partial f(\theta)}{\partial \theta} \quad (5.14)$$

On the other hand, when  $\theta = \theta^*$ ,  $f(\theta)$  can be developed in Taylor series around its maximum,

where  $\left. \frac{\partial f(\theta)}{\partial \theta} \right|_{\theta=\theta^*} = 0$ , thus

$$f(\theta) \approx f(\theta^*) + \frac{1}{2} \left. \frac{\partial^2 f(\theta)}{\partial \theta^2} \right|_{\theta=\theta^*} (\theta - \theta^*)^2 \quad (5.15)$$

Let us to define the estimation error as  $\tilde{\theta} = \hat{\theta} - \theta^*$ , thus  $\dot{\tilde{\theta}} = \dot{\hat{\theta}}$ . Substituting (5.15) into (5.14), the dynamic of the estimation error is given by

$$\dot{\tilde{\theta}} = \frac{1}{2} k a \left. \frac{\partial^2 f(\theta)}{\partial \theta^2} \right|_{\theta=\theta^*} \tilde{\theta} \quad (5.16)$$

The (5.16) shows that choosing properly  $a$  and  $k$ , the estimation error is locally asymptotically stable and it converge to zero, that is  $\hat{\theta} = \theta^*$ .

In our case, we use a modified schematic, as shown in figure 5.11

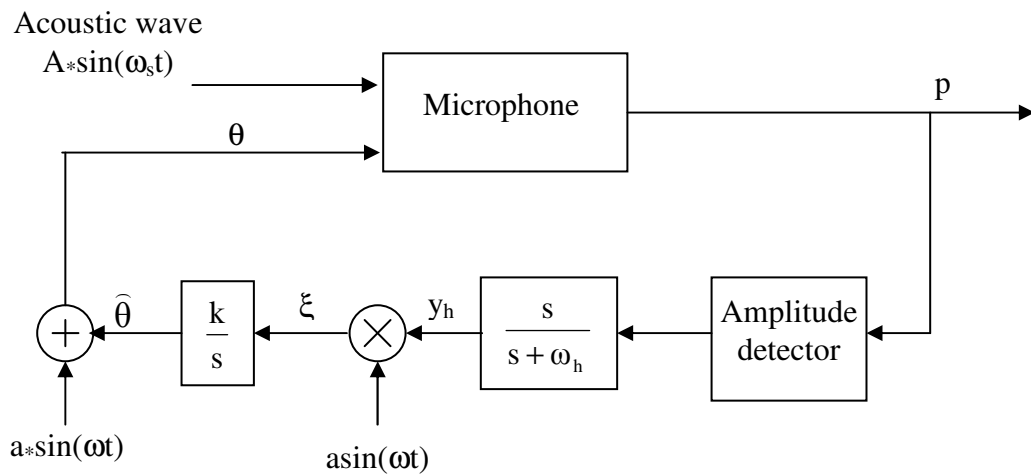


Figure 5.11 Schematic of the proposed extremum control loop

At the output of the microphone, an amplitude detector has been used. Indeed, the aim of this control loop is to maximize the amplitude of microphone output voltage, thus an amplitude detector has been used at the output of the microphone to measure such an amplitude. It is basically the detector proposed in [42] and here briefly reported.

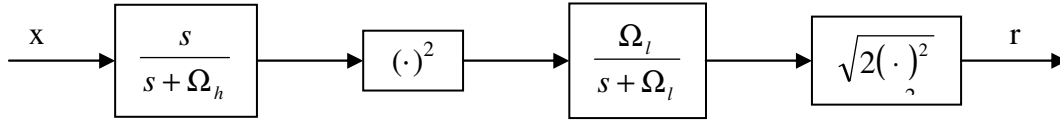


Figure 5.12 Schematic of the amplitude detector

The output of the microphone can be represented as  $x(t) = x_0 + r(t)\sin(\omega t)$ . The amplitude  $r(t)$  will be slowly varying because of the perturbation applied by the extremum seeking controller. To get  $r(t)$  amplitude first the constant term  $x_0$  is removed by the high pass filter, thus is squared. The square produce two terms: one constant,  $r^2(t)/2$ , and the other one oscillating  $r_2(t)\cos(2\omega t)$ . The low pass filter removes the oscillating part, thus we finally can get the information on the slowly varying amplitude  $r(t)$ .

### 5.2.2 Stability analysis

In this section proof of the stability of the proposed solution is given. The system resembles closely to the system presented in [68] and we can follow the same procedure.

To simplify the stability analysis we approximate the envelop detector with a square function. This simplification does not affect the conclusions [71] but simplify the analysis. We choose as a tuneable parameter  $\theta(t)$  the difference  $\omega_m^2 - \omega_s^2$ , so that  $\omega_m^2 = \omega_s^2 + \theta(t)$ . The simplified closed loop system is described by the following equations:

$$\begin{aligned} \ddot{p} + 2\xi \omega_m \dot{p} + (\omega_s^2 + \hat{\theta} + a \sin(\omega_p t))p &= A \sin(\omega_s t) \\ \dot{\eta} &= \omega_h (p^2 - \eta) \\ \dot{\hat{\theta}} &= k(p^2 - \eta)a \sin(\omega_p t) \end{aligned} \quad (5.17)$$

where  $\eta$  is the mean value of the microphone output.

We change the time scale of the system from  $t$  to  $\omega_s t$  to get the following system:

$$\begin{aligned} \frac{d^2 p}{d\tau^2} + \frac{2\xi \omega_m}{\omega_s} \frac{dp}{d\tau} + \left( \frac{\omega_s^2 + \hat{\theta} + a \sin(\omega_p t)}{\omega_s^2} \right) p &= \frac{A}{\omega_s^2} \sin(\omega_s t) \\ \frac{d\eta}{d\tau} &= \frac{\omega_h}{\omega_s} (p^2 - \eta) \\ \frac{d\hat{\theta}}{d\tau} &= \frac{k}{\omega_s} (p^2 - \eta) a \sin(\omega_p t) \end{aligned} \quad (5.18)$$

Defining

$$\varepsilon\alpha = \frac{A}{\omega_s^2} \quad \varepsilon\beta = \frac{2\xi \omega_m}{\omega_s} \quad \varepsilon\tilde{\theta} = \frac{\hat{\theta}}{\omega_s^2} \quad \varepsilon\gamma = \frac{a}{\omega_s^2} \quad \varepsilon\delta = \frac{\omega_h}{\omega_s} \quad \varepsilon\rho = \frac{k a}{\omega_s^3}$$

we get

$$\begin{aligned} \frac{d^2 p}{d\tau^2} + p &= \varepsilon g\left(p, \frac{dp}{d\tau}, \tilde{\theta}, t, \tau\right) \\ \frac{d\eta}{d\tau} &= \varepsilon\delta(p^2 - \eta) \\ \frac{d\hat{\theta}}{d\tau} &= \varepsilon\rho(p^2 - \eta) \sin(\omega_p t) \end{aligned} \quad (5.19)$$

where  $g\left(p, \frac{dp}{d\tau}, \tilde{\theta}, t, \tau\right) = \alpha \sin(\omega_s t) - \beta \frac{dp}{d\tau} - \tilde{\theta} p - \gamma \sin(\omega_p t) p$

Representing the system using a Van der Pol transformation, we get a system in the form suitable to apply averaging. Let's change the coordinates:

$$\begin{aligned} y = u \cos(\tau) - v \sin(\tau) &\quad u = y \cos(\tau) - \frac{dy}{d\tau} \sin(\tau) &\quad \frac{du}{d\tau} = -\left(\frac{d^2 y}{d\tau^2} + y\right) \sin(\tau) \\ \frac{dy}{d\tau} = -u \sin(\tau) - v \cos(\tau) &\Rightarrow v = -y \sin(\tau) - \frac{dy}{d\tau} \cos(\tau) &\Rightarrow \frac{dv}{d\tau} = -\left(\frac{d^2 y}{d\tau^2} + y\right) \cos(\tau) \end{aligned} \quad (5.20)$$

Substituting (5.20) in (5.19) we get

$$\begin{aligned}
 \frac{du}{d\tau} &= -\varepsilon g(u, v, \tilde{\theta}, t, \tau) \sin(\tau) \\
 \frac{dv}{d\tau} &= -\varepsilon g(u, v, \tilde{\theta}, t, \tau) \cos(\tau) \\
 \frac{d\eta}{d\tau} &= \varepsilon \delta [u^2 \cos^2(\tau) + v^2 \sin^2(\tau) - 2u v \sin(\tau) \cos(\tau) - \eta] \\
 \frac{d\hat{\theta}}{d\tau} &= \varepsilon \rho [u^2 \cos^2(\tau) + v^2 \sin^2(\tau) - 2u v \sin(\tau) \cos(\tau) - \eta] \sin(\omega_p t)
 \end{aligned} \tag{5.21}$$

Now the system is  $2\pi$ -periodic with respect to  $\tau$  and it is in the canonical form to apply averaging, obtaining the following averaged system:

$$\begin{aligned}
 \frac{du_a}{d\tau} &= -\frac{1}{2\pi} \int_0^{2\pi} \varepsilon g(u, v, \tilde{\theta}, t, \tau) \sin(\tau) d\tau = -\frac{\varepsilon \alpha}{2} - \frac{\varepsilon \beta u_a}{2} - \frac{[\tilde{\theta}_a + a \sin(\omega_p t_a)] v_a}{2} \\
 \frac{dv_a}{d\tau} &= -\frac{1}{2\pi} \int_0^{2\pi} \varepsilon g(u, v, \tilde{\theta}, t, \tau) \cos(\tau) d\tau = \frac{[\tilde{\theta}_a + a \sin(\omega_p t_a)] u_a}{2} - \frac{\varepsilon \beta v_a}{2} \\
 \frac{d\eta_a}{d\tau} &= \varepsilon \delta \frac{1}{2\pi} \int_0^{2\pi} [u^2 \cos^2(\tau) + v^2 \sin^2(\tau) - 2u v \sin(\tau) \cos(\tau) - \eta] d\tau = \varepsilon \delta \left( \frac{u_a^2 + v_a^2}{2} - \eta_a \right) \\
 \frac{d\hat{\theta}_a}{d\tau} &= \varepsilon \rho \frac{1}{2\pi} \int_0^{2\pi} [u^2 \cos^2(\tau) + v^2 \sin^2(\tau) - 2u v \sin(\tau) \cos(\tau) - \eta] d\tau \sin(\omega_p t) = \varepsilon \rho \left( \frac{u_a^2 + v_a^2}{2} - \eta_a \right) \sin(\omega_p t_a)
 \end{aligned}$$

The dynamic of the system is faster than the dynamic of the control loop. We can exploit this property to apply the singular perturbation method. Changing the time scale from  $t_a$  to  $\sigma = \omega_p t_a = \omega_p \tau_a / \omega_s$ , the system can be transformed in the standard form:

$$\begin{aligned}
 \frac{\omega_p}{\omega_s} \frac{du_a}{d\tau} &= -\frac{\varepsilon \alpha}{2} - \frac{\varepsilon \beta u_a}{2} - \frac{[\tilde{\theta}_a + a \sin(\sigma)] v_a}{2} \\
 \frac{\omega_p}{\omega_s} \frac{dv_a}{d\tau} &= \frac{[\tilde{\theta}_a + a \sin(\sigma)] u_a}{2} - \frac{\varepsilon \beta v_a}{2} \\
 \frac{d\eta_a}{d\tau} &= \frac{\omega_s}{\omega_p} \varepsilon \delta \left( \frac{u_a^2 + v_a^2}{2} - \eta_a \right) \\
 \frac{d\hat{\theta}_a}{d\tau} &= \frac{\omega_s}{\omega_p} \varepsilon \rho \left( \frac{u_a^2 + v_a^2}{2} - \eta_a \right) \sin(\sigma)
 \end{aligned} \tag{5.22}$$

$\omega_p / \omega_s$  is small, so that (5.22) is in standard form to apply the singular perturbation method separating the fast dynamics of the microphone from the slow dynamic of the control loop. To

find the reduced model we set  $\omega_p/\omega_s = 0$  in the first two equations of (5.22), solve the equation in  $u_a$  and  $v_a$ , finding the quasi-steady state solution and substitute those values in the second two equations of (5.22):

$$\begin{aligned} 0 &= \frac{\varepsilon\alpha}{2} - \frac{\varepsilon\beta u_a}{2} - \frac{[\tilde{\theta}_a + a \sin(\sigma)]v_a}{2} \\ 0 &= \frac{[\tilde{\theta}_a + a \sin(\sigma)]u_a}{2} - \frac{\varepsilon\beta v_a}{2} \end{aligned} \Rightarrow \begin{aligned} u_{a,qss} &= \frac{\alpha\beta}{\beta^2 + [\tilde{\theta}_a + a \sin(\sigma)]^2} \\ v_{a,qss} &= \frac{\alpha[\tilde{\theta}_a + a \sin(\sigma)]}{\beta^2 + [\tilde{\theta}_a + a \sin(\sigma)]^2} \end{aligned} \quad (5.23)$$

Substituting the (5.23) in the last two equations of (5.22) we get the quasi-steady state model:

$$\begin{aligned} \frac{d\eta_{a,qss}}{d\tau} &= \frac{\omega_s}{\omega_p} \varepsilon\delta \left( \frac{1}{2} \frac{\alpha^2}{\beta^2 + [\tilde{\theta}_{a,qss} + a \sin(\sigma)]^2} - \eta_{a,qss} \right) \\ \frac{d\hat{\theta}_{a,qss}}{d\tau} &= \frac{\omega_s}{\omega_p} \varepsilon\rho \left( \frac{1}{2} \frac{\alpha^2}{\beta^2 + [\tilde{\theta}_{a,qss} + a \sin(\sigma)]^2} - \eta_{a,qss} \right) \sin(\sigma) \end{aligned} \quad (5.24)$$

The reduced model (5.24) is  $2\pi$ -periodic with respect to  $\sigma$  and  $O(\varepsilon_1)$ , where

$$\varepsilon_1 = \max \left\{ \frac{\omega_s}{\omega_p} \varepsilon\delta, \frac{\omega_s}{\omega_p} \varepsilon\rho \right\}, \text{ and the system can be averaged again:}$$

$$\begin{aligned} \frac{d\eta_{aa,qss}}{d\tau} &= \frac{1}{2\pi} \int_0^{2\pi} \frac{\omega_s}{\omega_p} \varepsilon\delta \left( \frac{1}{2} \frac{\alpha^2}{\beta^2 + [\tilde{\theta}_{aa,qss} + a \sin(\sigma)]^2} - \eta_{aa,qss} \right) d\sigma = \frac{\omega_s}{\omega_p} \varepsilon\delta (\alpha^2 I_1(\tilde{\theta}_{aa,qss}) - \eta_{aa,qss}) \\ \frac{d\hat{\theta}_{aa,qss}}{d\tau} &= \frac{1}{2\pi} \int_0^{2\pi} \frac{\omega_s}{\omega_p} \varepsilon\rho \left( \frac{1}{2} \frac{\alpha^2}{\beta^2 + [\tilde{\theta}_{aa,qss} + a \sin(\sigma)]^2} - \eta_{aa,qss} \right) \sin(\sigma) d\sigma = \frac{\omega_s}{\omega_p} \varepsilon\rho \alpha^2 I_2(\tilde{\theta}_{aa,qss}) \end{aligned} \quad (5.25)$$

where

$$I_1(\tilde{\theta}_{aa,qss}) = \frac{1}{2\pi} \int_0^{2\pi} \frac{1}{2} \frac{1}{\beta^2 + [\tilde{\theta}_{aa,qss} + a \sin(\sigma)]^2} d\sigma \quad I_2(\tilde{\theta}_{aa,qss}) = \frac{1}{2\pi} \int_0^{2\pi} \frac{1}{2} \frac{\sin(\sigma)}{\beta^2 + [\tilde{\theta}_{aa,qss} + a \sin(\sigma)]^2} d\sigma$$

Defining a new state vector  $x = [\bar{\eta}_{aa,qss}, \tilde{\theta}_{aa,qss}]$ , where  $\bar{\eta}_{aa,qss} = \eta_{aa,qss} - \alpha^2 I_1(0)$ , the system can be expressed as a simple time-invariant system  $\dot{x} = f(x)$ , with

$$f(x) = \begin{bmatrix} \frac{\omega_s}{\omega_p} \varepsilon \delta (\alpha^2 [I_1(\tilde{\theta}_{aa,qss}) - I_1(0)] - \bar{\eta}_{aa,qss}) \\ \frac{\omega_s}{\omega_p} \varepsilon \rho I_2(\tilde{\theta}_{aa,qss}) \end{bmatrix} \quad (5.26)$$

The system has an equilibrium point in  $(0,0)$ . Indeed, the integral of  $I_2(0)$  is zero, because integral of an odd function over its period. This equilibrium point is exponentially stable. Indeed the Jacobian matrix of the system is

$$J_{f(x)}|_{x=0} = \begin{bmatrix} -\frac{\omega_s}{\omega_p} \varepsilon \delta & 0 \\ 0 & \frac{\omega_s}{\omega_p} \varepsilon \rho I_3 \end{bmatrix} \quad (5.27)$$

where

$$\frac{\partial}{\partial \tilde{\theta}_{aa,qss}} \left( \frac{1}{2\pi} \int_0^{2\pi} \frac{1}{\beta^2 + [\tilde{\theta}_{aa,qss} + a \sin(\sigma)]^2} d\sigma \right) \Big|_{\tilde{\theta}_{aa,qss}=0} = -\frac{1}{2\pi} \int_0^{2\pi} \frac{a \sin(\sigma)}{\beta^2 + a \sin^2(\sigma)} d\sigma \quad (5.28)$$

$$I_3 = \frac{\partial}{\partial \tilde{\theta}_{aa,qss}} \left( \frac{1}{2\pi} \int_0^{2\pi} \frac{\sin(\sigma)}{\beta^2 + [\tilde{\theta}_{aa,qss} + a \sin(\sigma)]^2} d\sigma \right) \Big|_{\tilde{\theta}_{aa,qss}=0} = -\frac{1}{2\pi} \int_0^{2\pi} \frac{\sin^2(\sigma)}{[\beta^2 + a \sin^2(\sigma)]^2} d\sigma \quad (5.29)$$

(5.28) is the integral of an odd function over its period, and it is zero. (5.29) is the integral of a non-positive function, so that the integral  $I_3$  will be negative, thus the Jacobian matrix (5.27) is Hurwitz and the equilibrium point of (5.26) is exponentially stable. Thus, using the averaging theorem [72, Theorem 10.4], the system (5.24) converges exponentially to zero in a

$O(\varepsilon_1)$ -neighbourhood, where  $\varepsilon_1 = \max \left\{ \frac{\omega_s}{\omega_p} \varepsilon \delta, \frac{\omega_s}{\omega_p} \varepsilon \rho \right\} = \max \left\{ \frac{\omega_h}{\omega_p}, \frac{k a}{\omega_p \omega_s^2} \right\}$ , that is

$$\eta_{a,qss} - \alpha^2 I_1(0) \rightarrow O(\varepsilon_1) \text{ exponentially}$$

$$\tilde{\theta}_{a,qss} \rightarrow O(\varepsilon_1) \text{ exponentially}$$

The system (5.24) is the reduced model of the singularly perturbed system (5.22) and by the Tikhonov theorem [72, Theorem 11.2] we have that

$$\eta_a - \eta_{a,qss} \rightarrow O(\omega_p/\omega_s) \text{ exponentially}$$

$$\tilde{\theta}_a - \tilde{\theta}_{a,qss} \rightarrow O(\omega_p/\omega_s) \text{ exponentially}$$

because the boundary-layer model associated to the system (5.22)

$$\begin{aligned} \frac{du_b}{d\tau} &= -\frac{\varepsilon \beta u_b}{2} - \frac{\varepsilon [\tilde{\theta}_a + a \sin(\sigma)] v_b}{2} \\ \frac{dv_b}{d\tau} &= \frac{\varepsilon [\tilde{\theta}_a + a \sin(\sigma)] u_a}{2} - \frac{\varepsilon \beta v_a}{2} \end{aligned} \quad (5.30)$$

where  $u_b = u_a - u_{a,qss}$  and  $v_b = v_a - v_{a,qss}$ , has an exponential equilibrium point at (0,0).

Eventually, the system (5.22) is the average of the system (5.21) and by the average theorem [72, Theorem 10.4] the trajectories of (5.21) are  $O(\varepsilon)$  far from the trajectories of (5.22), that is

$$\eta - \eta_a \rightarrow O(\varepsilon)$$

$$\tilde{\theta} - \tilde{\theta}_a \rightarrow O(\varepsilon)$$

Thus, we can conclude that  $\tilde{\theta} \rightarrow O(\varepsilon + \omega_p/\omega_s + \varepsilon_1)$ . But  $\hat{\theta} = \varepsilon \omega_s^2 \tilde{\theta}$  and  $\theta = \hat{\theta} + a \sin(\omega_p t)$ , so that  $\theta \rightarrow O(a) + O(\varepsilon \omega_s^2 (\varepsilon + \omega_p/\omega_s + \varepsilon_1))$ . The adjustable parameter  $\theta$  was defined as  $\omega_m^2 - \omega_s^2$ , so that the resonance frequency of the microphone converges to a neighbourhood of the frequency of the acoustic sound wave:  $\omega_m^2 \rightarrow \omega_s^2$  in a  $O(a) + O(\varepsilon \omega_s^2 (\varepsilon + \omega_p/\omega_s + \varepsilon_1))$  neighbourhood.

### 5.2.3 Simulation results

Some simulation has been performed to verify the feasibility of the proposed control loop.

The microphone is approximated by a second order model and described by the following equation:

$$m_D \ddot{x} + R \dot{x} + k_D x = F_{EL}(x) + F_S \quad (5.13)$$

where  $m_D$  is the moving membrane mass,  $R$  is the damping coefficient due to the air gap resistance and  $k_D$  is the spring constant of the membrane.  $F_{EL}$  is the electrostatic force due to the biasing voltage and  $F_s$  is the acoustic force due to a wave sound. The frequency tuning can be achieved only if the system is lightly damped, that is has a high quality factor and a resonant peak is present in the microphone frequency response. The first microphone design was overdamped due to the high air gap resistance value, but the second design manages to reduce it and the microphone presents a resonance peak. The sensor parameters are reported in table 5.1.

Parameter	Value
$m_D$	1.9e-9 kg
$R$	4.6e-5 kg/s
$k_D$	28.7 N/m

Table 5.1 Microphone parameters

As shown in section 5.2.2, the proposed control loop can be successfully applied to the microphone, if three different time scale can be distinguished:

- a fast time scale, associated with the vibration of the moving membrane
- a medium time scale, associated with the perturbation frequency
- a slow time scale, associated with the transient of the filters of the extremum seeking control loop.

The parameters of the extremum seeking controller are chosen accordingly to those considerations, as shown in table 5.2.

Parameter	Value
$k$	3e2
$a$	0.02
$\omega$	100Hz
$\omega_h$	10Hz

Table 5.2 Controller parameters



An estimation of the map  $f(\theta)$  of the microphone has been derived applying an input of 1Pa at 17kHz and varying the polarization voltage, which is our tuneable parameter. The map is given in figure 5.13.

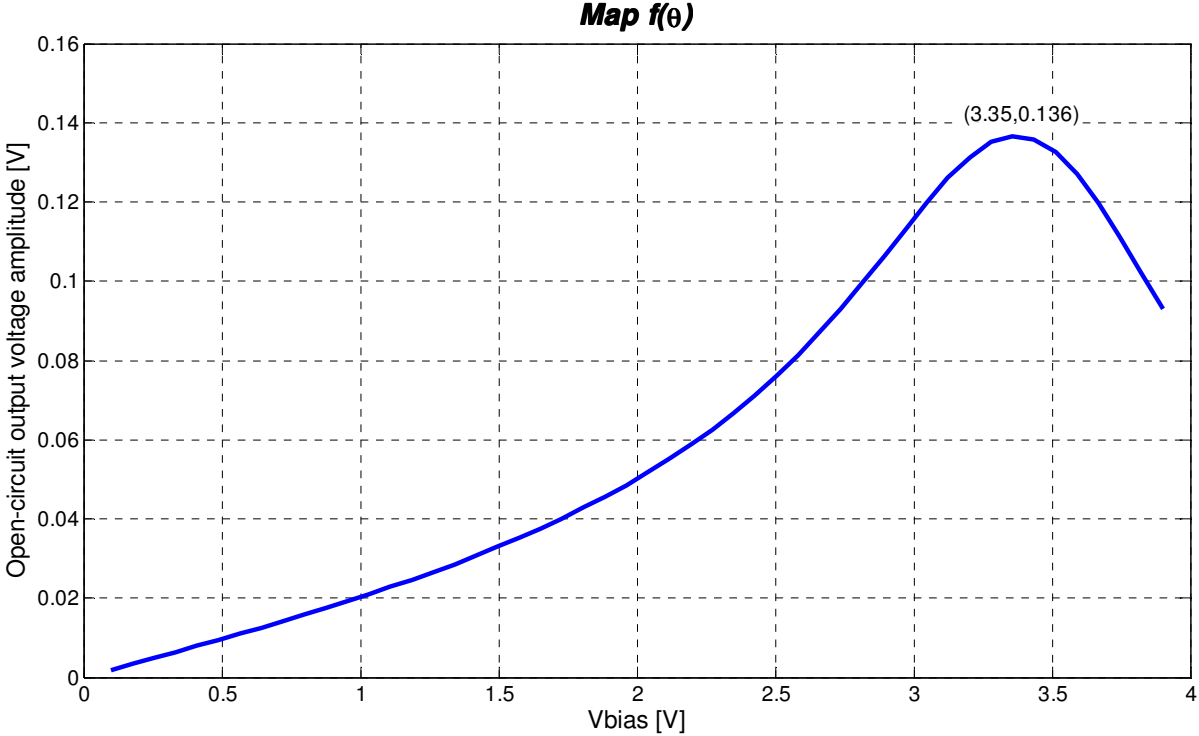


Figure 5.13 Map of  $f(\theta)$  for an acoustic sound pressure of 1Pa@17kHz

The map shows that the maximum output voltage of the microphone is 0.135V and is reached for  $V_{BIAS} \approx 3.35V$ . Figures 5.14-5.17 report the simulation results of the controller.

The simulations have been performed in two conditions: starting below the optimal bias voltage (2.5V) and above (3.55V). In both cases the controller has been able to drive the tuneable parameter to the optimum value to reach the maximum of the microphone output voltage.

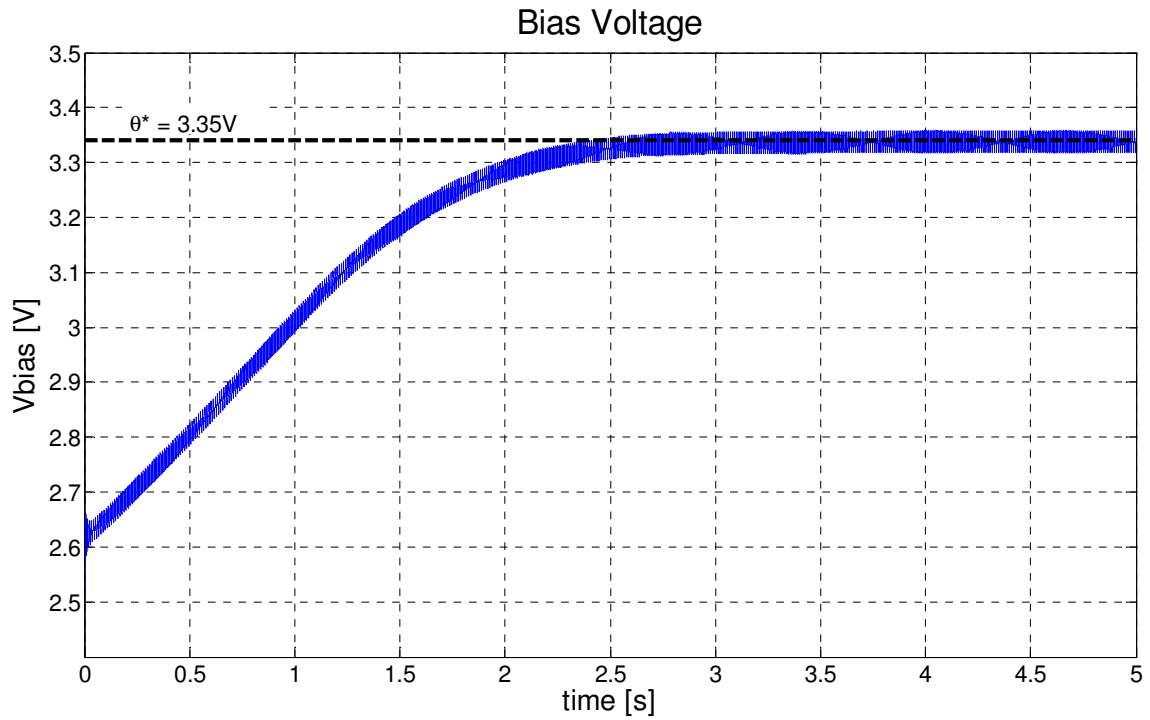


Figure 5.14 Evolution of the bias voltage of the microphone with a starting polarizing voltage of 2.5V

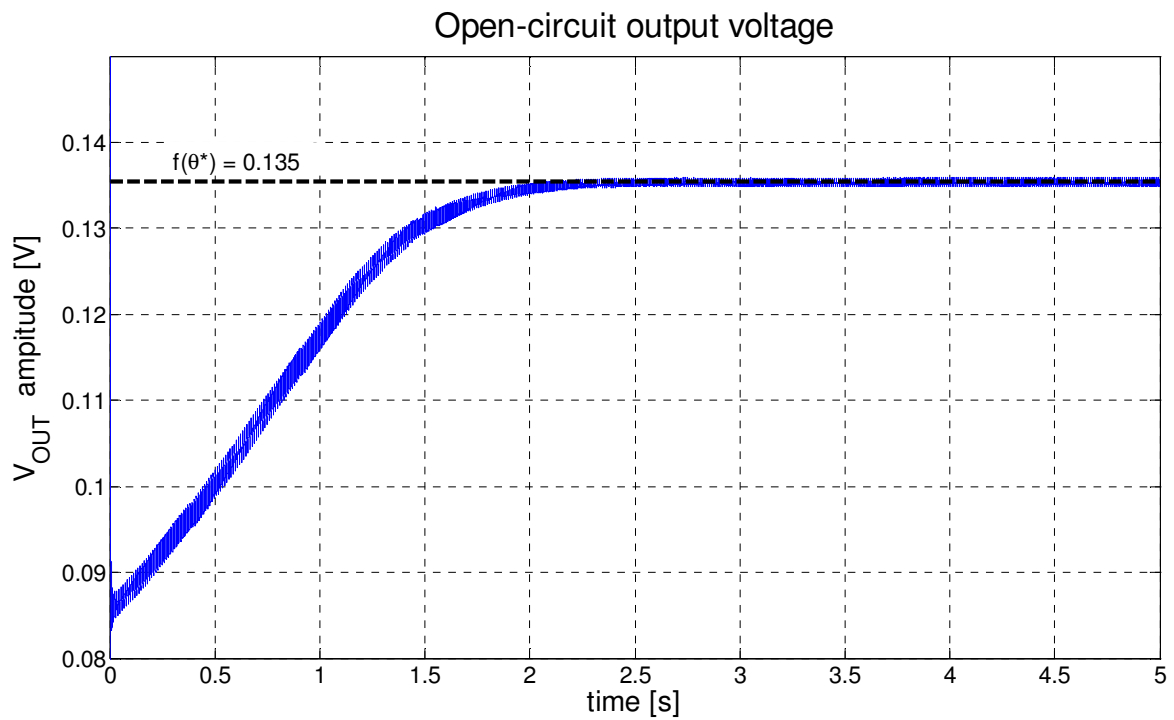


Figure 5.15 Evolution of the open-circuit output voltage of the microphone with a starting bias voltage of 2.5V

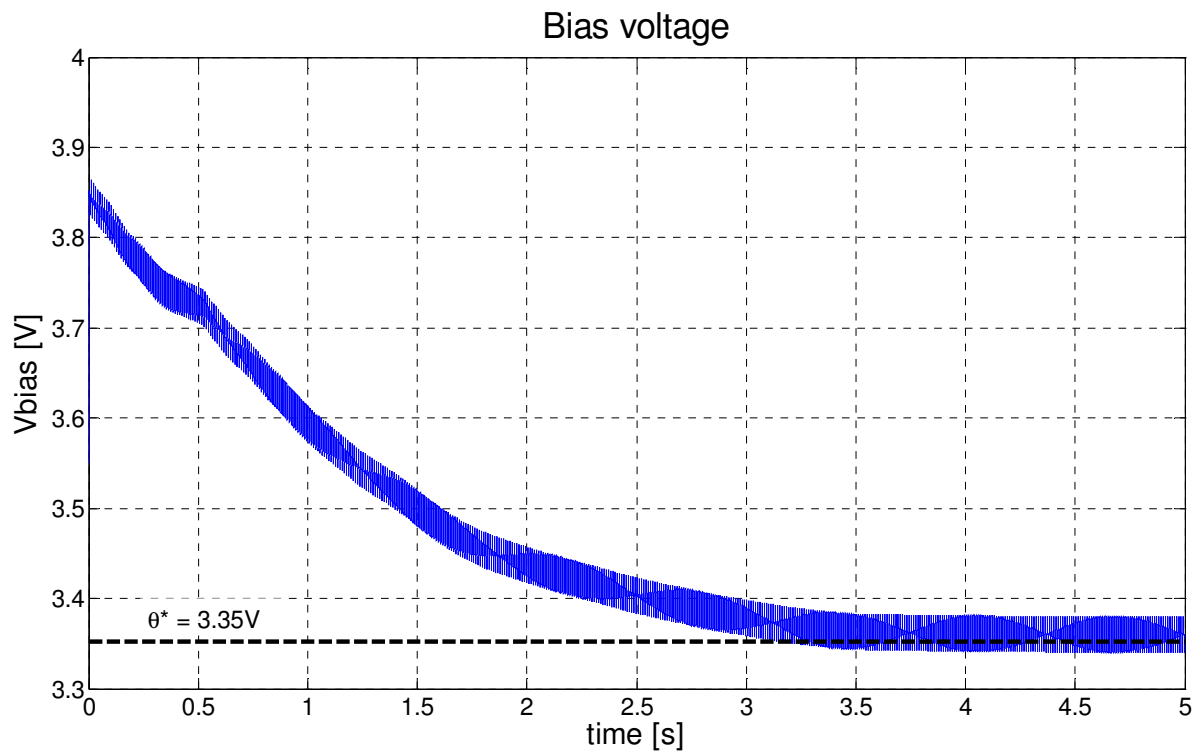


Figure 5.16 Evolution of the bias voltage of the microphone with a starting polarizing voltage of 3.5V

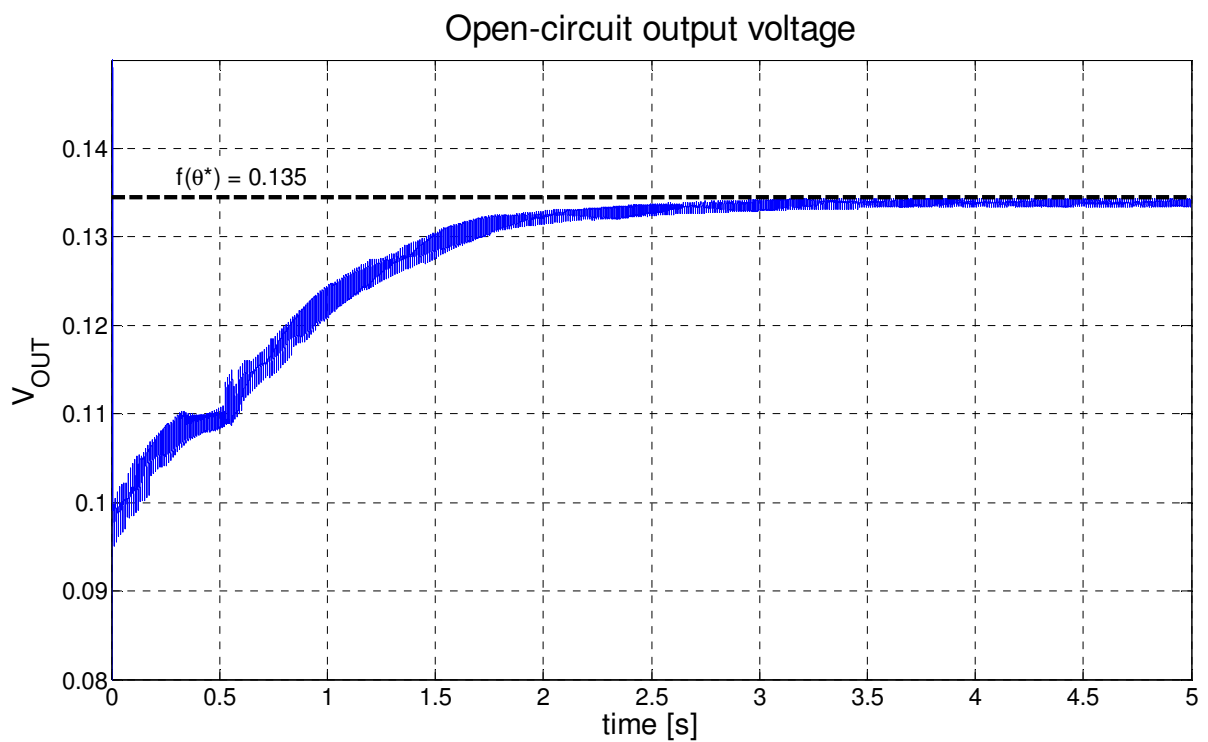


Figure 5.17 Evolution of the open-circuit output voltage of the microphone with a starting bias voltage of 2.5V

To steer the bias voltage to its optimum value, the controller takes a little time, and this is one of the issues of this kind of controller [69]. To speed up the convergence, we can increase the amplitude of the perturbation signal, or increase the gain of the integrator. As to the former solution, increasing the amplitude of the perturbation signal affects the output voltage. As to the integral gain, we cannot increase it too much, because it is like decreasing the damping of the system and it can make the system unstable [70]. Because of high integrator gain, overshoots can appear at the output. In our case overshoots can be particularly dangerous because of the pull-in limit of the bias voltage. If during the transient the bias voltage exceeds this limit the moving membrane could snap down to the backplate. In the performed simulation we used a quite high gain, and we can see the outcome in both the simulated cases. In figure 5.14 the starting bias voltage is set to 2.5, but the simulation seems to start at more than 2.6V and even more in figure 5.15, where the starting bias voltage is set at 3.5V, but because of the initial overshoot it is like the system starts from about 3.85V.

# Chapter 6

## 6. Conclusions

In this thesis a complete model of a capacitive MEMS microphone has been developed and validated comparing the simulation with the experimental results.

The microphone has been studied by the means of the electro-mechanical analogy. Each element has been studied in detail and modelled accurately with particular attention to the air gap, which has a big influence on the dynamic and noise performances of the microphone. Indeed, the air gap defines the main part of the damping coefficient of the microphone and most of all is the main source of noise. The model can fit the experimental data, as verified in Ormon, and using the same knowledge the model of IRST microphone can properly describe the designed microphone. The model of the package, which is often neglected, was included as well.

The main contribution at this level was the evaluation of the noise model. Measurements were performed and they permitted to separate the noise depending on the microphone from that one depending on the measurement setup. It was clear from the data collect that there is two main components: the well-known Brownian noise, due to the thermal agitation of the particle of air inside the air gap, and another one more subtle, the  $1/f$  component. Usually it has been confused with electronic flicker noise, but the accurate measurements performed in Omron permit to discern the low frequency electronic noise from that one inherent in the microphone. A very simple model has been developed and it can estimate with good accuracy the spectrum noise of the device. With this model, coupled with the model of the microphone, it is possible to estimate the SNR of the designed microphone, a key index and one of the main constrains concerning a microphone design.

The experimental characterizations of the produced samples permit to estimate the values of some key components of the microphone, such as the spring constant and the air gap when the microphone is not biased. The mismatching between the expected values and those found experimentally permits to highlight the residual stress present on the surface of the moving membrane.

The deep characterization of the parasitic component unveiled another relevant problem due to the non-perfect isolation of the moving membrane frame and the substrate due to the difficulties arose during the sacrificial oxide removal operation on the rear part of the microphone.

All the data collect and the following considerations permit to design the new generation of microphone.

Unfortunately, even from the preliminary test, the new generation of microphones presents high value of spring constant, and the frequency response shows a heavy roll off at low frequency. This means there is a problem with the flow-by slots around the membrane, because they do not present a high enough acoustic impedance. Maybe this is due again to the bending of the membrane because of superficial stress, which makes the moving membrane stiffer and due to the bending the flow-by slots are enlarged, reducing the acoustic impedance.

To solve partially this kind of problems, a force feedback has been applied along with the digital readout interface. Indeed, a force feedback has the property to counterbalance the displacement of the moving membrane reducing its movement, thus attenuating, at least partially, defects of the device. Using the quasi-linear approximation, the stability of both stand alone sigma delta modulator (SDM) and the whole system microphone+SDM has been proven.

Another advantage is the extra noise shaping due to the introduction of the sensor in the loop of the SDM, realizing a so-called electromechanical sigma delta converter. Indeed the sensor acts as an extra low pass filter that attenuates the noise caused by the quantizer. The effectiveness of the proposed configuration has been proved experimentally on a dummy sensor.

Finally to improve the performance of the microphone in a specific application, it has been proposed an extremum seeking controller to tune the resonance frequency of the microphone. Simulation reports the effectiveness of the solution proposed.

## 6.1. Future works

MEMS devices are revealing themselves as a very promising technology, especially concerning the condenser MEMS microphones. Due to the more and more demanding requirements, however, a deeper knowledge of the devices is necessary and modelling is becoming fundamental to design properly a microsystem. Furthermore, the uncertainties in the devices due to defects during the manufacturing process require a tiny tuning of the production process. To attenuate this problem and relax the constrains in the manufacturing process, it is possible to apply a control law. The control to tune the resonance frequency, for example, proves the flexibility of a system when supported by a controller.

Force feedback turns out to be a helpful solution to improve the performance of the microphone, such as noise, nonlinearities and dynamic range. Further investigation should be performed in order to characterize more in detail the closed loop system, such as the noise and harmonic recycling, as well as a deeper study on the stability of the electromechanical sigma delta converter.

# Bibliography

- [1] J. Bergqvist, "Finite element modelling and characterization of a silicon condenser microphone with a highly perforated back plate", *Sensors and Actuators A*, vol. 39, 1993, pp 191-200.
- [2] G. W. Elko, F. Pardo, D. López, D. Bishop and P. Gammel, "Capacitive MEMS Microphones", *Bell Labs Technical Journal*, vol. 10, issue 3, 2005, pp. 187-198.
- [3] P.R. Scheeper, A.G.H. Van Der Donk, W. Olthuis and P. Bergveld, "A review of silicon microphones", *Sensors and Actuators A*, 1994, vol. 44, pp. 1-11
- [4] G. M. Sessler, "SiliconMicrophones", . *Audio Eng. Soc.*, Vol. 44, no. 1/2, 1996 Jan/Feb, pp. 16-21.
- [5] Y. B. Ning, A. W. Mitchell<sup>1</sup> and R. N. Tait, "Fabrication of a silicon micromachined capacitive microphone using a dry-etch process", *Sensors and Actuators A*, Vol. 53, May 1996, pp 237-242
- [6] M. Royer, J. O. Holmen, M. A. Wurm, O. S. Aadland and M. Glenn, "ZnO on Si integrated acoustic sensor", *Sensors and Actuators A*, 1983, vol.4, pp. 357-362.
- [7] T. Bourouina, S. Spirkovitch, F. Baillieu and C. Vauge, "A new condenser microphone with a p+ silicon membrane", *Sensors and Actuators A*, vol. 31, 1992, pp. 149-152.
- [8] W. Kuhnel and G. Hess, "Micromachined Subminiature Condenser Microphones in Silicon", *Sensors and Actuators A*, vol 32, 1992, pp. 560-564.
- [9] J.Bergqvist and F. Rudolf, "A silicon Condenser microphone using bond and etch-back technology", *Sensors and Actuators A*, vol. 45, 1994, pp.115-124.
- [10] M. Pedersen, W. Olthuis and P. Bergveld, "A silicon condenser microphone with polyimide diaphragm and backplate", *Sensors and Actuators A*, vol. 63, 1997, pp. 97-104.
- [11] A. Torrkeli, H. Sipola, H. Sepa, J. Saarilahti, O. Rusanen and J. Hietanen, "Capacitive Microphone with Low-stress Polysilicon Membrane and High-stress Polysilicon Backplate", *Euroensors XIII*, September 12-15, 1999, The Hague, The Netherlands.
- [12] R. Kressmann, M. Klaiber, G. Hess, "Silicon Condenser microphones with corrugated silicon oxide/nitride electret membranes", *Sensors and Actuators A*, vol. 100, 2002, pp. 301-309.
- [13] P.R. Scheeper, W. Olthuis and P. Bergvwld, "The design, fabrication and testing of corrugated silicon nitride diaphragms", *IEEE J. Microelectromech. Syst.*, 1994, vol 13, issue 1, pp. 36-42.
- [14] A.G.H. Van Der Donk, P.R. Scheeper, W. Olthuis and P. Bergveld, "Modelling of silicon condenser microphones", *Sensors and Actuators A*, vol. 40, 1994, pp. 203-216.
- [15] C. W. T. and J. Miaob, "Analytical modeling for bulk-micromachined condenser microphones", *J. Acoust. Soc. Am.*, vol. 120, issue 2, August 2006.
- [16] B. A. Ganji and B. Y. Majlis, "Condenser Microphone performance Simulation using equivalent circuit method", *ICSE2004 Proc. 2004*, Kuala Lumpur, Malaysia, pp. 22-29.
- [17] M. Földner, A. Dehé, and R. Lerch, "Analytical Analysis and Finite Element Simulation of Advanced Membranes for Silicon Microphones", *IEEE Sensors Journal*, vol. 5, no. 5, october 2005, pp. 857-863.
- [18] P. Gangemi, *Dynamic Responses of Rectangular and Circular Plates with Various Boundary Conditions*", Bachelor Thesis, University of New South Wales.
- [19] D. Maier-Schneider, J. Maibach and E. Obermeier, "A New Analytical Solution for the Load-Deflection of Square Membranes" *J. Microelectromech. Systems*, vol. 4, no. 4, December 1995, pp. 238-241.

- [20] C. T. Loy, S. C. Pradhan, T. Y. Ng and K. Y. Lam, "A series solution approach to an analytical load-deflection relation for the measurement of mechanical properties of thin films", *J. Miromech. Microeng.*, vol. 9, 1999, pp. 341-344.
- [21] Z. Skvor, "On the acoustical resistance due to viscous losses in the air gap of electrostatic Transducers", *Acustica*, vol. 19, 1967/68, pp. 295-299.
- [22] A. J. Zuckerwar, "Theoretical response of condenser microphones" *J. Acoust. Soc. Amer.*, vol 64, Nov. 1978pp. 1278-1285.
- [23] T. Veijola, "End Effects of Rare Gas flow in Short Channels and in Squeezed-Film Dampers", *Proc. of MSM 2002*, San Juan, Puerto Rico, April 21-25, pp. 104-107.
- [24] T. Veijola, T. Tintunen, H. Nieminen, V. Ermolov and T. Ryhanen, "Gas Damping Model for a RF MEM Switch and its Dyamic Characteristics", *Proc. of IMS 2002*, Seattle, WA, June 2-7, pp. 1213-1216.
- [25] T. Veijola and T. Mattila, "Compact Squeezed-Film Damping Model for Perforated Surface", *Proc. of Transducers 2001*, Munchen, Germany, June 10-14, pp. 1506-1509.
- [26] T. Veijola, "Analytic Model for Perforated Squeezed-Film Dampers", *Proc. of DTIP 2006*, Stresa, April 26-28, pp. 36-41.
- [27] L. L. Beranek, "Acoustics", 1996, Acoustical Society of America, New York.
- [28] S. B. Horowitz, "Design and characterization of compliant bakcplate helmholtz resonators", M. Sc. Thesis, 2001, University of Florida.
- [29] A. Selametb and I. Lee, "Helmholtz resonator with extended neck", *J. Acoust. Soc. Am.*, vol. 113, issue 4 , Pt 1, April 2003, pp. 1975-1985.
- [30] A. S. Hersh amd B. Walker, "Fluid Mechanical Model of the Helmholtz Resonator", NASA Contractor Report, September 1977.
- [31] H.L. Chau and K. D. Wise, "Scaling Limits in Batch Fabricated Silicon Pressure Sensors", *IEEE Trans. On Electron Devices*, vol. ED-34, no. 4 April 1987, pp. 850-858.
- [32] V. Tarnow, "The lower limit of detectable sound pressures", *J. Acoust. Soc. Am.*, vol. 81, Issue 1, July 1987.
- [33] T. B. Gabrielson, "Mechanical Thermal Noise in Micromachined Acoustic and Vibration Sensors", *IEEE Trans. on Electron Devices*, vol. 40, no. 5, May 1993.
- [34] A. J. Zuckerwar, "Measured 1/f noise in the membrane motion of condenser microphones", *J. Acoust. Soc. Am.*, vol. 95, issue 3, March 1994.
- [35] A. S. Jawed, "CMOS Readout Interfaces for MEMS Capacitive Microphones", PhD Thesis, 2009.
- [36] S. Chowdhury, M. Ahmadi and W. C. Miller, "Nonlinear Effects in MEMS Capacitive Microphone Design", *Proc. of ICMENS'03*, 20-23 July, Banff, Alberta, Canada, pp. 297-302.
- [37] M. Vogels and G. Gielen, "Stability Analysis of  $\Delta\Sigma$  Modulators Using Wavelets", *Analog Integrated Cicruits and Signal Processing*, vol. 41, 2004, pp. 279-291.
- [38] S.H. Ardalan and J.J. Paulos, "An analysis of nonlinear behavior in delta-sigma modulators" *IEEE Trans. Circ. and Syst.*, vol. 41, no.6, 1987, pp. 593-603.
- [39] R. Schreier, "An Empirical Study o High-Order Single-Bit Delta-Sigma Modulators", *IEEE Trans. on Circ. and Syst. II: Analog and Digital Signal. Processing*, vol 40, no.8, August 1993, pp. 461-466.
- [40] M. Guaya and T. Zhang, "Adaptive extremum seeking control of nonlinear dynamic systems with parametric uncertainties", *Automatica*, vol. 39, 2003, pp.283-1293.
- [41] Hai Yu, "The Adaptive Seeking Control Strategy and Application in Automotive Control Technology", PhD Thesis, 2006, Ohio State University



- [42] H.H. Wang and M. Krstic, "Extremum Seeking for Limit Cycle Minimization", IEEE Trans. on Automatic Control, vol. 45, no. 12, December 2000.
- [43] M. Guarnieri and G. Malesani, "Elementi di Elettrotecnica – Reti elettriche", Ed. Progetto, Padova, 1999.
- [44] Mohamed Gad-el-Hak "The MEMS Handbook", Virginia Commonwealth University, Richmond, USA
- [45] B. Margesin, A. Bagolini, A. Faes, F. Giacomozzi and V. Guarnieri, "Progettazione, disegno, fabbricazione e caratterizzazione di un microfono capacitivo in silicio con tecnologie MEMS", Tech. Report, October 2002.
- [46] F. Sharipov and V. Seleznev, "Data on Internal Rarefied Gas Flow", J. Phys. Chem. Ref. Data. Vol. 27, no 3, 1998.
- [47] M. Pedersen, W. Olthuis and P. Bergveld, "On the Mechanical Behaviour of thin perforated plates and their application in silicon condenser microphones", Sensors and Actuators A, Vol. 54, Issue 1-3, June 1996, pp. 499-504.
- [48] P. C. Hsu, C. H. Mastrangelo and K. D. Wise "A high sensitivity polysilicon diaphragm condenser micropophone", Proc. of The Eleventh Annual International Workshop on MEMS, 25-29 Jan 1998, pp. 580-585.
- [49] H. L. Chau and K. D. Wise, "Noise Due to Brownian Motion in Ultrasensitive Solid-State Pressure Sensors", IEEE Trans. Electron Devices., vol. ED-34, Issue 4, April 1987, pp 859-865.
- [50] T. J. Hoffler and S. L. Garret, "Thermal noise in a fiber optical sensor", J. Acoust. Soc. Am. Vol. 84, Issue 2, pp. 471-475.
- [51] J. B. Johnson, "The Schottky effect in low frequency circuits", Physical Review, Vol. 26, pp. 71-85.
- [52] W. Schottky, "Small-Shot Effect and Flicker Noise", Physical Review, Vol. 28, July 1926, pp. 74-103.
- [53] P. Dutta and M. Horn, "Low-Frequency fluctuation in Solids: 1/f Noise", Rev. Mod. Phys., Vol. 53, no. 3, July 1981, pp. 497-516.
- [54] J. J. Lennon, "Red-shifts and red herrings in geographical ecology", Ecography, Vol. 23, 2000, pp. 101-113.
- [55] A. J. Zuckerwar and G. C. Herring, "Calibration of the pressure sensitivity of microphones by a free-field method at frequencies up to 80kHz", J. Acoust. Soc. Am. Vol. 119, Issue 1, January 2006, pp 320-329.
- [56] J. Bay, "Silicon Microphone for hearing aid applications", PhD Thesis 1997, Mikroelektronik Centret, Technical University of Denmark.
- [57] A. M. Elshurafa and Ezz I. El-Masry, "Effects of Etching Holes on Capacitance and Tuning Range in MEMS Parallel Plate Variable Capacitors", 6<sup>TH</sup> Int. Workshop on System-on chip for Real Time Applications, Cairo 27-29 Dec. 2006, pp. 221-224.
- [58] R. C. Batra, M. Porfiri and D. Spinello "Review of modeling electrostatically actuated microelectromechanical systems", Smart Mater. Struct. Vol. 16, no. 6 December 2007, pp. R23–R31.
- [59] V. L. Rabinovich, R. K. Gupta and S. D. Senturia, "The Effect of Release-Etch Holes on the Electromechanical Behavior of MEMS Structures", Transducers 97, International

- Conference in Solid-State Sensors and Actuators, Chicago June 16-19, 1997, pp. 1125-1128.
- [60] A. Faes, “Micromachined Condenser Microphone with Piston Diaphragm”, PhD Thesis, 2003
- [61] B. Margesin, “Relazione scientifica sullo stato d’avanzamento del progetto libero del Fondo Unico della PAT MIDALCO – Microfono distribuito altamente configurabile”, 2006.
- [62] Reimund Gerhard, “Zeit- und Frequenzabhängigkeit der Orientierungspolarisation, Debye-Relaxation”, <http://canopus.physik.uni-potsdam.de/acmp.html>.
- [63] A.K. Jonscher, “Dielectric relaxation in solids”, London, 1983 Chelsea Dielectric Press Ltd.
- [64] L. Risbo, “Stability predictions for high-order SD modulators based on quasilinear modelling”, Proc. IEEE Int. Symp. Circuits Syst., 1994, vol. 5, pp. 361-364.
- [65] R. T. Baird and T. S. Fiez, “Stability Analysis of High-Order Delta-Sigma Modulation for ADC's”, IEEE Trans. On Circuits and Systems II: Analog and Digital Signal Processing, vol. 41, no. 1, January 1994, pp. 59- 62.
- [66] Y. Dong, M. Kraft and W. Redman-White, “Force feedback linearization for higher-order electromechanical sigma–delta modulators”, J. Micromech. Microeng., vol. 16, no. 6, June 2006, ppS54–S60.
- [67] K.B. Ariyur and M. Kristić, “Real-Time Optimization by Extremum Seeking Control”, 2003, Hoboken, New Jersey, John Wiley & Sons.
- [68] R. Antonello and R. Oboe ”Stability Analysis of an Extremum Seeking Controller for Mode-matching in Vibrating Microgyros”, 10<sup>TH</sup> IEEE Int. Workshop on Advanced Motion Control, 2008, 26-28 March, pp. 116-121.
- [69] E. Ruth, “Modelling and control of controllable pitch thrusters subject to large losses”, M. Sc. Thesis.
- [70] M. Kristic, “Performance improvement and limitations in extremum seeking control”, Systems & Control Letters vol. 39 (2000), pp. 313-326.
- [71] H. H. Wang and M. Krstic, “Extremum Seeking for Limit Cycle Minimization”, IEEE Trans. on Automatic Control, vol. 45, no. 12, December 2000.
- [72] H. Kalil, “Nonlinear Systems”, 3. ed. Upper Saddle River, N.J., Prentice-Hall, 2002.